Master Degree Thesis

Variation in photosynthetic electron requirements for carbon fixation by *Dunaliella tertiolecta* during transient phases with different phosphorus availability

Universiteit Utrecht

Royal Netherlands Institute for Sea Research

Yue Lei (5895677)
y.lei@students.uu.nl

Supervisors:
Dr. J. C. Kromkamp
Dr. L. Polerecky

Contents

Statement of originality of the MSc thesis

I declare that:

1. this is an original report, which is entirely my own work,
2. where I have made use of the ideas of other writers, I have acknowledged the source in all instances,
3. where I have used any diagram or visuals I have acknowledged the source in all instances,
4. this report has not and will not be submitted elsewhere for academic assessment in any other academic course.

Student data:

Name: **Yue Lei**

Registration number: **5895677**

Date:
06/09/2018

Signature:

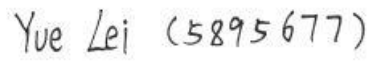

Variation in photosynthetic electron requirements for carbon fixation by *Dunaliella tertiolecta* during transient phases with different phosphorus availability

Abstract:

Marine phytoplankton is an essential contributor to global primary production (PP). Conventional methods to measure PP are time-consuming and the results are usually influenced by bottle effect. Radio isotope tracking methods using radioactive labels are very expensive and limited by health/safety regulations. Measuring PP through variable chlorophyll a (*Chla*) fluorescence based techniques is a potential cheaper, handier and safer choice. Especially its much higher temporal resolution is quite attractive. However, the regulation of the conversion factor -- the electron requirement for carbon fixation ($\Phi_{e,C}$) -- from photosynthetically produced electrons to carbon based PP, is still not fully understood, especially under fluctuating conditions which are typical in natural environments. We investigated the robustness of $\Phi_{e,C}$ and the contributions of the xanthophyll cycle and alternative sinks of electron to $\Phi_{e,C}$ during transient phases, through *Dunaliella tertiolecta* culture experiments in which the phosphorus supply was varied. Besides, we also investigated whether the theory developed to obtain absolute rates of ETR_{PSII} by Oxborough et al. 2012 and Silsbe et al. 2015 holds under such transient phase. Our results revealed that: 1) $\Phi_{e,C}$ doesn't remain stable and could increase 3-fold from a P-replete condition to a P-limited environment. 2) The roles of the xanthophyll cycle in NPQ is limited, but cyclic electron flow around PSII (or PSI) by PTOX can contribute about 50% to electrons sink and it decreased a lot when transformed into P-limited environment. 3) The assumption used for derivations of [RCII] from sigma algorithm and optical absorption coefficient of PSII (a_{LHII}) for the new absorption algorithm, that K_R is constant, proposed by Oxborough et al. 2012 doesn't hold during fluctuating environment with different P concentrations, and the K_R values we got were quite higher than the default value. Our finding points to the limitations of ETR_{PSII} derivations, and provides more information on the conversion of photosynthetically produced electrons to carbon-based PP. More studies are required before the wide spread of *Chla* fluorescence in measuring primary production.

Key words:

Chla fluorescence; electron requirement for carbon fixation; *Dunaliella tertiolecta*; FRRf; K_R

1 Introduction

Annual primary production (PP) by marine phytoplankton is estimated to be about 45-50 Gt C globally and contributes about 50% to the total global primary production (Longhurst et al. 1995) although the estimate varies from 35 to75 Gt C, depending on the models used (Carr et al. 2006). Mainstream conventional methods for measuring PP are the ^{14}C-carbon fixation method (Steemann Nielsen 1952) and gas exchange methods (Riley 1939; Cox et al., 2015), although other methods, like absorption or chlorophyll concentration based methods, are also feasible (for an overview see Kromkamp et al 2017). However, both of them need time-consuming incubations, and the results are influenced by the bottle effect. Besides, the result of ^{14}C technique is thought to be something lying between net and gross carbon fixation depending on the incubation time scale (Marra 2002; Milligan et al. 2015). Furthermore, application of radioisotopes is expensive, and their use is often limited by health/safety regulations. Quantification of PP based on variable chlorophyll a (*Chla*) fluorescence is an alternative approach that can overcome these constraints. Special user-friendly fluorometers which can measure "active fluorescence" can be deployed directly *in situ*, not requiring lengthy incubation. Also, without requiring costly consumable materials, information could be obtained in a more economical way (Goltsev et al. 2016). As such, they provide a cheaper, handier, safer, and higher temporal resolution measurements for PP. However, this active fluorescence technique measures the production of photosynthetically produced electrons, and this requires conversion to C-units. The conversion from electron flux to C-based production is quite complicated and varies with many factors such as different species, environments or even equipments used for measurement. That is the main problem that limites the development of this alternative method, and also one of the main topics in this study. The basic theory of variable fluorescence is also explained below.

1.1 Theory of variable Chlorophyll a fluorescence

1.1.1 Introduction of Chlorophyll a fluorescence

Fluorescence is the re-emission of energy in the form of light by a substance that has absorbed light or other electromagnetic radiation. The re-emitted light has lower energy than that of original absorbed light, and consequently, has longer wavelength. For the light harvesting complex (LHC) of a photosystem, a photon with 670 nm wavelength contains enough energy to make a *Chla* molecule be excited (Bolhàr- Nordenkampf and Öquist 1993). If the energy is not completely utilized in charge separation or heat dissipation, the photon will be red-shifted and re-emitted as *Chla* fluorescence with peak at ~685 nm. For photosystem II (PSII) in vivo, the absorption of antenna pigments peaks at about 435 nm and 678 nm, while the absorption peak of down-hill PSII core is red-shifted to 680 nm. This small difference causes the excitation energy being able to easily escape from the reaction center back to its antenna system (making PSII a shallow trap) (Krause & Weis 1988). In contrast, the divergence between the absorption maximum of photosystem I (PSI) antenna pigments and its reaction center is about 20 nm. With such large gap, the probability for the energy to escape back is much lower (Falkowski and Raven 2013). Therefore, it's generally assumed

that, at normal room temperature, all fluorescence (actually ~90–95%) stems from PSII antennae molecules (Krause and Weis 1991; Papageorgiou et al. 2007).

1.1.2 Link of fluorescence signal with photosynthesis

The characteristic change in *Chla* fluorescence yield upon transferring dark-adapted photosynthetic material into the light was firstly observed by Kautsky and Hirsch (1931): they observed that the *Chla* fluorescence yield rose rapidly to reach a peak after approximately 1 s. This pattern was the topic of intense research (e.g. review Dau 1994), leading to the development of useful tools to probe the photosynthetic apparatus and get information about reduction of electron acceptors downstream of PSII (Schreiber et al. 1986; Kolber and Falkowski, 1993; Dau, 1994; Maxwell and Johnson 2000). According to the fundamental biophysical model described by Kolber and Falkowski in 1993, in the dark, the primary electron donor – a special *Chla* molecule (P_{680}) – in the reaction center of PSII (RCII) is reduced while the primary electron acceptor – a quinone (Q_a) – is oxidized. In this situation, all the photosynthetic reaction centers are said to be "open". Upon exposure to light, the photosynthetic pigments absorb photons and transfer this excitation energy to the reaction center, then P_{680} is oxidized to P_{680}^+, and Q_a is reduced to Q_a^-. In this reduced state, Q_a is no longer able to accept another electron from P_{680} until it has passed an electron to the subsequent electron carrier, a quinone Q_b. Under such circumstances, the RCII is said to be "closed". The absorbed light energy by PSII can be used through three pathways: 1) photochemistry, which is the actual photosynthetic process that includes primary charge separation and photosynthetic electron transfer; 2) thermal dissipation; and 3) fluorescence emission, which only accounts for a small portion of the absorbed light (only 1% or 2%) (Maxwell and Johnson 2000). Due to energy conservation, the sum of the efficiencies of these three pathways is assumed to be unity. Since PSI does not emit fluorescence at room temperature, thus negligible to that from PSII, we are able to gain knowledge of the relationship among these three pathways through the measurement of changes in fluorescence emission from PSII.

In darkness, in the absence of any non-photochemical quenching process, when all the photosynthetic reaction centers are "open", they are capable of transferring absorbed light energy to chemical energy. The oxidized Q_a act as the main quencher of fluorescence, so fluorescence is at a minimal level, F_0 (see the notation list in Table 1). Under ambient light, as part of the photochemistry pathway is blocked by closed RCII, the fluorescence yield can increase to a level F', due to the fact that reduced Q_a does not quench fluorescence. When all RCII are closed in high light, the maximum level, F_m is reached. See Van Kooten and Snel 1990 and Kromkamp and Forster 2003 for terminology (or notation). The maximum quantum efficiency of PSII, F_v/F_m, is defined as $(F_m - F_0)/F_m$. In ambient light, F_0 rises to F' (< F_m'), the effective quantum efficiency of PSII F_q'/F_m' (φ_{PSII}) then equals $\Delta F/ F_m' = (F_m'-F')/F_m'$ (Genty et al. 1989). Therefore, in this manner, the relative change of fluorescence yield reflects the charge separation status of Q_a (Butler and Kitajima 1975; Kolber and Falkowski, 1993). There is a large body of evidence that F_v/F_m can be used as a sensitive indicator of plant photosynthetic performance or abiotic stress such as nutrient deficiency (Berges et al. 1996; Boyd et al. 1999; Ly et al. 2014), although results obtained by Kruskopf and Flynn 2006 suggested that F_v/F_m can recover when the cells have the time to adapt to the limiting nutrient conditions.

1.1.3 Fates of absorbed photons within photosystem II

As there are three pathways for the de-activation of PSII from excited states induced by absorption of photons, the relationship between fluorescence and photochemistry rarely follows a simple negative linear trend. Both photochemistry and non-radiative decay act as quenching paths of the fluorescence signal, which are called photochemical- (q_P) and non-photochemical quenching (q_N or NPQ, see Table 1 for a definition of the terms and abbreviations used in this thesis), respectively. The corresponding coefficients of them can be quantified by the application of saturation pulse method, firstly proposed by Bradbury and Baker in 1984 and further ameliorated by Schreiber and his colleagues two years later (Schreiber et al.1986). As shown in Figure 1, we assume that no non-photochemical quenching will be stimulated by short light pulse (Schreiber 2004). For a dark-adapted sample whose non-photochemical quenching is negligible, a short dim measuring light (<0.5 μmol photons m^{-2} s^{-1}; ~10 μs) is applied to measure the minimum fluorescence yield (F_0) (Suggett et al. 2010). That dim measuring light is weak enough to induce no reduction of Q_a and thus no closure of any RCII. Then a strong short light pulse (>10,000 μmol photons m^{-2} s^{-1}; 0.4–0.8 s) is used to close all RCII, giving rise to the maximum fluorescence yield (F_m) (Schreiber et al 1986; Ralph and Gademann 2005). This high intensity light pulse is called the saturation pulse. As the flash is short enough, it is commonly assumed that the nonphotochemical quenching rise is negligible. Nevertheless, in actinic (ambient) light, non- photochemical quenching might be activated and is no longer negligible, thus a drop of F_m to a lower level (F_m') might happen. Accordingly, this principle can be used to quantify both q_P and q_N (or NPQ). q_P here is defined as the chance that a RCII is capable of charge separation in photochemical process at a given instant (Kolber and Falkowski, 1993), while q_N is the measure of the absorbed light that is quenched under actinic light (Suggett et al. 2010). The calculations of them from the method described above are summarized in Table 1.

Calculation of q_P and q_N requires knowledge of the minimal fluorescence of PSII in the light adapted state (F_0'), i.e. the minimum fluorescence measured immediately after darkening a sample. Since F_0' may be difficult to measure technically, Oxborough and Baker described an alternative method to calculate F_0' in 1997:

$$F_0' = \frac{F_0}{F_v/F_m + F_0/F_{m'}} \quad \text{-- (1)}$$

Nonetheless, there is another drawback of q_N that it may vary with the rate constant of photochemistry (Krause and Jahns 2004). The Stern-Volmer coefficient – NPQ – is generally considered more robust and takes precedence over q_N (Ralph and Gademann, 2005). Hence, in this thesis below, NPQ is used as the non-photochemical quenching coefficient, instead of q_N.

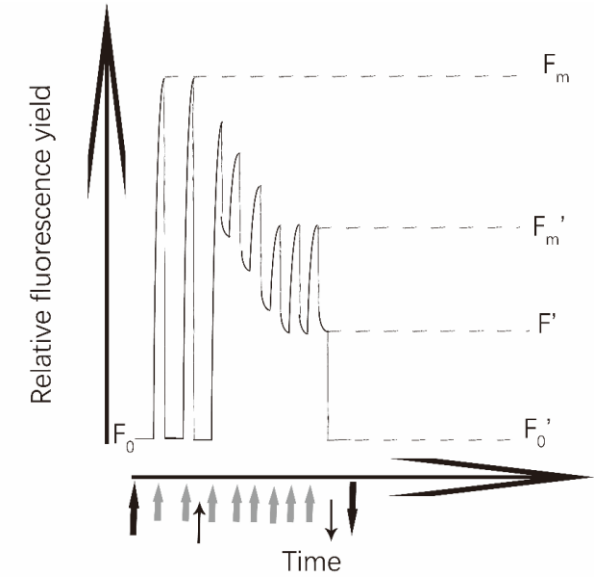

Figure 1. Schematic diagram of fluorescence induction kinetics with the application of the saturation pulse method. Thick black arrows indicate the start (up) and end (down) of the measuring light; grey arrows indicate the saturating light pulse application; Thin black arrows indicate the start (up) and end (down) of actinic light (Modified from Suggett and Borowitzka 2010).

Table 1 Fluorescence parameters used in this thesis.

Parameters	Definition	Derivation	units
E_{LED}	photon output from the FRRf measuring LEDs		µmol photons m^{-2} s^{-1}
E_{PAR}	photosynthetically active radiation		µmol photons m^{-2} s^{-1}
Φ_{RCII}	the quantum yield of charge separation within PSII		mol e^- (mol photon)$^{-1}$
F_0 or F_0'	minimum fluorescence yield induced by a weak probe flash in the dark, or immediately after turning off the ambient light.		dimensionless
F_m or F_m'	maximum fluorescence yield measured in dark adapted algae, or in algae under ambient light		dimensionless
F'	fluorescence yield under ambient light		dimensionless
F_q', ΔF	difference between fluorescence yields F_m' and F'	$F_m' - F'$	dimensionless
F_v	maximum variable fluorescence yield	$F_m - F_0$	dimensionless
φ_{PSII}, $\Delta F/F_m'$, F_q'/F_m'	effective photochemical efficiency of RCIIs	$(F_m' - F') / F_m'$	dimensionless
q_P	photochemical quenching coefficient, or proxy of fraction of open RCII	$(F_m' - F') / (F_m' - F_0')$	dimensionless

q_N	non-photochemical quenching	1- (F_m' - F_0') / (F_m – F_0)	dimensionless
NPQ	non-photochemical quenching (Stern-Volmer)	(F_m – F_m') / F_m'	dimensionless
q_T	state transition non-photochemical quenching		dimensionless
q_E	thermal energy non-photochemical quenching		dimensionless
q_I	photoinhibition non-photochemical quenching		dimensionless
a*	chlorophyll-specific optical absorption cross section	Average absorption between 400nm and 700nm ×100×2.303/ [*Chla*]	m^2 (mg *Chla*)$^{-1}$
a_{PSII}	chlorophyll-specific optical absorption cross section of PSII		m^2 (mg *Chla*)$^{-1}$
a_{LHII}	optical absorption cross section of PSII	a_{PSII} × [*Chla*] or $\frac{Fm \times Fo}{Fm - Fo} \times \frac{K_R}{1 \times 10^6}$	m^{-1}
F_{II}	the ratio of PSII absorption to total absorption	a_{PSII} / a*	dimensionless
σ_{PSII}	functional absorption cross section of PSII		nm^2 $PSII^{-1}$
n_{PSII}	the number of PSII		mol RCII (mol *Chla*)$^{-1}$
[RCII]	concentration of photosystem II reaction center		mol RCII m^{-3}
K_R	instrument specific constant	[RCII] × σ_{PSII} ×E_{LED} /F_0	m^{-1}
$\Phi_{e,C}$	electron requirement for carbon fixation		mol e^- mol^{-1} C
$rETR_{PSII}$	relative electron transport rate through PSII	F_q'/F_m' × E_{PAR}	dimensionless
ETR_{PSII}	electron transport rate through PSII per mg *Chla*		µmol e^- mg^{-1} *Chla* s^{-1}
JV_{PSII}	PSII flux per unit volume		electrons m^{-3} s^{-1}

Commonly, NPQ contains at least three components: thermal energy quenching (q_E), quenching due to state transitions (q_T) and quenching linked to photoinhibition (q_I). q_E is the most efficient component of NPQ in higher plants (Horton and Ruban 1994; Adams and Demmig-Adams 1995; Holt et al. 2004; Horton and Ruban 2005) and most eukaryotic algae (Goss et al. 2006; Lavaud 2007). Full q_E activation requires both a suitable proton gradient across the thylakoid membrane (trans-thylakoid-pH-gradient, ΔpH gradient) and the activation of the xanthophyll cycle (Nilkens et al. 2010). In green algae, the xanthophyll cycle involves three pigments: zeaxanthin, antheraxanthin and violaxanthin. Violaxanthin is converted to zeaxanthin via the intermediate antheraxanthin by the enzyme violaxanthin de-epoxidase, which is activated by the build-up of ΔpH, while the reverse reaction in dark is carried out by zeaxanthin epoxidase. In diatoms and dinoflagellates (contain

chlorophyll-c), this cycle consists of only two kinds of pigment: diadinoxanthin (DD) and diatoxanthin (DT, diatoms and haptophytes) or dinoxanthin (dinoflagellates), where the former is transformed into the latter under high light (Goss et al., 2006; Taiz and Zeiger, 2006). Another difference between higher plants (V/A/Z-cycle) and diatoms (DD/DT cycle) is that the latter requires a smaller drop in the lumen pH (thus the DD-de-epoxidase is activated earlier) and stays in the light activated state when transferred from high light to darkness. Lower light is required for the DD → DT conversion (Goss et al., 2006). For a long time it has been assumed that a xantophyll cycle driven q_E has been lacking for cyanobacteria, but with the discovery of the Orange Carotenoid Protein a q_E type non-photochemical quenching has now also been established (Kirilovsky 2007). The second component q_T lasts for 5-20 min and is effective especially in cyanobacteria and red algae but also in green algae although less significant (Campbell et al. 1998; Finazzi and Forti 2004; Suggett et al. 2010). During state-transitions, absorbed light energy can be re-distributed between the two photosystems -- PSII and PSI – by adjustment of the cross sections of light-harvesting antennas. For the detailed mechanism please see the study of Lemeille and Rochaix in 2010. Photoinhibition can also cause non-photochemical quenching (q_I). q_I is considered to be related to damage caused by strong light. It is generally agreed that the D1 protein (PSII core protein) seems to be among the first proteins which get damaged by photoinhibition. q_I can be distinguished from other forms of NPQ as it takes usually a longer time to relax (>h) after the cells are returned to the darkness or low light (Aro et al. 1993, Campbell et al. 1996, Pocock et al. 2007). In addition, a fourth component of NPQ has been suggested – reaction center quenching. It can cause heat emission as well as fluorescence quenching in a xanthophyll independent manner and could be particularly important in prokaryotic phototrophes (Ivanov et al. 2008a; 2008b).

1.1.4 Alternative electron sinks

For light energy that goes into the PSII photochemistry pathway, not all electrons produced from water-splitting are utilized in fixing carbon dioxide. When exposed in high light condition, PSII may produce more electrons than the amount that the dark reaction can use in carbon fixation. To avoid damage to photosynthetic apparatus in this case, the algae usually adopt other mechanisms to channel redundant electrons into alternative sinks. An important one is alternative electron cycling. Examples are: (a) Water Water Cycle (WWC) or Mehler reaction, where oxygen is reduced by electrons coming from ferredoxin of PSI to form superoxide, which is then dismutated to H_2O_2 and finally be further reduced to water and oxidized ascorbate (Flameling & Kromkamp 1998; Asada 2000; Claquin et al. 2004); (b) cyclic electron flow around PSII (or PSI) directly (Prasil et al. 1996, Lavaud et al. 2002) which might involve a plastid terminal oxidase (PTOX) (Berg et al. 2011). Channeling of electrons towards the synthesis of other biochemical compounds apart from carbohydrates, such as lipids or proteins that can be stored inside the cell or excreted, can be another alternative sink of electrons (Suggett et al. 2010). Excess energy can be extinguished by cyclic electron transport by PSI, even when linear electron transport is limited by low dissolved inorganic carbon (DIC) concentration (Bukhov and Carpentier 2004). In general, PSII is more sensitive to photodamage than PSI (Ihnken et al., 2014).

1.2 Use of *Chla* fluorescence in measuring primary production

1.2.1 Fluorescence-light response curves and ETR_{PSII} calculation

According to the work by Genty et al in 1989 and others (Kolber and Falkowski 1993; Baker and Oxborough 2004; Kromkamp et al. 2008), fluorescence-based measures of PSII photochemical efficiency correlates well with carbon fixation, indicating the PSII quantum yield to be a good proxy of photosynthesis production measurement. Similar with traditional photosynthesis-irradiance curves (P–E curve or P–I curve; Falkowski and Raven,1997) for photosynthetic rate measurements, we use fluorescence-light response curves (FLCs) to monitor changes of effective quantum yield in response to step-wise increased light intensities. In terms of the length of duration exposed to different light intensities, there are two kinds of FLCs: prolonged one (3-4 min) and rapid one (10-20 s) (Serôdio et al. 2006; Hennige et al. 2008). The former one can achieve possible steady state during each light step, which could indicate the ability and time duration of the photochemistry reactions to adjust the electron flow with changing light intensity (Suggett et al. 2003). But when we want to know the photosynthetic activity in the field environment, sampling time should be short to allow measurements in fast changing micro-environment *in situ* without altering the acclimation state of the photosynthetic apparatus. In this case, we would apply the rapid one, and a dark acclimation period should also be avoided (White and Critchley 1999).

The quantum efficiency of PSII ($\Delta F/ F_m'$) can be multiplied by the flux of photosynthetically active radiation (E_{PAR}) to get relative photosynthetic electron transfer rate through PSII ($rETR_{PSII}$) (eq. 2):

$$rETR_{PSII}\ (\mu mol\ e^{-}\ m^{-2}\ s^{-1}) = \frac{\Delta F}{F_m'} \times E_{PAR} \times \Phi_{RCII} \quad \text{-- (2)}$$

The Φ_{RCII} (mol e^-/mol photon) is the quantum yield of charge separation in PSII, representing the ratio of electrons produced per photon absorbed by PSII. It is taken to be unity (Kolber and Falkowsky 1993). If we know how much light is absorbed by PSII, we can derive the absolute rate of photosynthetic electron transfer through PSII (ETR_{PSII}). This light absorption rate can be obtained from the optical absorption cross section (a*, m^2/mg *Chla*) which can be obtained from spectrophotometer, and a fraction F_{II} which represents the ratio of PSII absorption to total absorption ($a_{PSII} = a^* \times F_{II}$). Thus, the absolute rate of ETR_{PSII} is (eq. 3):

$$ETR_{PSII}(\mu mol\ e^{-}mg^{-1}chla\ s^{-1}) = \frac{\Delta F}{F_m'} \times E_{PAR} \times \Phi_{RCII} \times a^* \times F_{II} \quad \text{-- (3)}$$

The fraction F_{II} is often assumed to be a certain value, such as 0.5 for green algae, thus this algorithm for deriving ETR_{PSII} is not so accurate as F_{II} can deviate from 0.5 (Johnsen and Sakshaug 2007). An alternative algorithm mostly used is the so-called "sigma algorithm", originally introduced by Kolber and Falkowski in 1993 (eq. 4):

$$ETR_{PSII}(\mu mol\ e^{-}mg^{-1}chla\ s^{-1}) = \frac{\Delta F}{F_m'} \times E_{PAR} \times \Phi_{RCII} \times \sigma_{PSII} \times n_{PSII} \times \frac{10^{18}}{893.5\times10^{3}} \quad \text{-- (4)}$$

Here, σ_{PSII} is the functional absorption cross section of PSII (nm^2 $PSII^{-1}$) that can be obtained from FRR fluorometers, and n_{PSII} is the number of PSII normalized to [*Chla*], which equals the RCII concentration per mol *Chla* (eq. 5):

$$n_{PSII}(\text{mol RCII } mol^{-1}Chla) = \frac{[RCII]}{[chla]/_{893.5}} \quad \text{-- (5)}$$

where 893.5 is a unit conversion from g/m^3 to mol/m^3 for *Chla*. The concentration of RCII can be obtained through the method described in methods part below. But that method requires high *Chla* concentration and specific instruments, therefore it is not so convenient in field work. Also, that "sigma algorithm" to derive ETR_{PSII} is based on two main assumptions that 1) connectivity among RCIIs is homogeneous; and that 2) σ_{PSII} values of open RCIIs within a sample don't vary a lot. Oxborough et al. 2012 and Silsbe et al. 2015 suggested a quicker and easier equation to deduce [RCII] without independent measurements (eq. 6):

$$[RCII](mol\ RCII\ m^{-3}) = \frac{K_R \times F_0}{\sigma_{PSII} \times E_{LED}} = \frac{F_0}{\sigma_{PSII} \times 10^{-18}} \times \frac{K_R}{10^6} \times \frac{1}{6.02 \times 10^{23}} \quad \text{-- (6)}$$

K_R is an instrument specific calibration factor, and E_{LED} is the light intensity used to measure F_0 and σ_{PSII}. The right part of this equation is based on the equipment we used in this study. This equation is based on an assumption that the ratio of fluorescence (k_f) and photochemistry (k_p) rate constants in dark acclimated samples is constant, thus K_R is constant. Based on that assumption, a new algorithm for the derivation of PSII electron transport rate per unit volume (JV_{PSII}), called "absorption algorithm", was further proposed by Oxborough et al. 2012 (eq. 7, 8, 9):

$$JV_{PSII} = \frac{\Delta F}{F'_m} \times a_{LHII} \times E_{PAR} \quad \text{-- (7)}$$

$$a_{LHII} = \frac{F_m \times F_0}{F_m - F_0} \times \frac{K_R}{E_{LED}} \quad \text{-- (8)}$$

Thus:

$$JV_{PSII} = \frac{F_m \times F_0}{F_m - F_0} \times \frac{\Delta F}{F'_m} \times \frac{K_R}{E_{LED}} \times E_{PAR} \quad \text{-- (9)}$$

where a_{LHII} is the optical absorption cross section of PSII (m^{-1}); E_{LED} is the photon output from the FRRf measuring LEDs. For the detailed theory behind, please look into Oxborough et al. 2012. But whether that assumption holds in variable environmental conditions and for all phytoplankton species still needs further test, and testing that assumption is an important part of the research described in this thesis.

1.2.2 Protocols

The earliest method for measuring photosynthetic parameters mentioned above is the"fluorescence induction technique", which is based on monitoring fluorescence transient of a dark-adapted sample under a short continuous light (Govindjee 1995). But since the excitation transported to RCII in a dark-adapted state is slower than the re-oxidation of PQH_2, and also because the stoichiometry of plastoquinone pool (PQ) is about 5-30 times higher than Q_a (Kolber and Falkowski, 1993), the fluorescence yield change is complicated due to multiple turnovers of PSII. Although this problem can be solved by application of 3-(3,4-dichlorophenyl)-1,1-dimethylurea (DCMU) that could prevent the re-oxidation of Qa^-, thus reducing photochemistry to zero, it is not practical to apply this herbicide solution *in situ*. Afterwards, single-turnover (ST) and multiple-turnover (MT) active fluorescence-based techniques were developed. The duration of MT flashes is long enough to allow several oxidation and reduction steps of Q_a, leading to also reduction of Q_b and PQ-pools. But the duration of ST flashes only allows a single reduction of Q_a. The principle is to expose samples to

one or more saturating light flashes, and then record changes in fluorescence yield. One of the applications of them is the “pulse amplitude modulated (PAM)” (also called “light doubling”) method proposed by Schreiber et al in 1986, using MT actinic flashes (~0.6 s) based on the saturation pulse method described above to induce the maximum fluorescence level. Another application is “pump and probe' (P&P)”, advocated by Mauzerall in 1972 and further developed by Kolber and Falkowski (Falkowski et al. 1986; Kolber et al. 1990). They recorded fluorescence yields with weak short probe flash before and after an ST (~10 μs) actinic pump flash of variable intensity. For more information between both methods see Kromkamp and Forster (2003). Through varying the intensity of pump flashes, we can derive σ_{PSII}. However, there are two drawbacks of these two techniques: First, it is not easy to track dynamic changes of electron transport and σ_{PSII} in microseconds to minutes time scale; Second, in the case of MT protocols, the excitation energy used may alter the redox status of electron carriers between PS II and PSI, as well as the non-photochemical quenching level (Kolber et al. 1998). The subsequently proposed “fast repetition rate fluorescence (FRRF)” by Kolber et al in 1998 is a great improvement, which measures fluorescence changes induced by a series of ST sub-saturating flashlets (~1 μs). Although the intensity of single flashlet is not saturating, the overall photon flux is more than saturating by virtue of the high frequency. The intensity, duration, and interval between them can be controlled independently, allowing separate control of Qa and PQ reduction, and consequently derivation of independent contribution of different processes to the fluorescence yield change. Besides, σ_{PSII} and the connectivity among RCIIs can also be calculated from this fluorescence transient kinetics. Moreover, the theory of the sigma and absorption algorithm for ETR_{PSII} derivation mentioned above were developed for the FRRF. So we choose the FRRf to carry out our experiment in this study.

1.3 Research aim

Although many studies found an obvious linear relationship between ETR_{PSII} and C-fixation or gross O_2 evolution rate (see Perkins et al 2010 for a summary), different results were discovered when the same research was done in broader conditions (Lawrenz et al 2014). The reason is linked with the different contributions of other electron sinks explained above under different environmental conditions, such as light history of the sample, temperature/nutrient/salinity/light stress, and by using different protocols. Additionally, several assumptions in the ETR_{PSII} calculation algorithms were necessary related to: 1) how to derive absolute rates of ETR from relative rates of ETR, and 2) a value for the electron requirement for carbon fixation ($\Phi_{e,C}$). Regulation of the latter is still not fully understood, especially under fluctuating environmental conditions where variable availability of nutrients or light leads to an unbalanced growth. Those limitations substantially prevent the variable fluorescence-based method from being expanded as a standard quantification method of PP.

In most laboratory studies, $\Phi_{e,C}$ has been investigated under the condition of a balanced growth, i.e., during constant environmental conditions, despite the fact that an unbalanced growth under fluctuating environment might be the most common condition for many phytoplankton communities. To which extent does $\Phi_{e,C}$ vary under unbalanced growth conditions is presently unknown. Phosphorus (P) is essential for the growth and reproduction of phytoplankton. It plays an important role in thylakoid structure and NADPH regeneration (Kalaji et al. 2016). Also, the internal P-content

is intimately tied to the growth rate via the rRNA content (Elser et al 2003). Although marine primary productivity is mainly considered to be nitrogen- or iron-limited (Moore et al. 2013), a growing number of marine environments are now recognized to be phosphorus limited (Elser et al 2007; Ly et al 2014; Lin et al. 2016; Reed et al. 2016). Apart from that, it is observed that light-dark cycles can induce large diurnal variability in ETR_{PSII} (Kromkamp, pers. Com). However, at present it is unknown whether this large diurnal variability is also observed in C-fixation rates.

The green algae *Dunaliella tertiolecta* is widely distributed in cosmopolitan estuaries and marine coastal waters (Flood et al. 2018). We used this species as our experimental organism as a model photosynthetic eukaryotic micro-organism. There are four objectives of this project: 1) explore the robustness of $\Phi_{e,C}$ during a transient phase – especially the initial stages – when the cells will go from a phosphate-replete to a phosphate-limited situation; 2) investigate whether the assumption (i.e. K_R is constant) made in the theory developed to obtain absolute rates of ETR_{PSII} by Oxborough et al. 2012 and Silsbe et al. 2015 holds under such transient phase; 3) explore the role of alternative sinks of electrons during such transient phase; 4) check whether there is large diurnal variability in C-fixation.

2 Materials and methods

The general experimental approach is based on manipulation of the inorganic phosphorus concentration during the growth of cells in a fed-batch culture coupled with the measurements of FRRf parameters, photosynthetic carbon fixation, and alternative sinks of electron. Photosynthetic carbon fixation is measured using incubations with ^{14}C-DIC. Alternative electron cycling of electron is measured by FRRf with addition of corresponding inhibitors. Channeling of electrons towards storage compounds is characterized by different patterns in the allocation of assimilated C and N. It is investigated through incubations with ^{13}C-DIC and ^{15}N-NH_4, followed by measurements of isotopic enrichment in bulk biomass with Isotope-ratio mass spectrometry (IRMS) and in single cells with Nanometer-scale Secondary Ion Mass Spectrometry (NanoSIMS).

2.1 Experimental design and culture conditions

Before the experiment, *Dunaliella tertiolecta* (Butcher 1959) (CSIRO strain CS-175) was grown in steady state continuous cultures (dilution rate 0.1 day $^{-1}$) in nutrient replete F/2 medium (the recipe is in Table i of Appendix I; Guillard and Ryther, 1962) under light-dark cycle (14h: 10h, 63 µmol photons m^{-2} s^{-1}), using a white LED Photopanel (Photon System Instruments, Czech Republi). Cultures were monitored daily by following the cell concentration and pH between 9:00 am and 10:00 am (in the same time period in order to avoid variability in the data caused by possible diurnal patterns) to make sure the cells are in steady state (growth rate "µ" equals dilution rate "D") before the experiment. The dilution rate was calculated as the flow rate (ml day^{-1}) divided by the volume (ml). Here the growth rate is calculated from eq. 8:

$$N_t = N_0 \times e^{(\mu - D)t} \quad \text{-- (8)}$$

where N_t and N_0 are the cell concentration at time t (day) and 0, respectively (Crow & Kimura, 1970).

In the first experiment (E1), after several measurements following the protocol of V.S.1 in Table 2, we started the P-limiting experiment by transferring algae suspension to two 1L pre-autoclaved Roux bottles (about 5 cm light path, named culture a (Ca) and culture b (Cb) respectively). Each bottle was filled with 650 ml cell suspension and sealed with cotton plug. During the transfer, cells were harvested by gentle centrifugation (2000 rpm) and the pelleted cells were re-suspended in F/2 medium with 10% of the normal phosphate concentration (Table 3). These two batch cultures were treated with the same conditions as previous continuous cultures, with daily dilution by P-limited F/2 medium (dilution rate: 0.1 day $^{-1}$). Suspension taken out from the culture was collected with 100 ml pre-autoclaved glass bottles and used as samples to conduct different measurements. But then a problem was found with the medium: it didn't contain DIC, Br, B and Sr, so we updated the medium immediately. After about one week with measurements following the protocol in Table 2, however, the algae were getting P-starved and dying, so we doubled the DIP in the cultures and medium. The cultures showed little improvement, so another 80% DIP of normal F/2 medium level was added into the cultures, and the dilution from then on was performed with normal F/2 medium. The experiment ended after about two weeks' monitoring following the protocol in Table 2. Cell

concentration and size were measured in triplicate through a Coulter Counter (model ZM connected to a Coulter Multisizer, Beckman Coulter), and the average value was used. pH was measured using a pH electrode which was regularly calibrated (DJ 113, 662-1385). Absorption was monitored by Cary BIO-100 UV-VIS dual-beam spectrophotometer (Varian, Palo Alto), equipped with a LabSphere integrating sphere (DRA-CA-3300), in the wavelength region of 400-750 nm. The average absorption was obtained by averaging the absorption from 400-700 nm after correction for backscatter at 740-750 nm.

As the first experiment (E1) was not ideal, we repeated the experiment for a second time (E2). As the cells didn't grow well in continuous cultures, we grew them in two 1 L Roux bottles as fed-batch cultures directly, each with 1L cell suspension. Except for the addition of air bubbling into cultures, growth conditions were the same as the first experiment. The cultures were diluted daily with fresh medium and the dilution rate was higher (0.4 day $^{-1}$) than the first experiment because of the updated medium with DIC, Br, B and Sr supplementary, thus the parameter monitoring was performed every day. The same parameters were measured as V.S.1 of the first experiment, except the addition of fluorescence-light response curves with dithiothreitol (DTT) and propyl gallate (PGal) for the investigation of the role of the xanthophyll cycle and plastid terminal oxidase (PTOX) involved cyclic electron flow respectively. After one week, when the cells were in semi-steady state, the cells were transferred to P-limited F/2 medium (Table 3) and daily diluted with P-limited F/2 medium. Two weeks later, the back-transient was started by adding another 80% P to normal F/2 medium level into the cultures and conduct the dilution with normal F/2 medium. The experiment was terminated after another one week.

Table 2 Parameters monitoring protocol for experiment 1. "Ca" and "Cb" are two replicate batch cultures. Constrained by the growth rate and culture volume, protocol V.S.1 and V.S.2 were conducted in turn, which means V.S.1 on day 1, V.S.2 on day 2, V.S.1 on day 3, V.S.2 on day 4... etc. The right two column are corresponding volume for measurements of different parameters. This complicated pattern was necessary as the volume and biomass in the cultures did not allow all measurements (V.S.1) to be measured every day. Otherwise, the sampled volume would disturb the transient state too much.

		Ca (650 ml)	Cb (650 ml)
V.S.1	Absorption, cell concentration	3 ml	3 ml
	^{14}C fixation	30 ml	30 ml
	$ETR_{PSII}/^{14}C$	3 ml	3 ml
	pH	30 ml	30 ml
	Chla	5 ml	5 ml
	Pigments (HPLC)	5 ml	5 ml
	FLCs	3 ml	3 ml
	[RCII]	30 ml	30 ml
	POC and PON, filtrate for DIP	10 ml	10 ml
V.S.2	Absorption, cell concentration	3 ml	3 ml
	FLCs	3 ml	3 ml
	$ETR_{PSII}/^{14}C$	3 ml	3 ml

Table 3 Phosphorus and nitrogen concentration plan of the medium in this study.

	DIP (μmol/l)	Percentage of DIP	DIN (μmol/l)	N/P ratio
Normal medium	32	100.0%	882	27.6
P-limited medium of experiment 1	3.2	10.0%	882	275.6
P-limited medium of experiment 2	6.4	20.0%	882	137.8

During the second experiment, we also conducted 2 h, 7 h and 24 h incubations with ^{13}C-DIC and ^{15}N-NH_4 (10% enrichment) at certain timepoint (to avoid variability caused by possible diurnal patterns) every other day, in order to study C/N allocation patterns during such transient phases both in bulk analysis level and single cell level through NanoSIMS measurements. 20 ml samples were filled into 20 ml glass vessels, thus little headspace, under same conditions as batch cultures. 20 μl of 88.2 mM $Na^{15}NO_3$ and 20 μl of 857.2 mM $NaH^{13}CO_3$ stock solution were spiked into the 20 ml samples, causing a 10% enrichment of the nitrate and DIC concentrations. The incubation protocol is summarized in protocol P2 in Table 4.

Besides, diurnal patterns of C_fixation rate were expolored by 2 h incubations with ^{13}C-DIC and ^{15}N-NH_4 (10% enrichment) at different four time points during single days (one day during the first P-replete period and one day during the P-limited period) (protocol P1 in Table 4). These incubations were only performed on culture Ca. The incubation operations were same with protocol P2 in Table 4. Meanwhile, we tracked ETR_{PSII} change of Ca through FLCs at the same four time points during same days to derive the diurnal pattern of electron requirement for carbon fixation. Constrained by the lab working time, we only did -- 09:30 am, 11:30 am, 13:30 pm and 15:30 pm -- four time points during the light period on day 4 during the first stage (P-replete) and day 18 during the second stage (P-limited).

2.2 FRRf measurements

A Fast Repetition Rate fluorometer (FRRf; FastOcean system, equipped with an Act2 accessory to measure fluorescent light curves (FLC), Chelsea Technology Group Ltd, UK) was used to measure variable *Chla* fluorescence by FLCs. A 3 ml sample was dark-adapted for 15 min for the relaxation of energy-dependent and state-transition NPQ (Kruskopf and Flynn 2006), and then added to the cuvette of FRRf, followed with 150 s exposure to ten different irradiances from 0 to 600 μmol photons m^{-2} s^{-1} white light which was separated by 5 s darkness between each two light periods to measure F_0'. (see example: Figure 2). The fluorescence response was measured by blue ST flashes only. Fluorescence induction curves during the 100 flashlets followed by 50 relaxation flashlets were fitted automatically by the Act2-software provided by the manufacturer. Fluorescence parameters F_0, F_m, σ_{PSII}, F_v/F_m, NPQ, and φ_{PSII} were given by the instrument. $rETR_{PSII}$ and ETR_{PSII} were calculated based on eq. 2 and eq. 4, respectively and fitted by Platt & Gallegos (1980) (eq. 10, 11) (P&G model) normalized to the irradiance as suggested by Silsbe and Kromkamp 2012 to give irradiance-saturated ETR_{PSII} ($ETR_{PSIImax}$), ETR_{PSII} efficiency alpha (α, i.e. the intial slope of the

FLC/PI-curve) and saturation irradiance E_k, using the FRRF R script (K Soetaert et al. 2014). All measurements were corrected for blank fluorescence of filtered f/2 medium by Whatman GF/F filters.

$$ETR_{PSII} = \left[ETR_{PSIIs} \times \left(1 - e^{\left(\frac{-\alpha E_{PAR}}{ETR_{PSIIs}}\right)}\right) \times e^{\left(\frac{-\beta E_{PAR}}{ETR_{PSIIs}}\right)}\right] / E_{PAR}. \quad \text{– eq (10)}$$

$$ETR_{PSIImax} = ETR_{PSIIs} \times \left(\frac{\alpha}{\alpha+\beta}\right) \times \left(\frac{\beta}{\alpha+\beta}\right)^{\frac{\beta}{\alpha}}. \quad \text{– eq (11)}$$

where Eopt is the optimum light point where photosynthesis reaches maximum; ETR_{PSIIs} is the scaling factor defined as the potential maximum ETR_{PSII}; the inhibition factor β is the slope of FLC where PSII start to decrease (Ralph and Gademann, 2005).

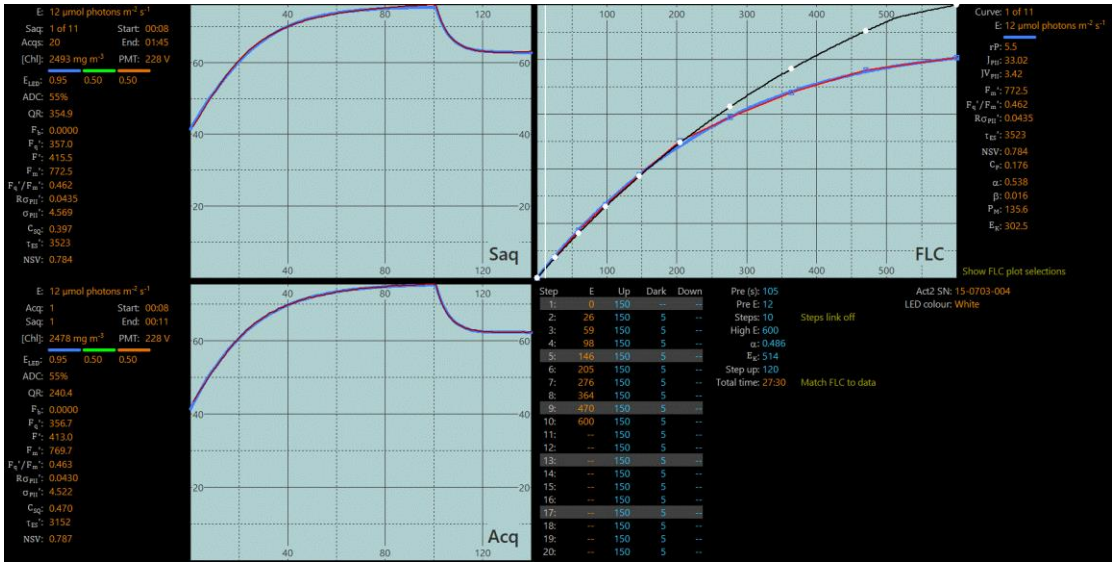

Figure 2 Example of a FLC file

For experiment 2, FLCs with inhibitors dithiothreitol (DTT) and propyl gallate (PGal) were performed. DTT is an inhibitor of violaxanthin de-epoxidase enzyme (VDE), and its effect on NPQ was investigated by treating the 15 min pre-dark-adapted sample with 1mM DTT for 10 min before the start of FLC (García-Mendoza & Colombo-Pallotta 2007). PGal is an alternative oxidase inhibitor, through which we can test whether electrons are used to reduce oxygen by PTOX or PTOX-like oxidase. Similar to the DTT treatment, a 3 ml 15 min pre-dark-adapted sample was treated with 2 mM PGal for 10 min before collecting fluorescence signal (Mackey et al. 2008). As Pgal was dissolved in ethanol, we tested the effect of ethanol through FLCs treated with the same volume ethanol (0.790 kg/l). In the meantime, FLCs treated without additions were run as controls. A control experiment in which only the same amount of ethanol was used turned out to have no effect on the results (Figure 3).

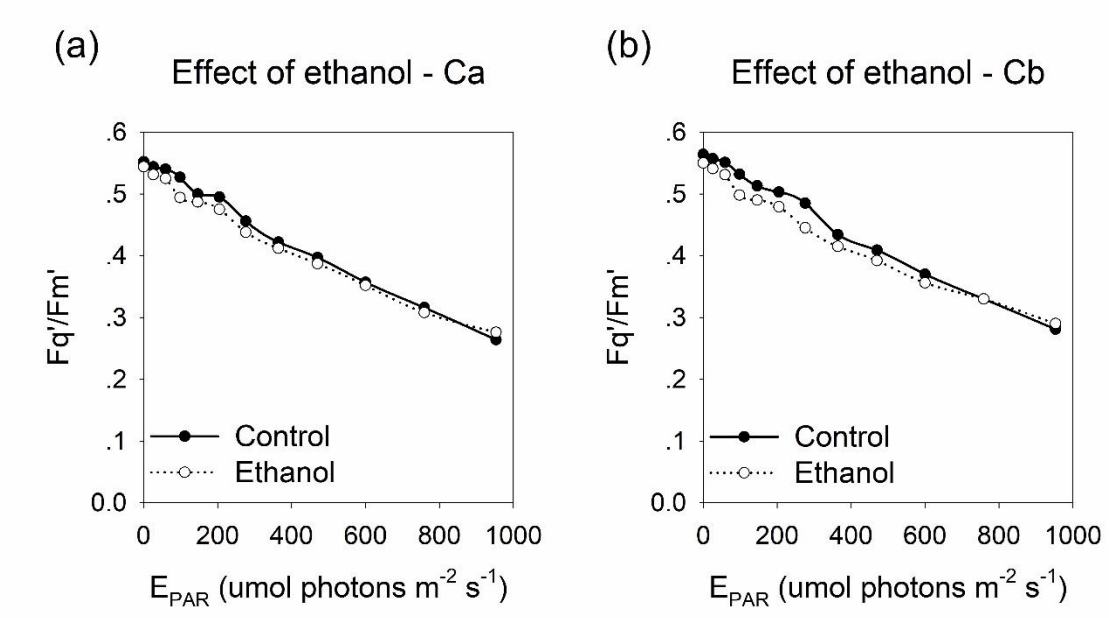

Figure 3 Fq'/F_m' in FLCs using samples treated with 50 µl ethanol (0.790 kg/l) (dotted line with white circle) and control samples treated with nothing (solid line with black circle) for Ca (a) and Cb (b).

Table 4 Protocol of incubations with ^{13}C-DIC and ^{15}N-NH_4 for the second experiment. P2 was conducted every other day, while P1 was conducted in one day during the first P replete period (day 4) and one day during the P-limited period (day 18).

	Incubation sequence	Volume	Start time	Duration	Replicate	Measurements
P1	1	20 ml	09:30	2h	Ca	FLCs, $PO^{13}C$/$PO^{15}N$, $DI^{13}C$
	2	20 ml	11:30	2h	Ca	FLCs, $PO^{13}C$/$PO^{15}N$, $DI^{13}C$
	3	20 ml	13:30	2h	Ca	FLCs, $PO^{13}C$/$PO^{15}N$, $DI^{13}C$
	4	20 ml	15:30	2h	Ca	FLCs, $PO^{13}C$/$PO^{15}N$, $DI^{13}C$
P2	1	20 ml	09:30	24h	Ca and Cb	NanoSIMS (only Ca), $PO^{13}C$/$PO^{15}N$, $DI^{13}C$
	2	20 ml	09:30	7h	Ca and Cb	NanoSIMS (only Ca), $PO^{13}C$/$PO^{15}N$,

						$DI^{13}C$
	3	20 ml	09:30	2h	Ca and Cb	$PO^{13}C/PO^{15}N$, $DI^{13}C$

2.3 [RCII] measurements

[RCII] was measured through an oxygen flash yield system as described by Myers and Graham (1971), Dubinsky and Falkowsky (1986) and Kromkamp and Limbeek (1993). 30 ml cell suspensions were concentrated by gentle centrifugation and re-suspension after removal of 25 ml supernatant liquid before the measurements were started. This was necessary in order to ensure sufficient biomass in order to be able to make detectable oxygen evolution. The oxygen concentration was measured by a Clarke-type electrode housed within an Hansatech Oxygraph sample chamber (DW1/AD), calibrated against 0% and 100% oxygen concentrations. A ST saturation flash system (Act 2 accessory) equipped with white LED's was positioned around the chamber and controlled by the corresponding Act2Run software. The oxygen evolution rate of the concentrated sample was recorded for 4 min in dark and then another three 4 min under ST saturating flashes (22932 µmol photons m^{-2} s^{-1}; 0.24 ms duration) of three different frequencies: 55.6, 41.7 and 31.3 s^{-1}. Mean O_2 flash yield was obtained through linear regression of O_2 evolution rates against flash frequencies (see example Figure 4). [RCII] was calculated as mean O_2 flash yield times 4 because 4 mol RCII are required for 1 mol of O_2 generated. [RCII] was then normalized to *Chla* concentration to give the number of PSII (n_{PSII}, mol RCII (mol *Chla*)$^{-1}$). The photosynthetic unit (PSU) size (Emerson and Arnold number) was calculated as *Chla* concentration normalized to the O_2 flash yield (mol *Chla* (mol O_2)$^{-1}$). The *Chla* concentration here was multiplied by a concentration factor calculated from cell concentration results.

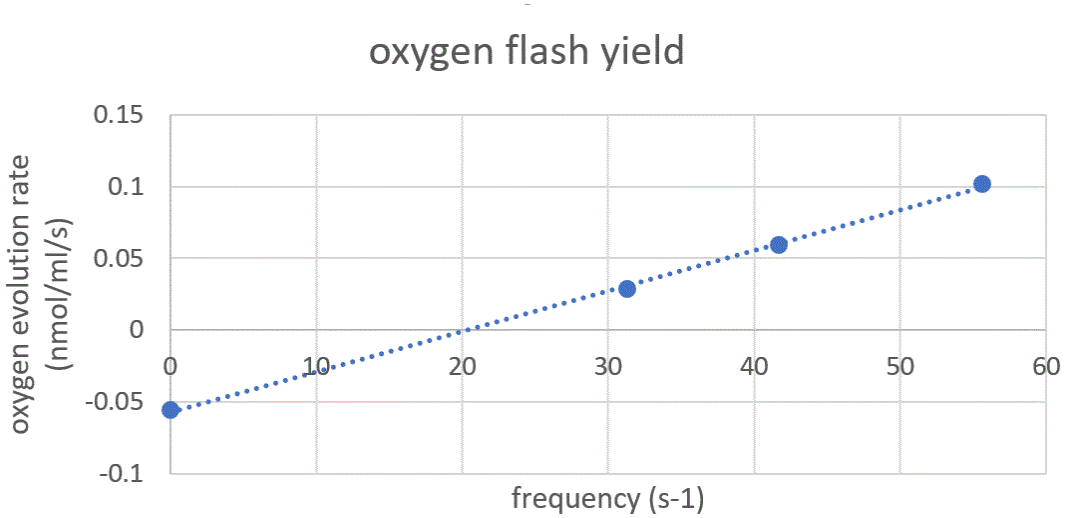

Figure 4 Example of O_2 flash yield derivation. The points are the oxygen evolution rate in dark and under three different frequency flashes (55.6, 41.7 and 31.3 s^{-1}). The dotted line is the trend line of those four points, and its slope is the O_2 flash yield.

2.4 $^{14}CO_2$ fixation rates

We used the ^{14}C technique (Steeman Nielsen, 1952) to measure the PP of the cells by adding 50 µl 0.925 MBq/ml $NaH^{14}CO3$ to a 2 ml sample in a 20 ml glass scintillation vial. Ten vials were exposed to a light gradient from 0 to 800 µmol photons m^{-2} s^{-1}, and incubated for 30 min. After that, 100 µl 37% HCl was added to stop the ^{14}C-fixation and to remove the remaining inorganic $^{14}CO_2$. After one night, 18 ml Insta-gel plus from Perkin-Elmer counting liquid was added, and the radioactivity of the sample was measured by a liquid scintillation counter (Perkin Elmer Tri-Carb 2910TR). PP was calculated using the formula in Nielsen & Bresta, 1984, and the ^{14}C fixation in the dark was subtracted from the results. These PP data were then fitted by P&G model (eq. 9, 10; but replace "ETR_{PSII}" with "P_{14C}") to give irradiance-saturated P_{14C} (P_{14Cmax}), P_{14C} efficiency α and saturation irradiance E_k.

2.5 Pigments, optical absorption cross section and PSII absorption ratio

For *Chla* measurement, a 5 ml sample was centrifuged at 2500 rpm for 10 min in 15 ml Falcon tubes, then 4.5 ml supernatant liquid was removed, and 4.5 ml acetone (99.8% purity) was added. The centrifuge tubes were wrapped with aluminum foil and kept overnight in 4°C fridge. The same sample was centrifuged again at 2500 rpm for 10 min in the next morning, and the green supernatant liquid was scanned in Cary BIO-100 UV-VIS dual-beam spectrophotometer (Varian, Palo Alto), equipped with a LabSphere integrating sphere (DRA-CA-3300). *Chla* concentration [*Chla*] was calculated from the absorbance results based on the equation in Ritchie (2006). And the optical absorption cross section, a*, was calculated as below (eq. 12):

$$a^* = \frac{(average\ absorption\ between\ 400nm-700nm)\times 100\times 2.303}{[Chla]} \quad \text{-- (12)}$$

where 100 is to transfer "cm" to "m"; 2.303 is the transfer factor from "ln" to "log".

The ratio of PSII absorption to total absorption, F_{II}, is then calculated as below (eq. 13, derived from eq. 8 and eq. 12) (Oxborough et al 2012; Silsbe et al 2015):

$$F_{II} = \frac{a_{PSII}}{a^*} = \frac{\frac{Fm\times Fo}{Fm-Fo}\times\frac{K_R}{1\times 10^6}}{(average\ absorption\ between\ 400nm-700nm)\times 100\times 2.303} \quad \text{-- (13)}$$

where a_{PSII} (m^2/mg Chla) is the optical absorption cross section of PSII normalized with [Chla]. Theoretically, we should use calculated K_R values from measured [RCII] data, but the F_{II} we got from that were much higher than 1, which is not possible, because the K_R values calculated from measured [RCII] data were about 10 times higher than 11800 m^{-1}. For the details, please see Section 3.2.3.

For a complete pigment profile, a 5 ml sample was filtered through a 25 mm Whatman GF/F filter. The filter was then folded in half , packed with aluminum foil, and stored in -80°C freezer until analyzed after extraction with 95% aceton. The aceton extracts were centrifuged and the supernatants were analyzed using a high-performance liquid chromatography (HPLC) equipment

with both diode array absorption and a fluorescence detector (nexera X2, Shimadzu, Japan).

2.6 NanoSIMS measurements

Before the experiment, in order to determine the right volume to filter, we did a number of tests and the filters were checked by epifluorescence microscopy to ensure that cells didn't fall on each other, and that the distance between them was < ~ 10 µm. During the experiment, a 1 ml sample was diluted 5 times with fresh f/2 medium (normal P concentration), and then treated with 0.5% formaldehyde for 1 h at room temperature. 1 h later, 200 µl was filtered through 3 µm polycarbonate filter. Three times washes by demineralized water were applied during the filtering. A mask on the filter limited the filtration area to 5mm in diameter. After the filters were dried in the air, they were collected in petri dishes and kept under dark at room temperature until analyzed with Nanometer-scale Secondary Ion Mass Spectrometry (NanoSIMS) (Cameca, Paris, France). Obtained data was processed using the Look@Nanosims (LANS) software.

2.7 POC, PON, DIC, DIP

10 ml sample was filtered through pre-combusted (450°C for 4 h) 25 mm Whatman GF/F filter. The filters were folded in half, packed with aluminum foil, and stored in -80°C freezer until analyzed for particulate organic carbon (POC) and particulate organic nitrogen (PON), while the filtrate was collected with plastic bottles and stored in -18°C freezer for later analysis for dissolved inorganic phosphorus (DIP). POC/PON was measured as described in Nieuwenhuize et al. 1994. DIP (here phosphate) was measured by QuAAtro continuous flow analyzer (Seal, UK) according to the manufacturers instruction. DIC samples were collected into 10 ml borosilicate vessels, poisoned with $HgCl_2$ to stop biological activity, sealed and stored in dark at room temperature until analyzed. They were analyzed later with DIC analyzer (AS-C3, Apollo, USA) by adding acid to the sample and measure the formed CO_2 through a no-dispersive infrared CO2 analyzer.

For isotope enrichment incubation samples, 5 ml samples were used for $PO^{13}C/PO^{15}N$ measurements, and 10 ml samples were used for $DI^{13}C$ measurements. The isotope components were quantified by IRMS (Flash1112-DeltaV, Thermo, Germany).

The carbon fixation rate was calculated from $PO^{13}C$ results (eq. 14-17), and the nitrogen incorporation rate was calculated in the same way from the $PO^{15}N$ results:

$$\delta 13C\ (‰) = (\frac{R_{sample}}{R_{standard}} - 1) \times 1000 \quad \text{-- (14)}$$

$$R_{sample} = \left(\frac{\delta 13C}{1000} + 1\right) \times R_{standard} \quad \text{-- (15)}$$

$$F^{13} = \frac{13C}{13C+12C} = \frac{R}{R+1} \quad \text{-- (16)}$$

$$P_{13C} = \frac{\mathrm{F}^{13}_{POC} - \mathrm{F}^{13}_{POC.backgrand}}{\mathrm{F}^{13}_{DIC} - \mathrm{F}^{13}_{DIC.backgrand}} \times \frac{[\mathrm{POC}]}{incubation\ time} \quad \text{-- (17)}$$

Where the $\delta^{13}C$ is the result measured with IRMS; R is the isotope ratio ($^{13}C/^{12}C$-ratio); F^{13}_{POC} and

$F^{13}_{POC.backgrand}$ are the fraction of ^{13}C in POC samples with and without isotope enrichment, respectively; F^{13}_{DIC} and $F^{13}_{DIC.backgrand}$ are the fraction of ^{13}C in DIC samples with and without isotope enrichment, respectively; [POC] is the concentration of POC in mg C L^{-1}; the unit of incubation time is h; P_{13C} is the C-fixation rate in mg C L^{-1} h^{-1}. For carbon, the international standard is Vienna PeeDeeBelemnite ($\delta^{13}C$ = 0 ‰, $R_{standard}$ = $^{13}C/^{12}C$-ratio = 0.0111802). For nitrogen, the international standard is atmospheric N_2 ($\delta^{15}N$ = 0 ‰, $R_{standard}$ = $^{15}N/^{14}N$-ratio = 0.0036782). As we didn't measure dissolved inorganic nitrogen (DIN) in this study, F^{13}_{DIC} - $F^{13}_{DIC.backgrand}$ from DIC data instead of F^{13}_{DIN} - $F^{13}_{DIN.backgrand}$ from DIN data were used in P_{15N} calculation.

2.8 Data processing

All data were calculated in Excel. The calculations of error of calculated parameters were based on the "Law of propagation of error": if we have Z= *f* (x1, x2, …, xn), then the error of Z (ΔZ) is calculated as:

$$\Delta Z = \left|\frac{\partial f}{\partial x1}\right| \times \Delta x1 + \left|\frac{\partial f}{\partial x2}\right| \times \Delta x2 + \cdots + \left|\frac{\partial f}{\partial xn}\right| \times \Delta xn \quad \text{-- (18)}$$

Where $\frac{\partial f}{\partial xn}$ (n = 1, 2, 3, …, n) is the partial derivative of the fuction *f* to each variable xn; Δxn is the error of each variable xn.

All photosynthetic production data were fitted by Platt & Gallegos (1980) model normalized to the irradiance as suggested by Silsbe and Kromkamp 2012 to give $ETR_{PSIImax}$ or P_{14Cmax}, α (i.e. the intial slope of the FLC/PI-curve) and saturation irradiance E_k, using the FRRF R script (K Soetaert et al. 2014).

Graphes in this report were generated from Excel, Sigmaplot, or R script.

3 Results

3.1 Experiment 1

Since there were more than one variable factors in the first experiment, making it difficult to relate the observed effects to the treatment intended, I will briefly display some basic part of the results here, and mainly focus on the second experiment. As mentioned above, the main milestones of this experiment are shown in Table 5.

Table 5 Main milestones of the first experiment.

Date number	Description
1-5	P-replete phase-I
5 (after sampling)	Transfer cells into P-limited medium.
7 (after sampling)	Addition to medium and cultures with DIC, Br, B and Sr supplementary*
6-20	P-limited phase-I
20 (after sampling)	Addition of 10% P to the medium and cultures.
21-26	P-limited phase- II
26 (after sampling)	Added 80% P into the culture
27-37	P-replete phase- II

*According to the recipe in Appendix I

Table 6 Actual P concentration of the medium used in this study.

	DIP (μmol/l)	Percentage of DIP
Normal medium	20.50	100.0%
P-limited medium of experiment 1	0.61	3.0%
P-limited medium of experiment 2	4.20	20.5%

The percentage of DIP we planned was 10% of normal level, but because of an operational error, the actual concentration was 0.61 μmol/l (3.0%) in the first experiment (Table 6), resulting instarvation and not a P-limitation during the low P-phase of the experiment. The DIP concentration of the culture at the first stage (P-replete phase) was 3.11 μmol/l (Figure 5 (a)). After transfer to P-limited medium, it showed a downtrend until the addition of another 10% P on day 20. After the supplementary of 80% P into the culture on day 26, DIP concentration of Cb kept stable at a level similar with that in the beginning, while that of Ca fluctuated a lot. Basically, its trend is in accordance to expectation that it would decrease when goes into P-limitation and then goes up with supplementary of P. But the magnitude of variation is much smaller than what we expected. We didn't measure DIN concentration in this study. If we assume that the DIN concentration was the

same with that in the recipe, that is 882 µmol/l, then the N/P ratio at the first stage was 43.0:1, which is about 2.7 times higher than the Redfield ratio (C:N:P=106:16:1) (Redfield 1958), indicating that the cells have already been potentially P limited from the beginning. However, DIP concentrations at the begaining of the experiment are higher than 2 µmol, which is way above the 0.1-0.2 µmol/L which is usually used as a P-limited threshold (Ly et al, 2014, Peeters et al, 1991). For some reasons the P-concentrations during the P-limited phase were quite variable and high. Normally, phosphate concentrations are hard to measure during P-starvation/limitation, so we think this has been due to the fact that we did not use acid washed glassware. Despite the high fluctuation of DIP, the cell number, Chla concentration and F_v/F_m (Figure 5 (b), (c), (d)) showed more obvious trend with DIP manipulation. After transferred to low DIP medium, the cell concentrations started to decrease, but recoverd afer addition of DIC and micronutrients on day 7. Cell number kept stable until day 13 when it started to decline, indicating that after the transfer to low-P medium the cells continued to growh for a few days using internally stored phosphate. Despite the fact that cell concentration remained more or less constant during the first 10 days, the chla concentrations showed a slight upward trend, indicating a rise in the *Chla*/POC content of the cells. And that is confirmed in Figure 5 (e). The increase in the *Chla* concentration was mirrored by an increase in F_v/F_m, again suggesting that the physiology (but not the cell concentrations) reacted favourably to the addition of DIC/micronutrients. During the P-limited phase, cell concentration, *Chla* concentration, Fv/Fm and *Chla*/POC content continued to decrease, although addition of an extra 10% DIP slowed down (*Chla*, cell concentration) or stopped (F_v/F_m, *Chla*/POC) the decrease. Then the cells reacted immediately on the larger addition of DIP to P-replete conditions: cell concentration rose quickly, as did the *Chla* concentration. F_v/F_m and *Chla*/POC reached maximal values in 5 days and then became constant. It seems that there still existed transient phases, thus the P-limited condition from the very begaining problem seems didn't cause serious undesirable effect on our experiment. So, we still use "P-replete phase" and "P-limited phase" to describe the first and second stages below. The third stage is thus the second "P-replete phase" after addition of extra P.

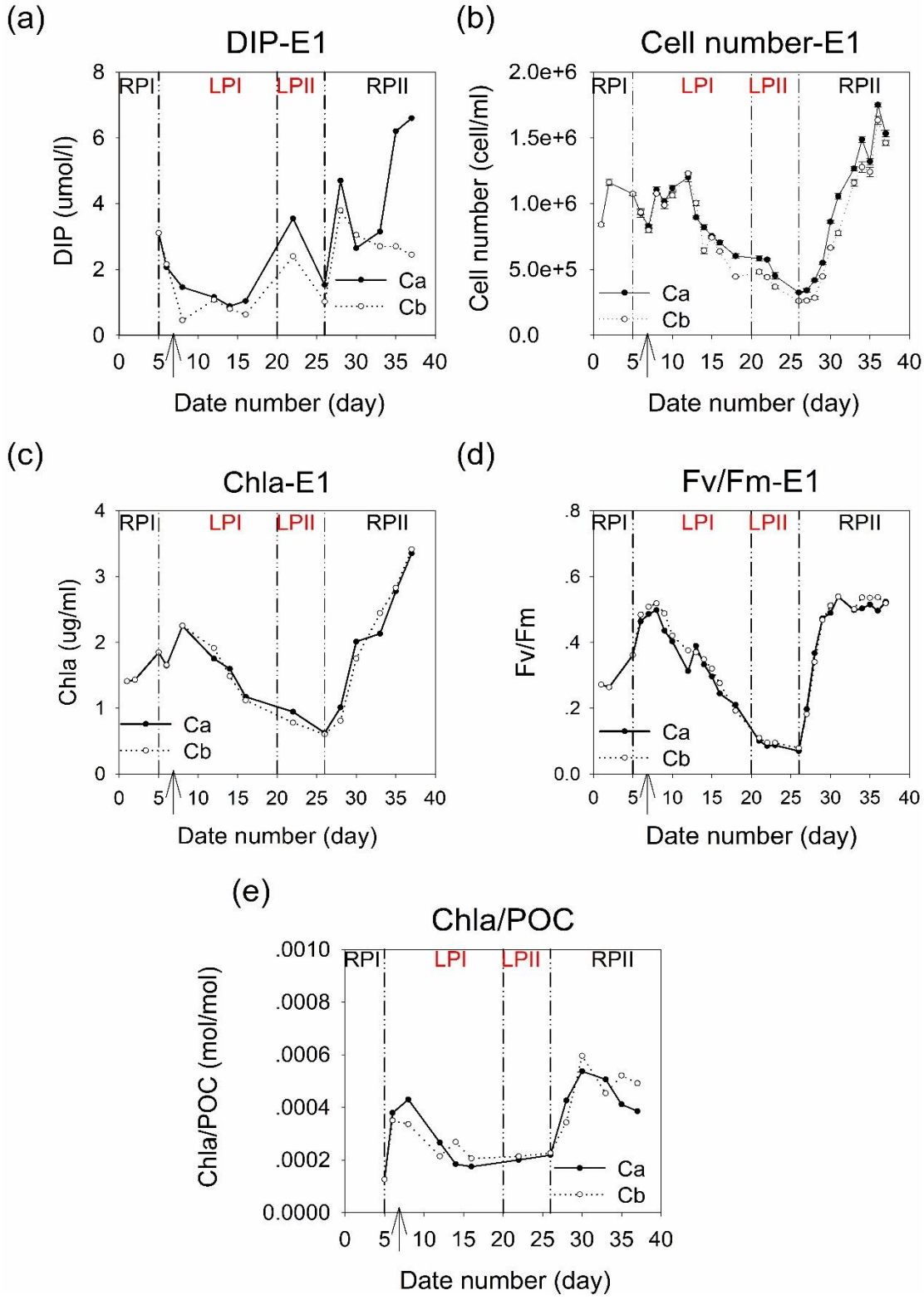

Figure 5 The DIP ((a)), cell concentration ((b)), *Chla* concentration ((c)), F_v/F_m ((d)) and *Chla*/POC ((e)) of cultures Ca (solid line with black circle) and Cb (dotted line with white circle) change with date in Experiment 1. At day 7 DIC and several micronutrients were added (black upward arrow). Day 1-5 is the P-replete phase-I (RPI), day 6-20 is the P-limited phase-I (LPI), day 21-26 is the P-limited phase-II (LPII), and day 27-37 is the P-replete phase-II (RPII) (see Table 5).

3.2 Experiment 2

3.2.1 Transfer effect

According to the results from experiment 1, cells did showed obvious changes after transferred to P-limited medium. Nevertheless, as we applied centrifugation and resuspension during the transfer process, it is necessary to know whether those processes caused any influence on the cells. So we measured the cell number, mean cell diameter, average absorption from 400 nm to 700 nm, and F_v/F_m before and just after the transfer from P-replete stage to P-limited stage in order to find the transfer effect (Figure 6). Table XX is the main milestones of the second experiment. The variations of mean cell diameter and F_v/F_m were around 1%, while those of cell number and average absorption were around 10% (Table 7), indicating loss of 10% of the biomass during the centrifugation/resuspension procedure. So we can conclude that the influence of transfer operation on the physiology of the cells was negligible.

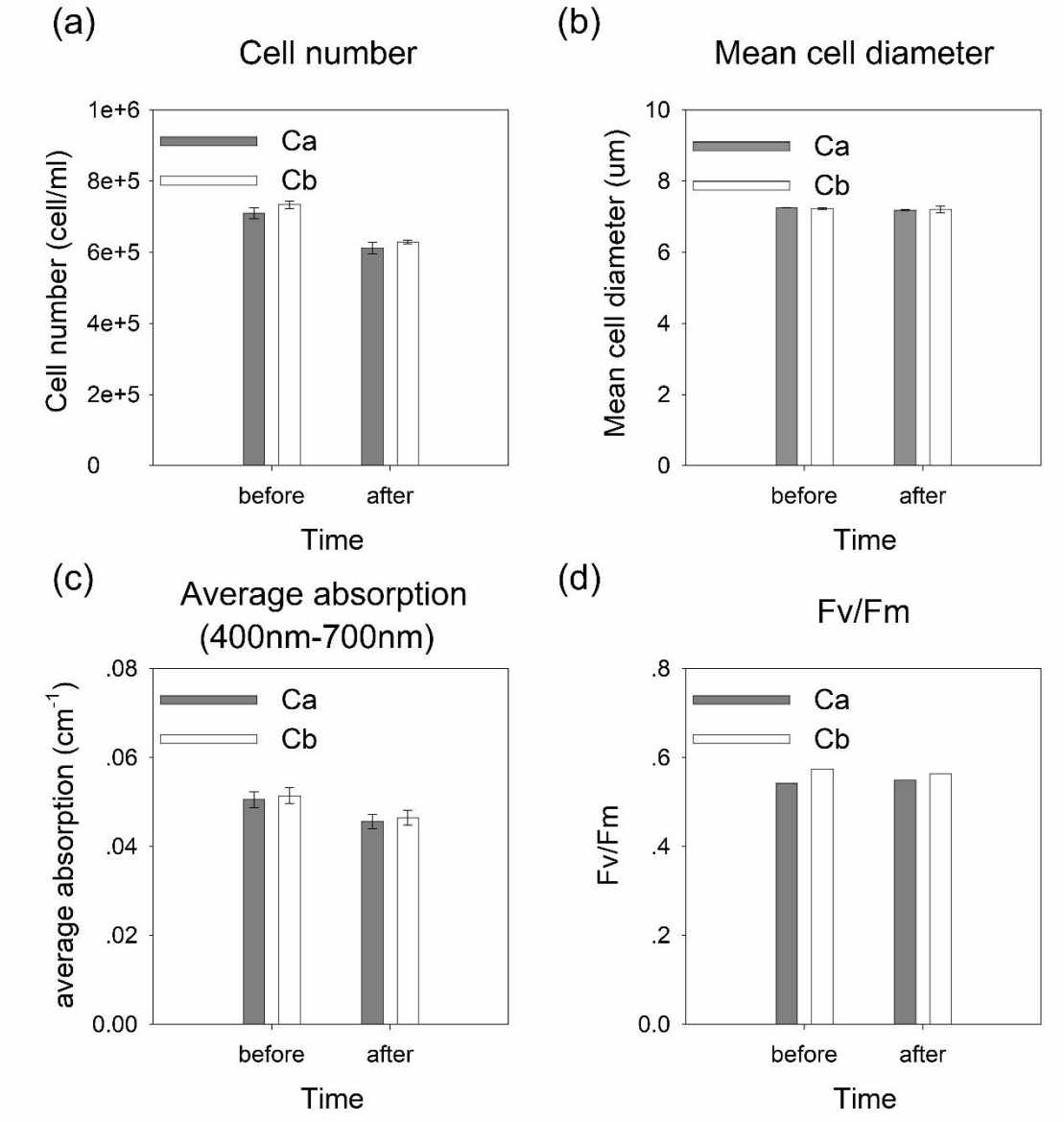

Figure 6 The cell number ((a)), mean cell diameter ((b)), average absorption between 400nm and 700nm ((c)) and F_v/F_m ((d)) of cultures Ca (grey bar) and Cb (white bar) before and after transfer from P-replete to P-limited medium in Experiment 2.

Table 7 Transfer effect on the cell number, mean cell diameter, average absorption from 400 nm to 700 nm, and F_v/F_m of the two cultures before and after the transfer from P-replete stage to P-limited stage. Variation equals: (before-after)/before×100%.

Culture		Cell number (cell/ml)	mean cell diameter (μm)	Absorption (cm^{-1})	F_v/F_m
Ca	Before	$7.097\times10^5 \pm 1.466\times10^4$	7.256 ± 0.005239	$5.051\times10^{-2} \pm 1.792\times10^{-3}$	0.543
	After	$6.113\times10^5 \pm 1.690\times10^4$	7.187 ± 0.02034	$4.561\times10^{-2} \pm 1.611\times10^{-3}$	0.549
	Variation	13.9% ± 4.7%	1.0% ± 0.4%	9.7% ± 7.1%	-1.1%
Cb	Before	$7.343\times10^5 \pm 1.048\times10^4$	7.228 ± 0.02034	$5.141\times10^{-2} \pm 1.765\times10^{-3}$	0.574
	After	$6.293\times10^5 \pm 4.910\times10^3$	7.199 ± 0.09166	$4.645\times10^{-2} \pm 1.617\times10^{-3}$	0.563
	Variation	14.3% ± 2.3%	0.4% ± 1.6%	9.6% ± 6.9%	1.9%

Table 8 Main milestones of the second experiment.

Date number	Description
1-7	P-replete phase-I
7 (after sampling)	Transfer cells into P-limited medium
8-20	P-limited phase
20 (after sampling)	Added 80% P into the culture
21-26	P-replete phase- II

3.2.2 Growth monitoring

3.2.2.1 DIP

The main milestones of the second experiment were summarized in Table 8. DIP concentration of Ca was highly variable and from 0.26 to 22.5 μmol/l; whereas that of Cb was smoother, from 0.14 to 1.38 μmol/l (Figure 7). Their change throughout the whole experiment 2 has no specific pattern. We expected DIP in the first and third period to be higher than the second period. As during P-limited growth the DIP concentrations should be very low, it is reasonable to assume that the variation is caused by contamination of the glassware, which was not acid washed. Assuming a mean C:*Chla* ratio in cells is 50 (Quere, C. L.,2005; Strickland, 1960), as the start *Chla* concentration of the culture was about 3 μg/ml (Figure 9(b)), then the C in algae was about 150 mgC/L, that is 12.5 mmol/l. According to the Redfield Ratio (C:N:P = 106:16:1), the P in algae should then be about 0.118 mmol/l, that is 118 μmol/l. But DIP concentration of the normal medium we used in this experiment is only 20.5 μmol/l (Table 6), which means that the cells' need for P is

much higher than the P concentration in our medium. That is to say, the culture is already in P-limited state at the start of this experiment.

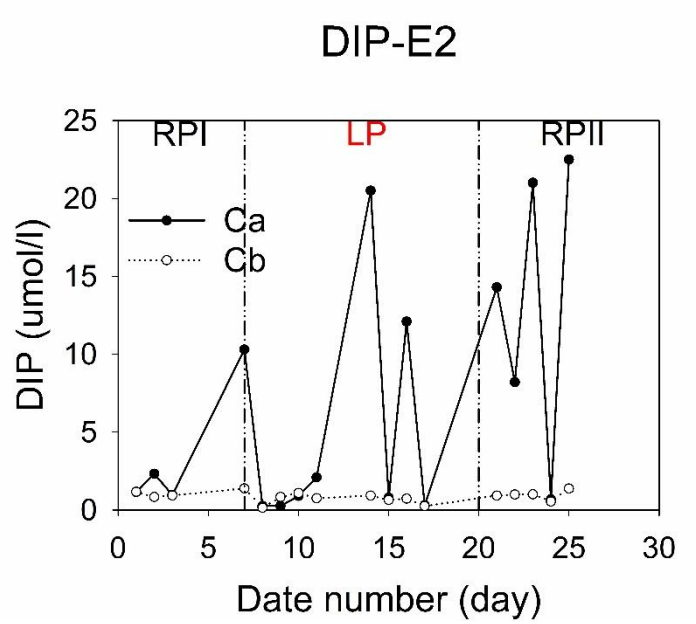

Figure 7 The DIP concentration of culture a (Ca, solid line with black circle) and culture b (Cb, dotted line with white circle) during the experiment 2. Day 1-7 is the P-replete phase-I (RPI), day 8-20 is the P-limited phase (LP), and day 21-26 is the P-replete phase-II (RPII) (see Table 8).

3.2.2.2 Cell number and pH

The cell number of both Ca and Cb at the start of the experiment were about 1.3×10^6 cells/ml and they kept relatively stable before we transferred the cells into P-limited medium on day 7 (Figure 8 (a)). During the first week after transfer, cell density of both cultures decreased slightly, and a divergence appeared between them. After one week, that descent speed became larger until the adding of extra P into cultures on day 20. At the end of P-limited stage, cell density of Ca dropped to 7.9×10^5 cell/ml and that of Cb declined to 8.5×10^5 cell/ml. The reduction magnitude was about 40%. The cell density started to increase rapidly after the addition of P but the growth rate showed a declining trend with time because of the enhanced competition for living resources like nutrients or light. The mean diameter of cells kept at around 6.9 μm at the beginning (Figure 8 (b)). After transfer to low P condition on day 7, it rapidly dropped by about 2.0 μm and then recovered to 6.9 μm in four days. From then on, a small decrease in cell size was observed till it reached a diameter of 6.4 μm at day 21. The addition of P caused a rapid rise, but after two days the cell diameter started to decrease again. Growth rate of cells fluctuated a lot throughout the whole experiment (Figure 8 (d)). But basically, there is no obvious change pattern except that it dropped a lot just after transferring cells to the P-limited medium and increased dramatically just after the addition of extra P on day 20. In both cases, it recovered in one or two days. It is noticeable that, during the P-limited stage, growth rate of both cultures seems showed a decrease trend from about 0.6 day^{-1} at the initial stage to around 0.4 day^{-1} at the end stage, which might caused by the limitation of P.

The pH of normal medium was 7.59 (pH for 20%P medium was 7.79) and that of both cultures were

around 9 during the initial steady state (Figure 8 (c)). After transfer, the pH value gradually decreased to about 8 until the addition of extra P. This is because there was less O_2 evolved (i.e. less CO_2/HCO^{3-} taken up) in the P-limited condition due to the drop of cell number as well as the photosynthetic ability (Figure 15). After the addition of P at day 20, it climbed back to its starting level in three days and then remained stable.

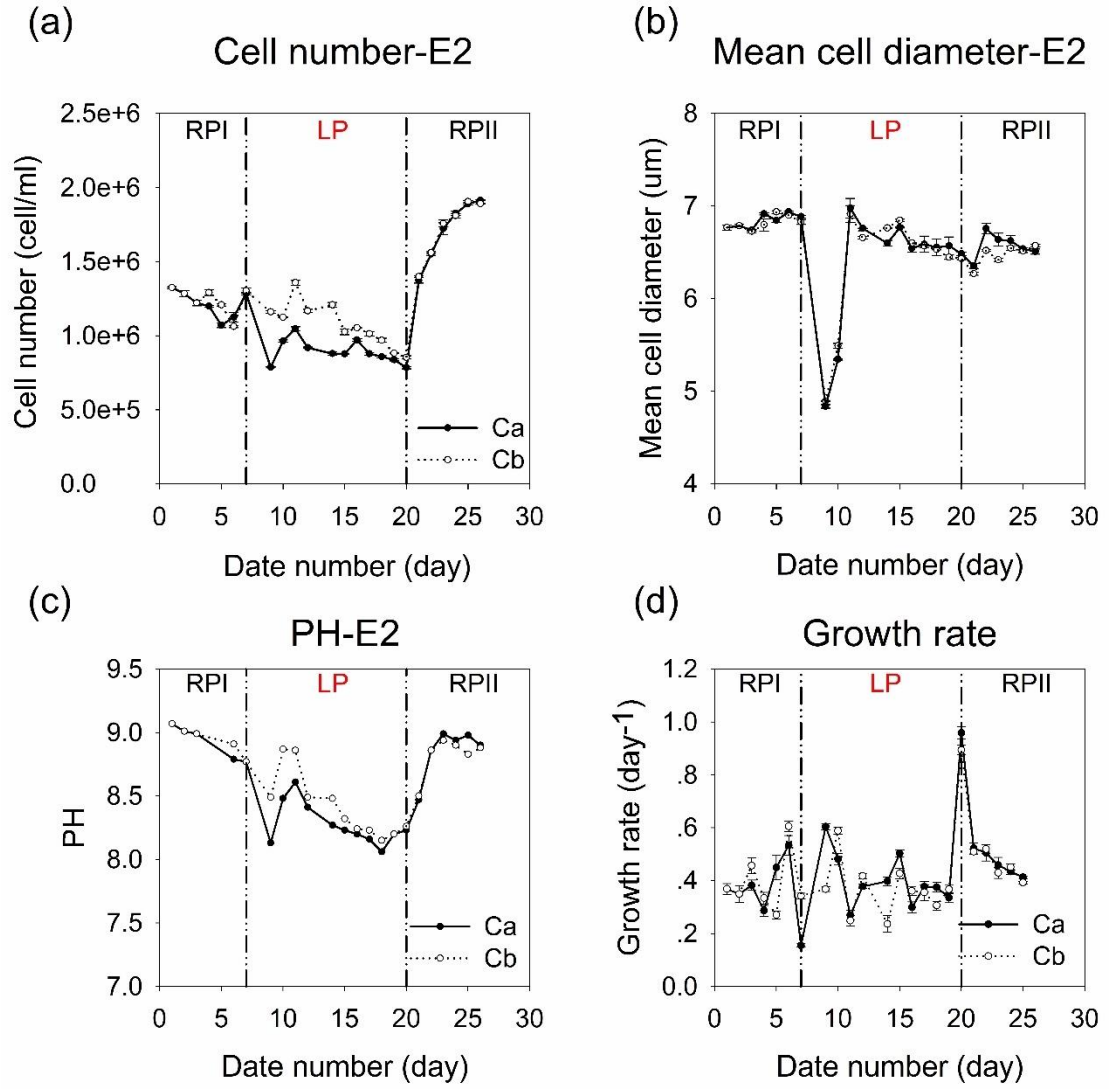

Figure 8 The cell concentration ((a)), mean cell diameter ((b)), pH value ((c)) and growth rate ((d)) of Ca (solid line with black circle) and Cb (dotted line with white circle) change with date in Experiment 2. Day 1-7 is the P-replete phase-I (RPI), day 8-20 is the P-limited phase (LP), and day 21-26 is the P-replete phase-II (RPII) (see Table 8).

3.2.2.3 Absorption, *Chla*, F_{II}

As might be expected, the cell density, the average absorption between 400 nm ~ 700 nm and the *Chla* concentration of the cultures were positively related and showed similar change pattern as the cell number (Figure 9 (a), (b)). The *Chla* concentration of cultures decreased by about 55% when

the cells were transferred from the first “P replete” to the P limited phase, whilethe change of the cell number is less (about 36%). This mismatch can be explained by a change in the *Chla* concentration per cell: it is clear that *Chla*/cell of both cultures decreased during the P-limited phase and increased again after the addition of DIP (Figure 9 (d)).

For the optical absorption cross section, a*, there was no visible trend, only some small fluctuation throughout the whole experiment 2 (Figure 9 (c)). That means the average absorption per *Chla* kept stable during such transient phases. Since the *Chla*/cell decreased when cells went into P-limited stage, the average absorption per cell also decreased consequently. The ratio of PSII absorption to total absorption, F_{II}, kept steady at around 0.4 before transfer (Figure 9 (e)). During the second period — P lacking stage, an apparent increase to about 0.8 was observed. Thus, the relative contribution of PSII absorption to total absorption increased. Following the adding of P on day 20, it fell back to its original level.

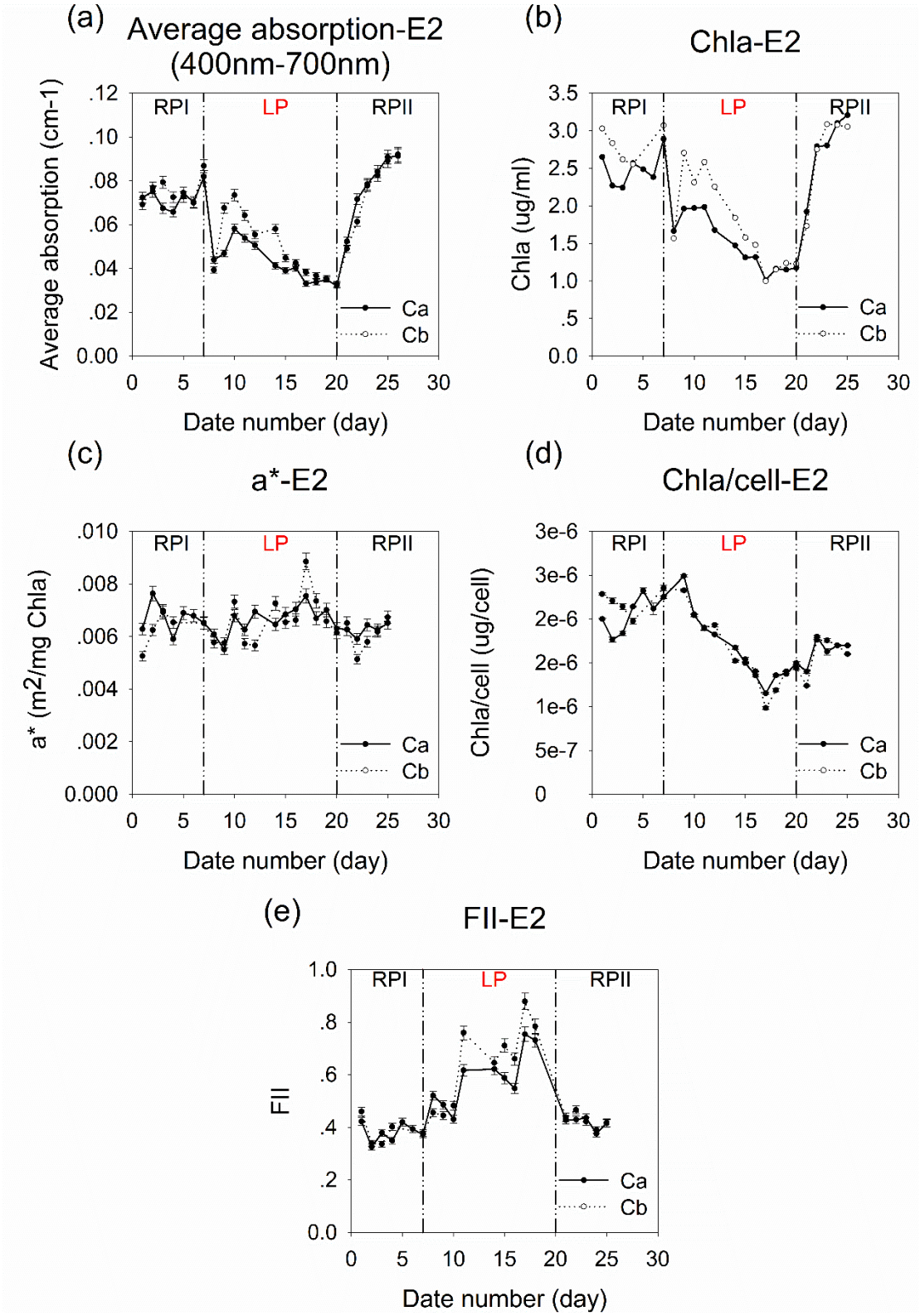

Figure 9 Changes in average absorption between 400nm and 700nm ((a)), *Chla* concentration ((b)), a* ((c)), *Chla* concentration per cell ((d)) and F_{II} factor ((e)) of cultures Ca (solid line) and Cb (dotted line) in Experiment 2. Day 1-7 is the P-replete phase-I (RPI), day 8-20 is the P-limited phase (LP), and day 21-26 is the P-replete phase-II (RPII) (see Table 8).

3.2.2.4 Carbon and nitrogen change

As we expected, the DIC concentration of cultures during the P-limited phase showed a climbing trend because of the decrease of both cell number and cell photosynthetic activity (Figure 10 (a)). The drop in *Chla*/cell weakened cells' photosynthetic capacity, so cells' ability to fix inorganic carbon decreased. Along with the decrease in cell number, cultures' need for carbon also dropped. Therefore, more DIC was left in the medium. Thepeak in DIC on day 8 is caused by the transfer to new fresh medium. After the transfer, almost all medium in the cultures was replaced by new medium with relatively higher DIC. The POC and PON concentration showed similar patterns: relatively lower values during P-limited phase and higher and relatively stable values at the beginning (Figure 10 (b), (c)). This change corresponds to our expectation and can be reflected from the decrease of cell number in P-limited stage (Figure 8 (a)). Nevertheless, the ratio of them -- POC/PON -- showed some expected fluctuation (Figure 10 (d)). It increased a little in the P-limited phase, which means that relatively more carbon than nitrogen was accumulated when the supply of P is insufficient. The interpretation could be: since the growth rate during the second period decreased, cells no longer need that much carbohydrates for growth, thus redundant C was stored as POC. That leads to the rise of POC/PON in the second period.

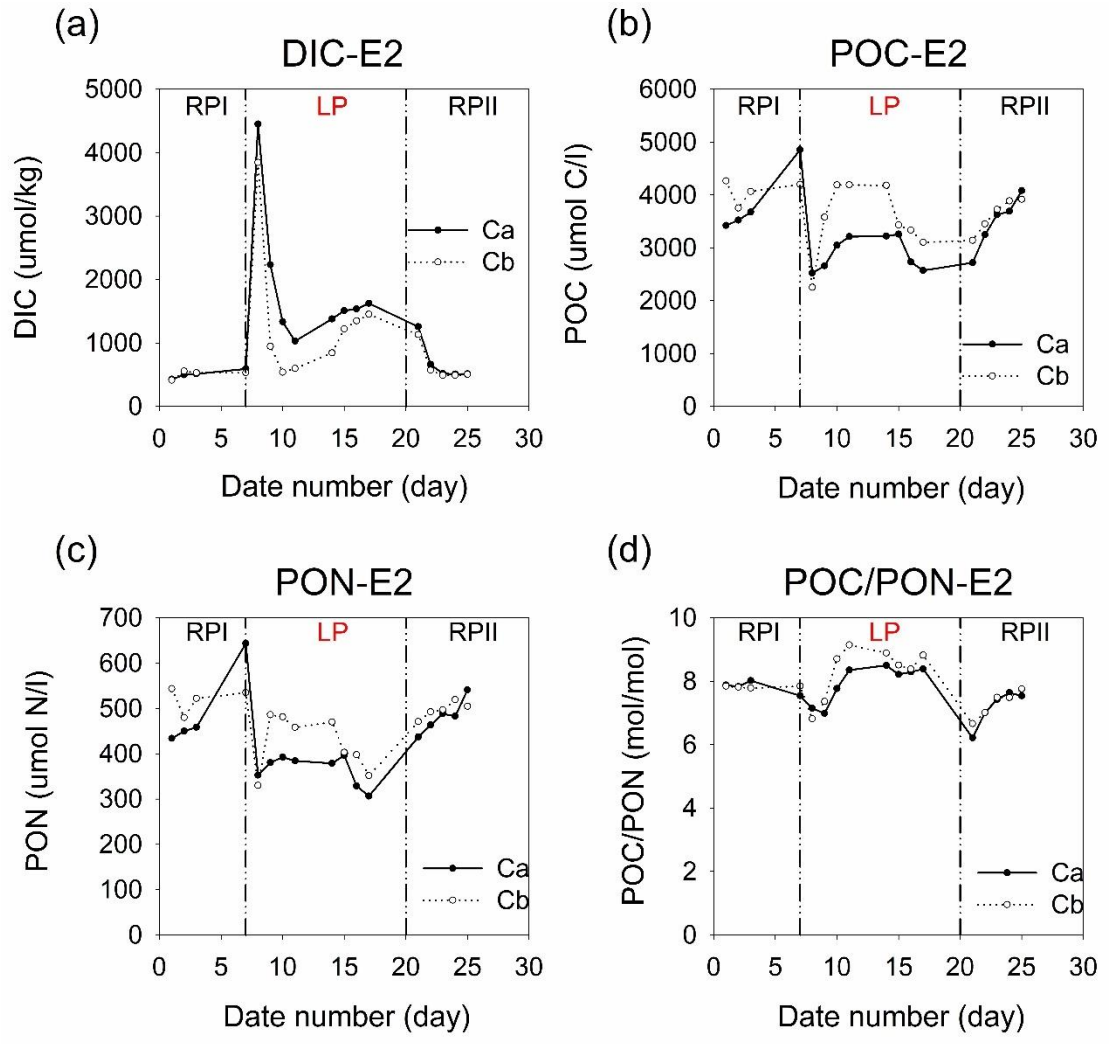

Figure 10 Changes in DIC ((a)), POC ((b)), PON ((c)) and POC/PON ratio ((d)) of Ca (solid line with black circle) and Cb (dotted line with white circle) with time in Experiment 2. Day 1-7 is the P-replete phase-I (RPI), day 8-20 is the P-limited phase (LP), and day 21-26 is the P-replete phase-II (RPII) (see Table 8).

3.2.2.5 PSU size and n_{PSII}

For both PSU size and n_{PSII}, there was some fluctuations throughout the whole experiment, but we cannot see any patent trend (Figure 11(a)(b)). That means both the amount of *Chla* molecules needed for per O_2 produced and the amount of RCII per *Chla* molecule didn't change much when the cells went into P lacking environment, indicating that the structure of the PSII unit hardly changed during the experiment. But the number of RCII per cell did change in that circumstance: it dropped to about half of its initial level from balanced growth to P-limited growth. After the addition of DIP at day 20, n_{RCII}/cell started to increase again, although the pattern was not so clear. If we kept monitoring it after day 25, it is foreseeable that it would rise to its original values (Figure 11(c)). Obviously, this variation is induced by the decline of *Chla*/cell in P-limited period (Figure 9(d)). So, we can say that the cells might reduced their intracellular RCII numbers through the reduction of *Chla* content in the cells to diminish their capability in absorbing light energy, for the sake of protecting themselves from photodamage.

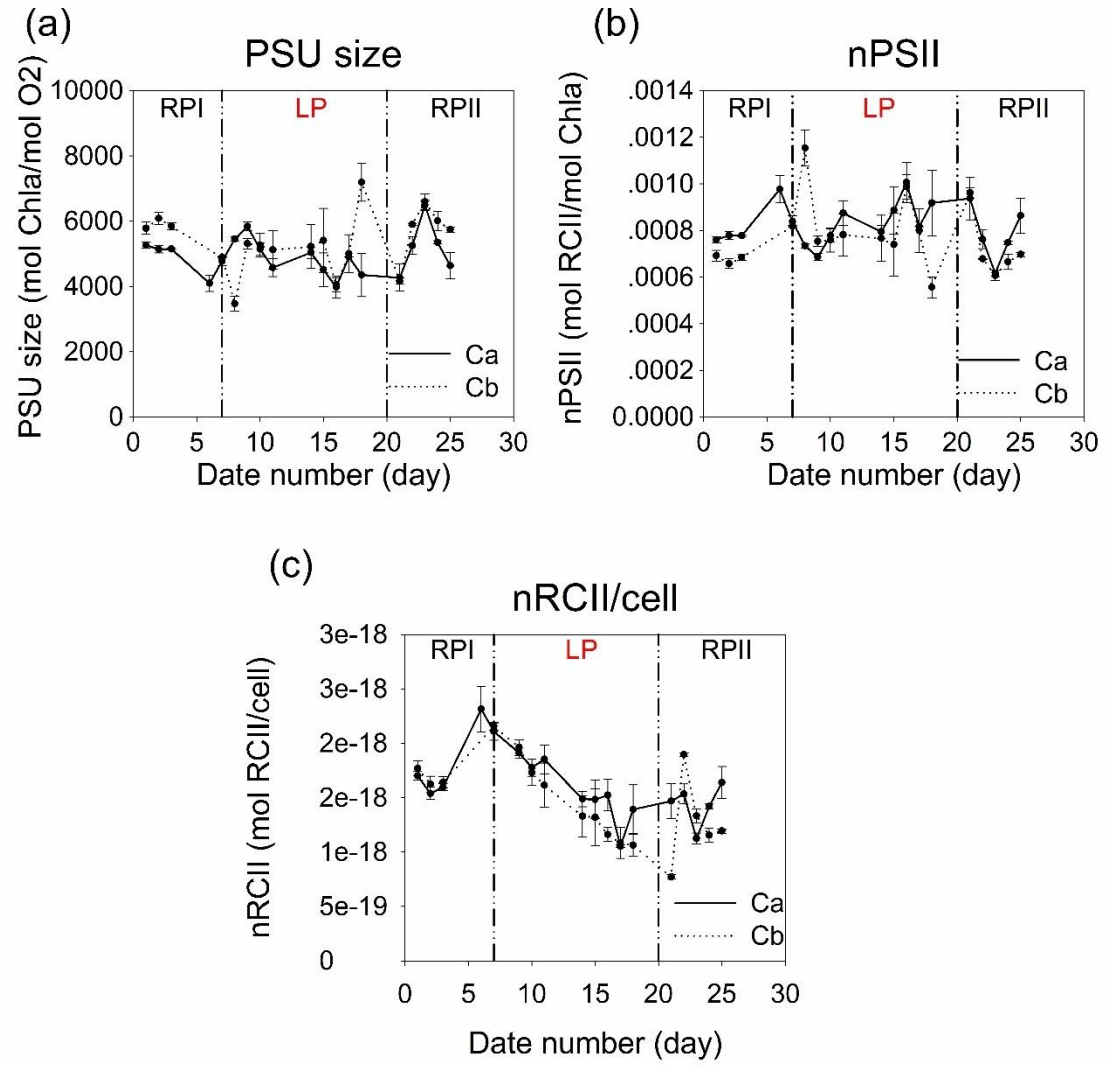

Figure 11 The PSU size ((a)), n_{PSII} ((b)) and n_{RCII}/cell ((c)) of cultures Ca (solid line) and Cb (dotted line) change with date in Experiment 2. Day 1-7 is the P-replete phase-I (RPI), day 8-20 is the P-limited phase (LP), and day 21-26 is the P-replete phase-II (RPII) (see Table 8).

3.2.3 K_R

3.2.3.1 K_R

One of the main aims of this work was to investigate whether K_R remains constant under conditions of unbalanced growth, here induced by transfer of the cells to P-constrainted medium. K_R values were calculated from eq. 6 with measured [RCII] from oxygen flash yield system, F_0 and σ_{PSII} from Frrf measurement. The Frrf measurement doesn't give error values for F_0 and σ_{PSII}, so the error of calculated K_R values here mainly comes from errors of [RCII] values. The errors of [RCII] values arise from the fitting of four points in Figure 4, the quality of which had already been controlled by abandoning points with large variation. Generally, the K_R values are about ten times higher than the value given in the manual—11800 (m^{-1}), which might result from the different light unit we used (Figure 12). Aside from that, this instrument specific factor declined slowly during the P-limited

phase from about 1.0×10^5 m^{-1} to about 5.0×10^4 m^{-1}. The decrease amplitude was about 30-40%.

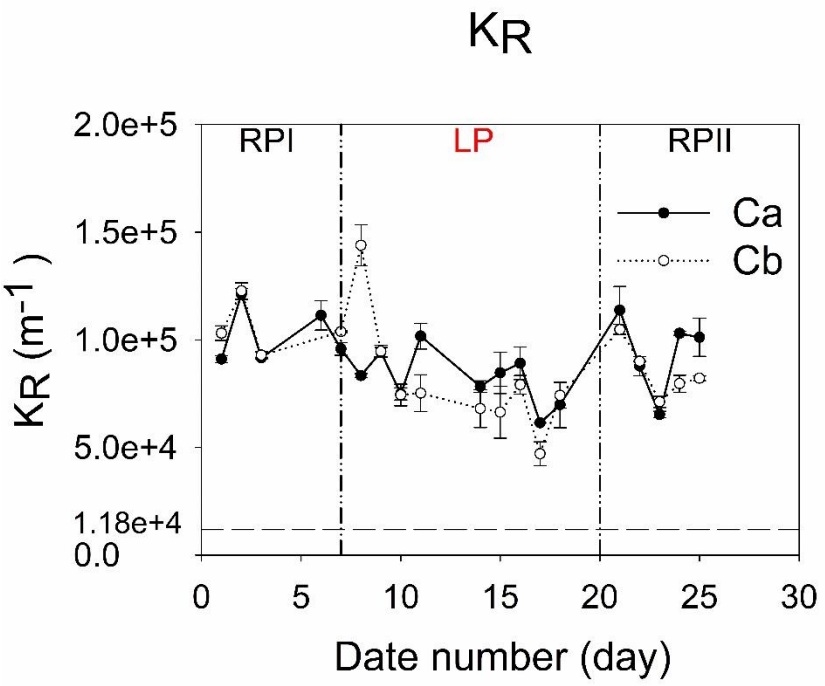

Figure 12 Calculated K_R of Ca (solid line with black circle) and Cb (dotted line with white circle) in Experiment 2 through eq. 6 -- the algorithms advocated by Oxborough et al. 2012 and Silsbe et al. 2015. Day 1-7 is the P-replete phase-I (RPI), day 8-20 is the P-limited phase (LP), and day 21-26 is the P-replete phase-II (RPII) (see Table 8).

3.2.3.2 Calculations based on K_R

Theoretically, we should use new K_R values we calculated in this study to derive a_{LHII} in the absorption algorithm and [RCII] in the sigma algorithm, thus F_{II} and ETR_{PSII} respectively. Here we plotted the new a_{LHII} calculated from new K_R values we got (here we call it "$a_{LHII.new}$") and F_{II} derived from $a_{LHII.new}$ ($F_{II.new}$) with time (Figure 13). $a_{LHII.new}$ kept stable at around 55 m^{-1} in the first P-replete stage and showed a downward trend in the P-limited stage to about 30 m^{-1} until the addition of P on day 20, after which it started to increase. $F_{II.new}$ showed opposite trend, with a slight increase trend in the P-limited stage. Nevertheless, all the values of $F_{II.new}$ are larger than 1and $a_{LHII.new}$ values were about ten times higher than the average absorption of culture, which is not possible. This problem arises from the abnormal K_R values we got in this study, which are about ten times higher than the value given by the manual. Therefore, for the a_{LHII} and FII calculation in this report, we used the K_R value given by the manual instead of the valus we got. Since the K_R values we got showed large variation in different P conditions, the calculation of [RCII] with eq. 6 based on the assumption that K_R keeps constant under different environment conditions and for different species doesn't hold in our case. So, we used measured [RCII] to calculate ETR_{PSII} instead of using calculated [RCII] from K_R to derive ETR_{PSII}.

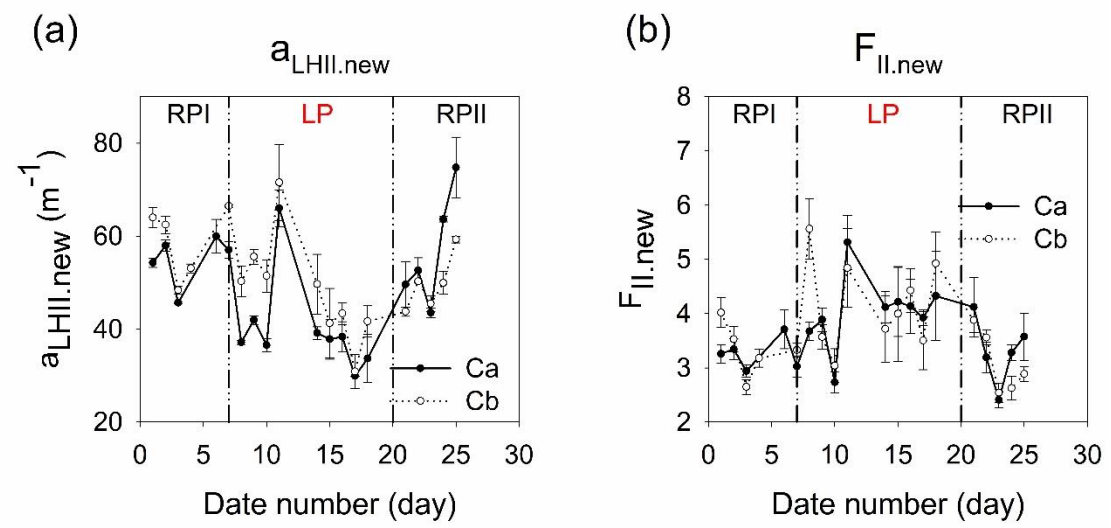

Figure 13 Change of new a_{LHII} ($a_{LHII.new}$) (a) calculated from new K_R values we got and F_{II} derived from $a_{LHII.new}$ ($F_{II.new}$) (b) with time. Day 1-7 is the P-replete phase-I (RPI), day 8-20 is the P-limited phase (LP), and day 21-26 is the P-replete phase-II (RPII) (see Table 8).

In the following sections we investigate the different photoacclimation processes to see how the cells cope with the P-stress and with the relative increase in irradiance.

3.2.4 Light absorption regulation

During the initial P-replete phase, the *Chla*/*Chlb* ratio was more or less constant at values around 3.3-3.4. After the transfer to the low P-medium, the *Chla*/*Chlb* ratio initially dropped after which started to rise to reach a maximum at day16-17. The increase in Ca was more pronounced than that in Cb. After addition of P, the values recovered to similar values at the start of the experiment (Figure 14(a)). The ratio of photosynthetic pigments *Chla* to photoprotective xanthophyll cycle pigments (*Zea*+*Viol*), and ratio of *Zea*/(*Zea*+*Viol*) of both two cultures all showed easily observed decreased values during the P-limited stage and evident recovery following the extra P addition (Figure 14(b)(c)). *Chla*, *Chlb*, *Zea*, and *Viol* here are the concentrations of chlorophyll a, chlorophyll b, zeaxanthin and violaxanthin, respectively. The ratios of both *Chla*/POC and *Chlb*/POC showed a valley during the P-limited period (Figure 14(d)(e)). The mechanisms of those changes are discussed in the Section 4.1.

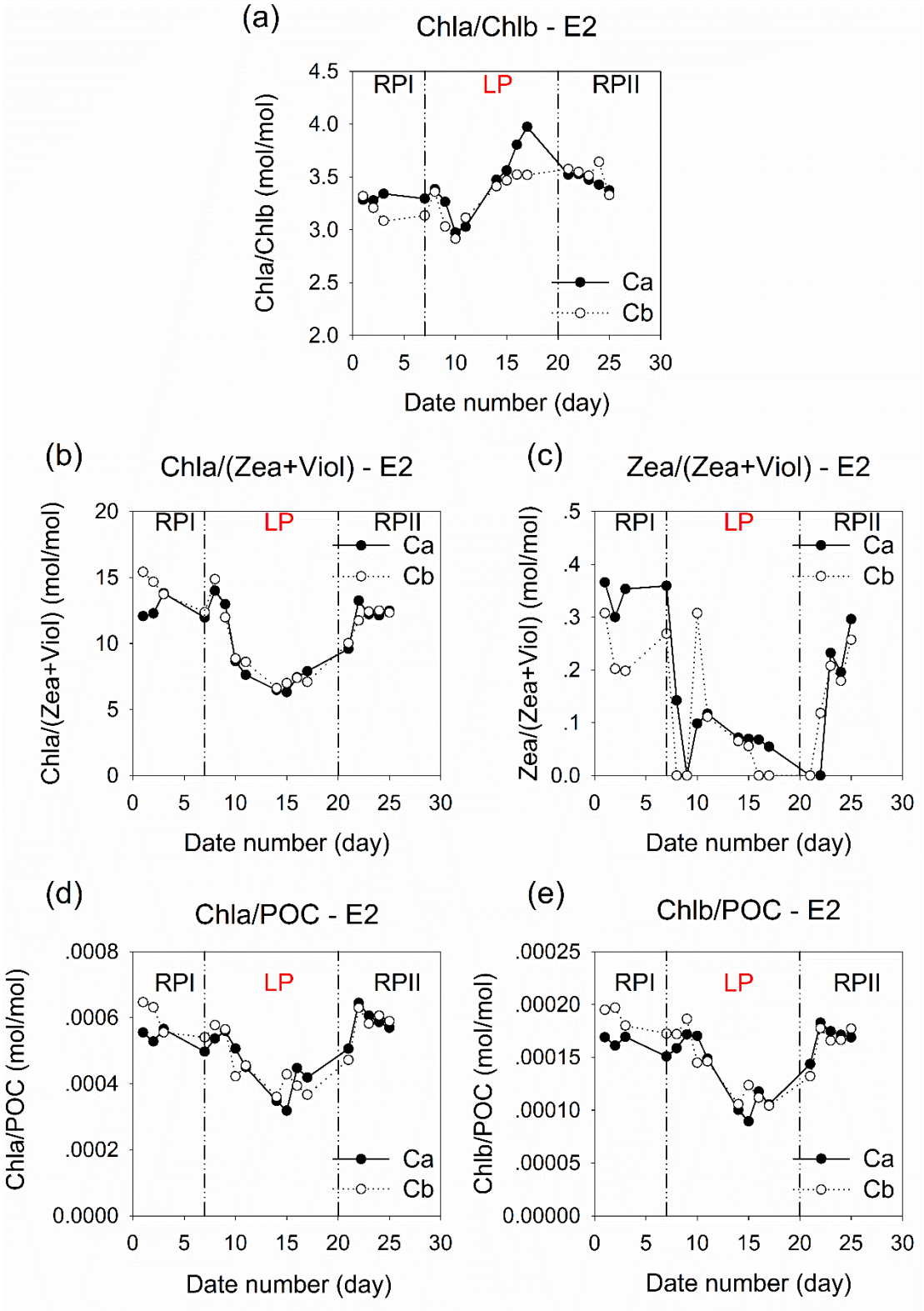

Figure 14 The ratios of *Chla*/*Chlb* (a), *Chla*/(*Zea*+*Viol*) (b), *Zea*/(*Zea*+*Viol*) (c), *Chla*/POC (d) and *Chlb*/POC (e) of cultures Ca (solid line with black circle) and Cb (dotted line with white circle) throughout the experiment 2. Pigments data were obtained from HPLC measurements. *Chla*, *Chlb*, *Zea*, *Viol* and POC are the concentrations of chlorophyll a, chlorophyll b, zeaxanthin, violaxanthin and particle organic carbon, respectively. Day 1-7 is the P-replete phase-I (RPI), day 8-20 is the P-limited phase (LP), and day 21-26 is the P-replete phase-II (RPII) (see Table 8).

3.2.5 Effect of inhibitors

F_v/F_m

Firstly, we look at the parameter of F_v/F_m. It kept steady at the first stage (around 0.53), declined to around 0.48 rapidly after transfer, and then drifted gradually back to about 0.52 on day 20. After the supplement of extra P into medium, it jumped to about 0.58 within one day but dropped back to the primary level (Figure 15). This means that the lack of P did influence the cells by reducing the photosynthetic activity, but this effect tapered off with time and F_v/F_m had nearly fully recovered at the day we added extra P.

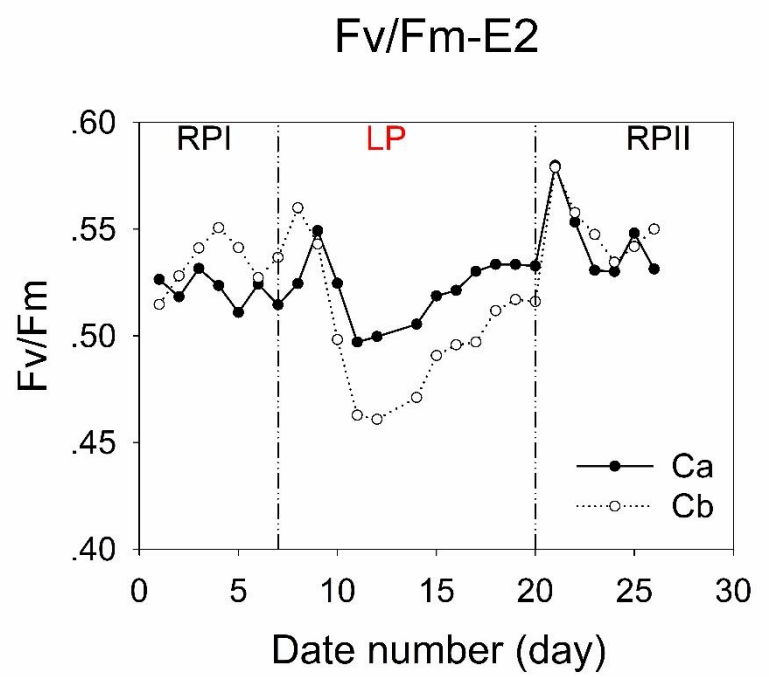

Figure 15 The F_v/F_m of cultures Ca (solid line with black circle) and Cb (dotted line with white circle) throughout the experiment 2. Day 1-7 is the P-replete phase-I (RPI), day 8-20 is the P-limited phase (LP), and day 21-26 is the P-replete phase-II (RPII) (see Table 8).

DTT

To know the importance of xanthophylls cycle in NPQ quenching mechanism as well as how this importance change during transient phase, we investigated changes in NPQ during a FLC measurement on different days, with and without DTT treatment. The mechanism is that DTT can inhibit the function of violaxanthin de-epoxidase enzyme (VDE), thus block the xanthophylls cycle. As there are too many graphs and similar results were observed for Cb, we only display those for Ca here. Graphs with grey background are in the P-limited stage (Figure 16(d)(e)(f)); the others are in the second P-replete stage (Figure 16(a)(b)(c) – the first P-replete stage; Figure 16(g)(h)(i) – the second P-replete stage). It is obvious that, for both P-replete phases, NPQ values started to decrease from about 0.1-0.2 in dark to values near zero around 100 μmol photons m^{-2} s^{-1}, and then it slightly rose to about 0.2 at 953 μmol photons m^{-2} s^{-1}. Thus some NPQ occurred in the dark. However, for the P-limited stage, NPQ values started from values near zero directly, and then rose to values around 0.6 at 953 μmol photons m^{-2} s^{-1}, which is about three times higher than 0.2. This phenomenon fits our expectation that cells would receive much more light energy than they need in the P-limited stage. In order to solve this excess energy unbalance, they would enhance NPQ mechanism to get rid of extra energy they absorbed. But despite the apparent NPQ present, the effect of DTT was limited in both the P-replete and P-limited stages. We expected the role of xanthophylls cycle in NPQ quenching woud be enhanced in P-limited stage, which means the ratio of NPQ decrease blocked by DTT would be larger, because cells need to dissipate more light energy received in P-limited stage and the xanthophylls cycle is a choice to consume extra light energy absorbed. But our study indicates that the role of xanthophylls cycle in the NPQ quenching mechanism of *Dunaliella tertiolecta* is small.

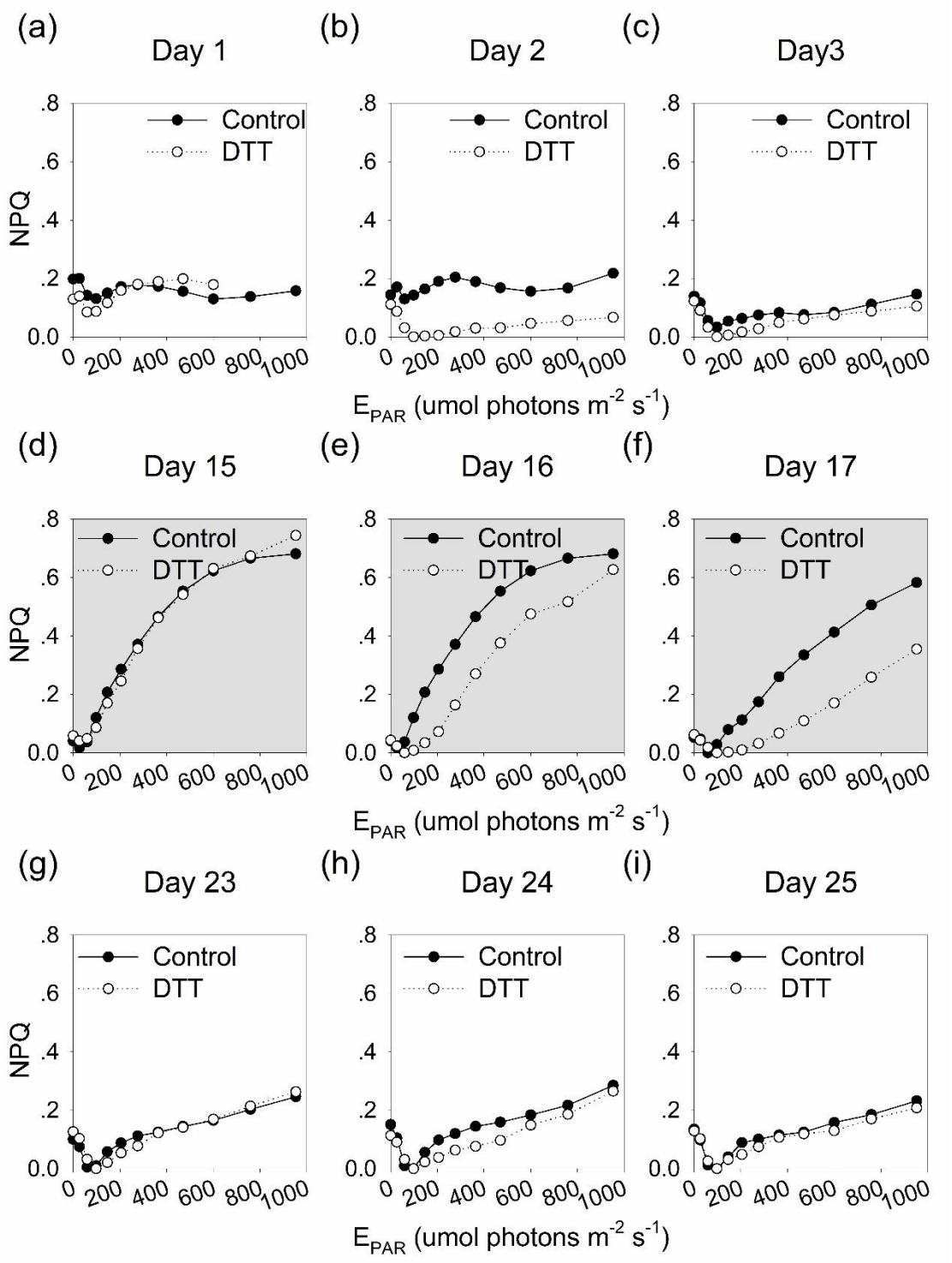

Figure 16 NPQ during fluorescence-light response curve measurements of culture Ca on different days. Day 1 (a), 2 (b) and 3 (c) are in the first P-replete stage; day 15 (d), 16 (e) and 17 (f) are in the P-limited stage (with grey fills); day 23 (g), 24 (h) and 25 (i) are in the second P-replete stage. Solid line with black circle stands for control samples without any treatment, while dotted line with white circle stands for samples with 1mM DTT treatment.

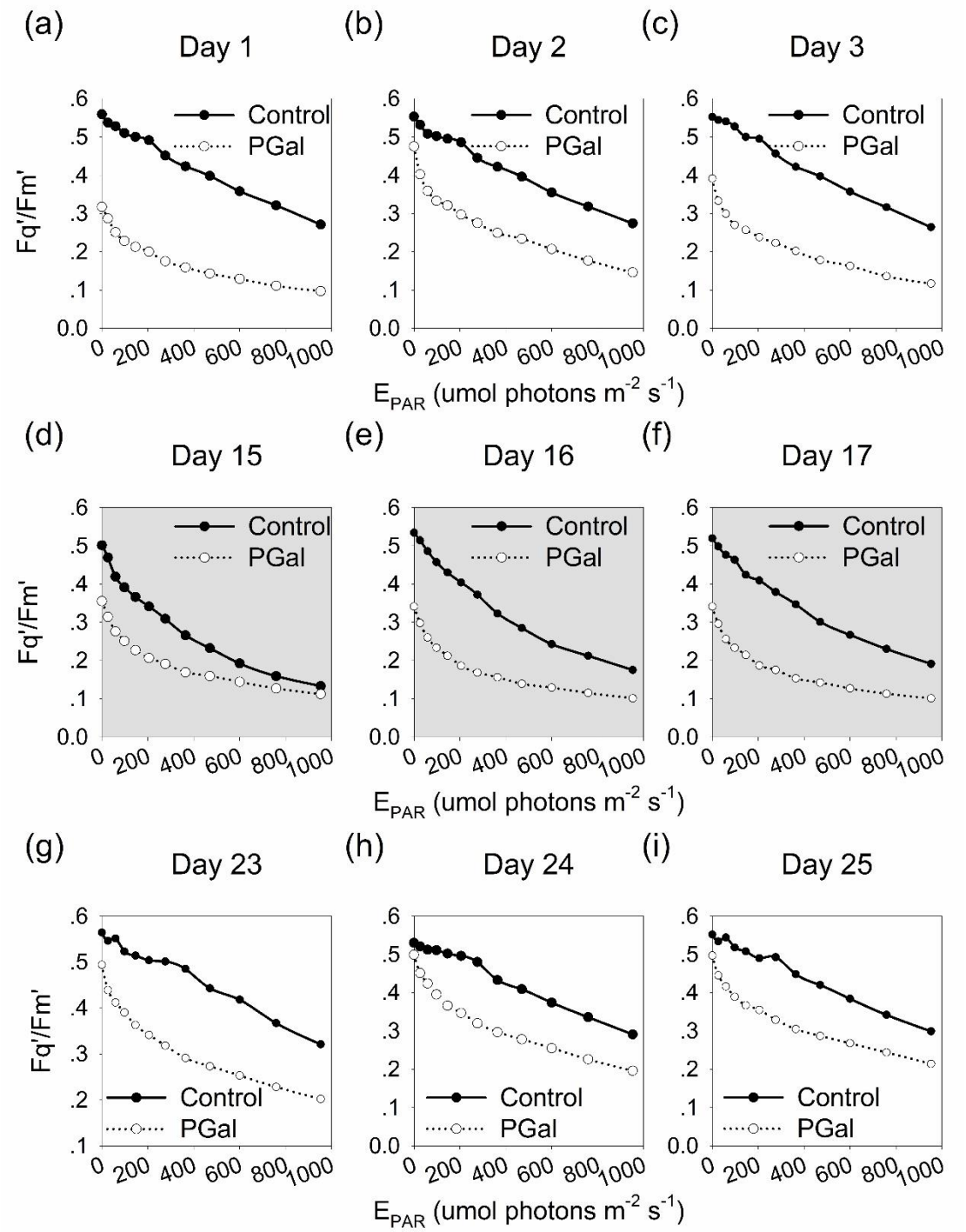

Figure 17 Fq'/F_m' during fluorescence-light response curve measurements of culture Ca on different days. Day 1 (a), 2 (b) and 3 (c) are in the first P-replete stage; day 15 (d), 16 (e) and 17 (f) are in the P-limited stage (with grey fills); day 23 (g), 24 (h) and 25 (i) are in the second P-replete stage. Solid line with black circle stands for control samples without any treatment, while dotted line with white circle stands for samples with 2mM PGal treatment.

PGal

As mentioned above, not all electrons produced from water-splitting are utilized in fixing carbon. To test whether there are some electrons used to reduce oxygen by PTOX or PTOX-like oxidase, we look at Fq'/F_m' values during a FLC measurement on different days, with and without PGal treatment (Figure 17). Also, we only display graphs for Ca here. Same with Figure 16, Graghs with grey background are in the P-limited stage; the others are in P-replete stages. Fq'/F_m' of all controls in whichever stage started with values between 0.5 and 0.6 in dark. It then progressively dropped to values near 0.3 at 953 μmol photons m^{-2} s^{-1} in P replete stages, whereas that value in P limited stages was about 0.2. That is to say, under high light intensity, photochemical quenching is weaker in P lacking environment, compared with that in P sufficient environment. That is because of reduced photosynthetic activity during P-limited stage. When comparing PGal treatments with controls, it is obvious that photochemical quenching was largely reduced in all days. But it is hard to find any pattern in different stages. So we quantified this change by calculating the change ratio of $rETR_{PSII}$ at 276 μmol photons m^{-2} s^{-1} (eq. 19). 276 μmol photons m^{-2} s^{-1} here is the closest light intensity to Ek among all the light intensities in FLCs.

$$\text{rETR}_{PSII} \text{ change ratio} = \frac{rETR_{PSII\ control} - rETR_{PSII\ PGal}}{rETR_{PSII\ control}} \quad \text{-- (19)}$$

The ratio we calculated thus reflects the remaining fraction of potential photosynthetic electron transport after addition of Pgal. Assuming no artefacts by using this inhibitor, we found that: about 50% electrons produced by PSII are used to reduce oxygen by PTOX or PTOX-like oxidase both in P-replete and P-limited conditions, and this percentage drops significantly and then recovers to previous level within a few days (about one week) during transient phases from P abundant environment to P lacking environment. For reverse transient phase from P lacking environment to P abundant environment, there is also a huge decrease of $rETR_{PSII}$ change ratio. But then, that of Cb started to increase, while that of Ca stopped the downward trend and showed small fluctuations. The reason of the different behaviors of Ca and Cb here is unknown. There might exist a delay before $rETR_{PSII}$ change ratio of Ca to rise, but further monitor is needed before we can get that conclusion.

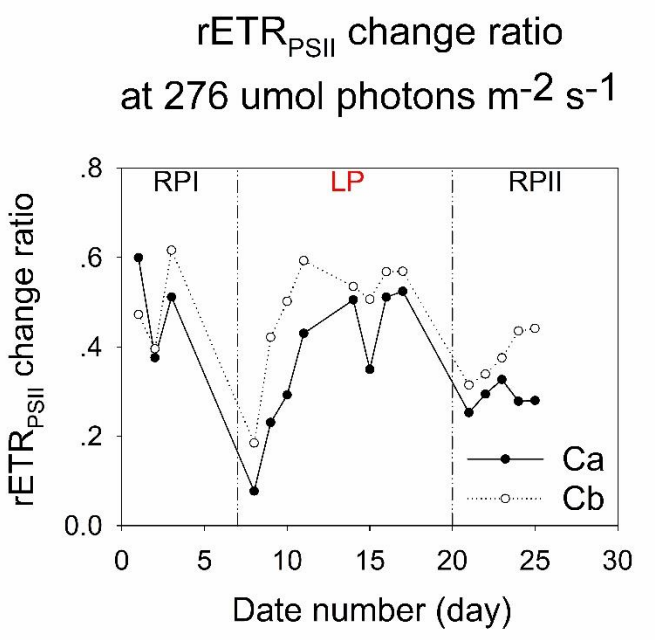

Figure 18 $rETR_{PSII}$ change ratio between PGal treatment and control of Ca (solid line with black circle) and Cb (dotted line with white circle) at 276 μmol photons m^{-2} s^{-1}. Day 1-7 is the P-replete phase-I (RPI), day 8-20 is the P-limited phase (LP), and day 21-26 is the P-replete phase-II (RPII) (see Table 8).

3.2.6 Primary production

As described in Section 2.4, we measured the primary production of cells by measuring the uptake of radioactively labeled $NaH^{14}CO_3$ under different light intensities. In the meantime, we also measured variable Chla fluorescence under progressively increased light intensities, and then calculated corresponding ETR_{PSII} through eq. 2 and eq. 4. An example of a photosynthesis light curve made from ^{14}C-incubations and an example of ETR_{PSII} light curve are shown in Fig. 19. We fitted the light curves from Frrf and ^{14}C fixation rate gained from ^{14}C isotope enrichment incubations with P&G model to get parameters: α, Ek, $ETR_{PSIImax}$ or P_{14Cmax} (Figure 20 and 21). Using these parameters, we predicted ETR_{PSII} and ^{14}C fixation rate between 0 and 80 μmol photons m^{-2} s^{-1}. The reason why "80 μmol photons m^{-2} s^{-1}" was choosed is that the average Ek of those curves were around 80 μmol photons m^{-2} s^{-1}, and divergence between ^{14}C-PP and ETR_{PSII}-PP started to occure in higher light intensities due to the role of NPQ or other alternative electron sinks. Then the results were plotted against each other in a xy-plot and from the slope the electron requirement for carbon fixation Φe,C was calculated.

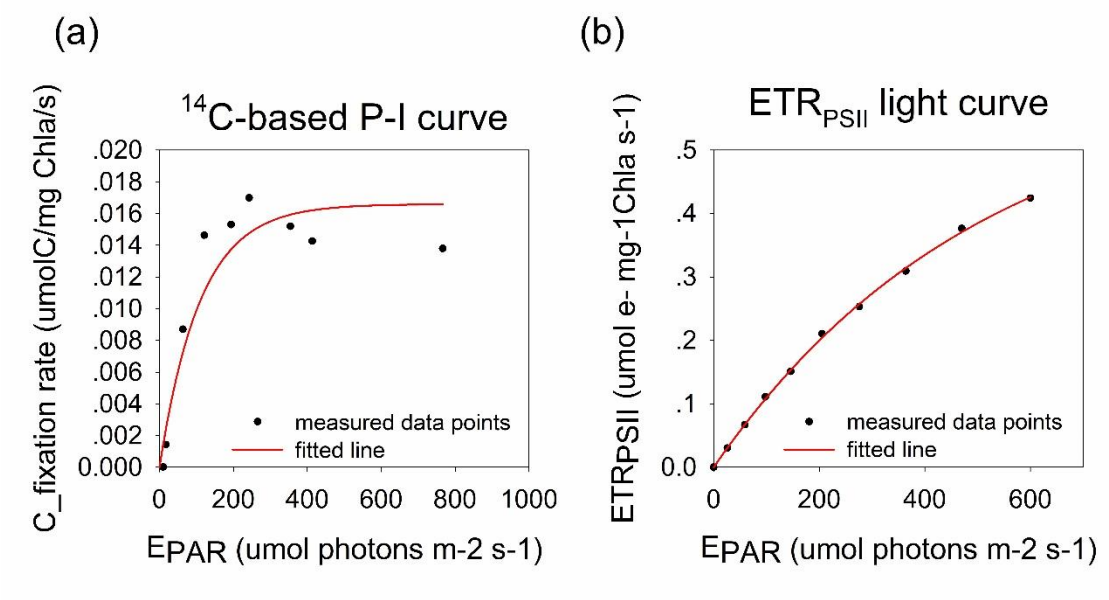

Figure 19 An example of photosynthesis light curve made from ^{14}C-incubations (a) and an example of ETR_{PSII} light curve (b). Dots are measured data points, red line is the fitted line with P&G model.

α obtained from ^{14}C isotope enrichment incubation data showed large fluctuations. But except that α of Cb at day 9 dramatically increased to 0.0007, α were around 0.0002 in the first P-replete stage, decreased to around 0.0001 in the P-limited stage, rose back to around 0.0002 one day after extra P-addition, and then started to drop again three days after extra P-addition (Figure 20 (a)). For P_{14Cmax}, the decrease trend after transfer is more manifest, from about 0.015 µmol C/mg *Chla*/s to about 0.005 µmol C/mg *Chla*/s, also except for Cb on day 9 – it markedly rose to 0.04 µmol C/mg *Chla*/s (Figure 20 (b)). Since it only happened once, and the value is far high above the values of its adjacent days, we checked the raw data of ^{14}C incubations and found that disintegrations per minute (DPM value) was super high on that day, compared with other days. So we think there might be an operation error on that sample. After the addition of P on day 20, it rapidly recovered to its original level, but then started to decrease again. Ek change is more fluctuating (Figure 20 (c)). Ek of Ca showed more variability than E_k of Cb, whereas that of Cb is kind of stable before day 22, only decreased by more than half on day 15. The upward trend of Ek of Cb after day 22 is distinct.

α obtained from FLCs showed marked variability with time, but no clear trend was observed throughout the whole experiment 2 (Figure 21 (a)). The values were much higher than those gained from ^{14}C isotope enrichment incubation data, and the behaviours were not similar. Except the abnormal data point of Cb on day 9, it seems that Ca displayed a inverse trend compared with Figure 20 (a) – increased a little during P-limited stage, but Cb showed no obvious pattern. The reason for this divergence is not clear. Similar with data from ^{14}C isotope enrichment incubation, both $ETR_{PSIImax}$ and Ek obtained from FLCs declined after transfer of the cells to P-limited conditions. The decrease seems to stabilize for a few days before P was added again (Figure 21 (b)(c)). The reason of this pattern can be explained by the decrease of photosynthetic activity during P-limited phase. Besides, it is noticeable that the Ek values obtained from FLCs are also much higher than those gained from ^{14}C isotope enrichment incubation. This is most likely due to the function of alternative electron pathways when exposed to irradiances higher than Ek values obtained from ^{14}C

isotope enrichment incubations. When exposed under gradually incremental light intensities, cells' rate of carbon fixation starts to decrease when the light intensity reaches Ek in Figure 20 (c), but the rate of electron transport through PSII would decrease later because electrons are still continually transported to alternative pathways described in Section 1.1.4 until alternative electron pathways are also saturated.

$\Phi_{e,C}$ was calculated from calculated photosynthetic rates using the fitted parameters obtained from the FLCs and the 14C-based P-I curves (slope of fitting line in Figure 22 (a)). $\Phi_{e,C}$ was stable during the first 7 days (i.e during the P-replete phase), with values of about 8 mole electrons/mole photons absorbed but it climbed to about 25 mol/mol in the P-limited phase (Figure 22 (b)). After addition of DIP on day 20, $\Phi_{e,C}$ went down back to previous level but started to rise again after day 23. That increase during P limited phase fits with our expectation because more electrons were used for one carbon fixation when alternative electron pathways are enhanced in undesirable P lacking environment. But the reason for the second rise after day 23 is unknown. It might indicate that cells hadn't reached balanced growth yet.

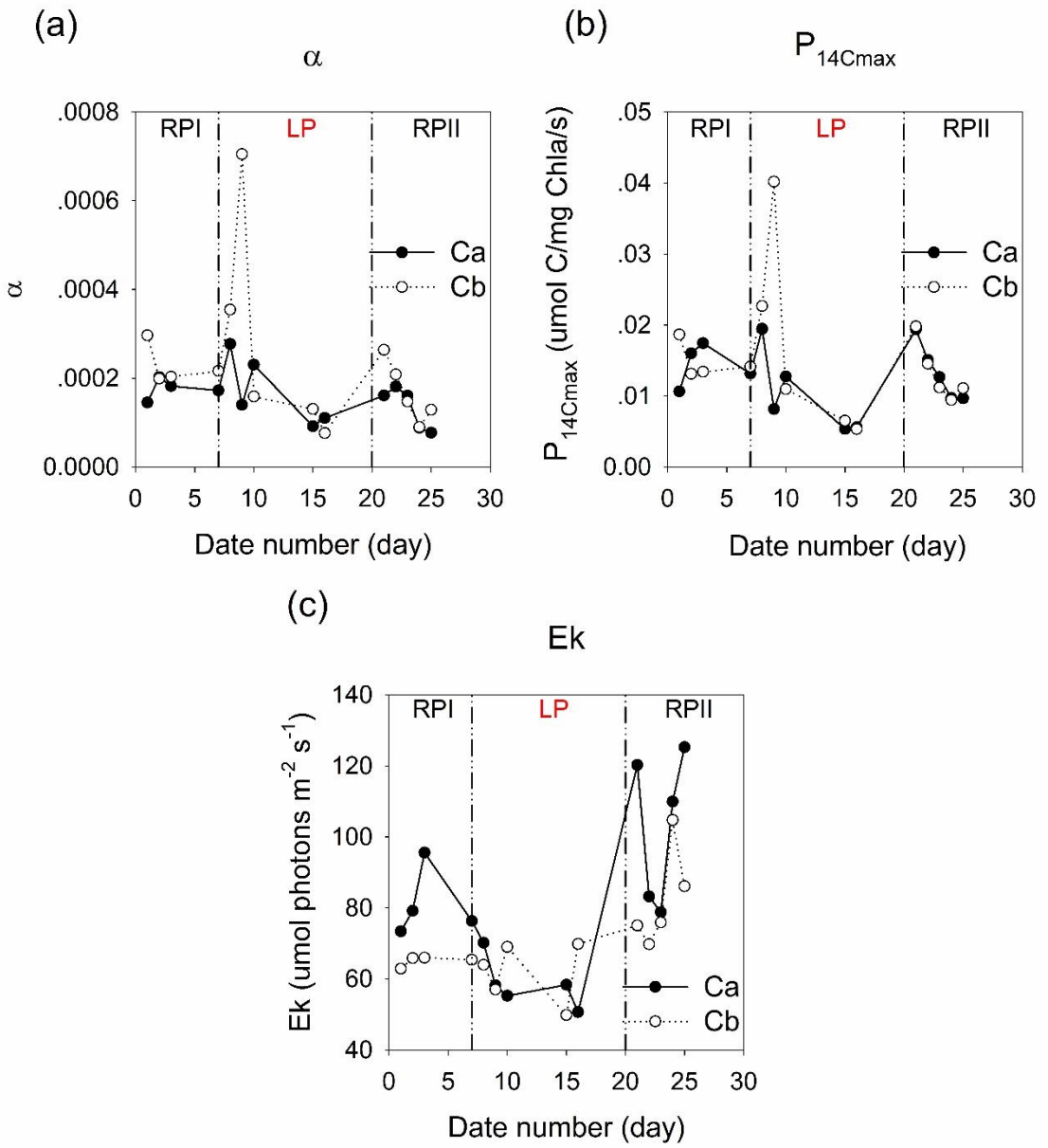

Figure 20 Fitted parameters α (a), P_{14Cmax} (b) and Ek (c) of both Ca (solid line with black circle) and Cb (dotted line with white circle) throughout the experiment 2, with C-fixation rate data from ^{14}C isotope enrichment incubations. Day 1-7 is the P-replete phase-I (RPI), day 8-20 is the P-limited phase (LP), and day 21-26 is the P-replete phase-II (RPII) (see Table 8).

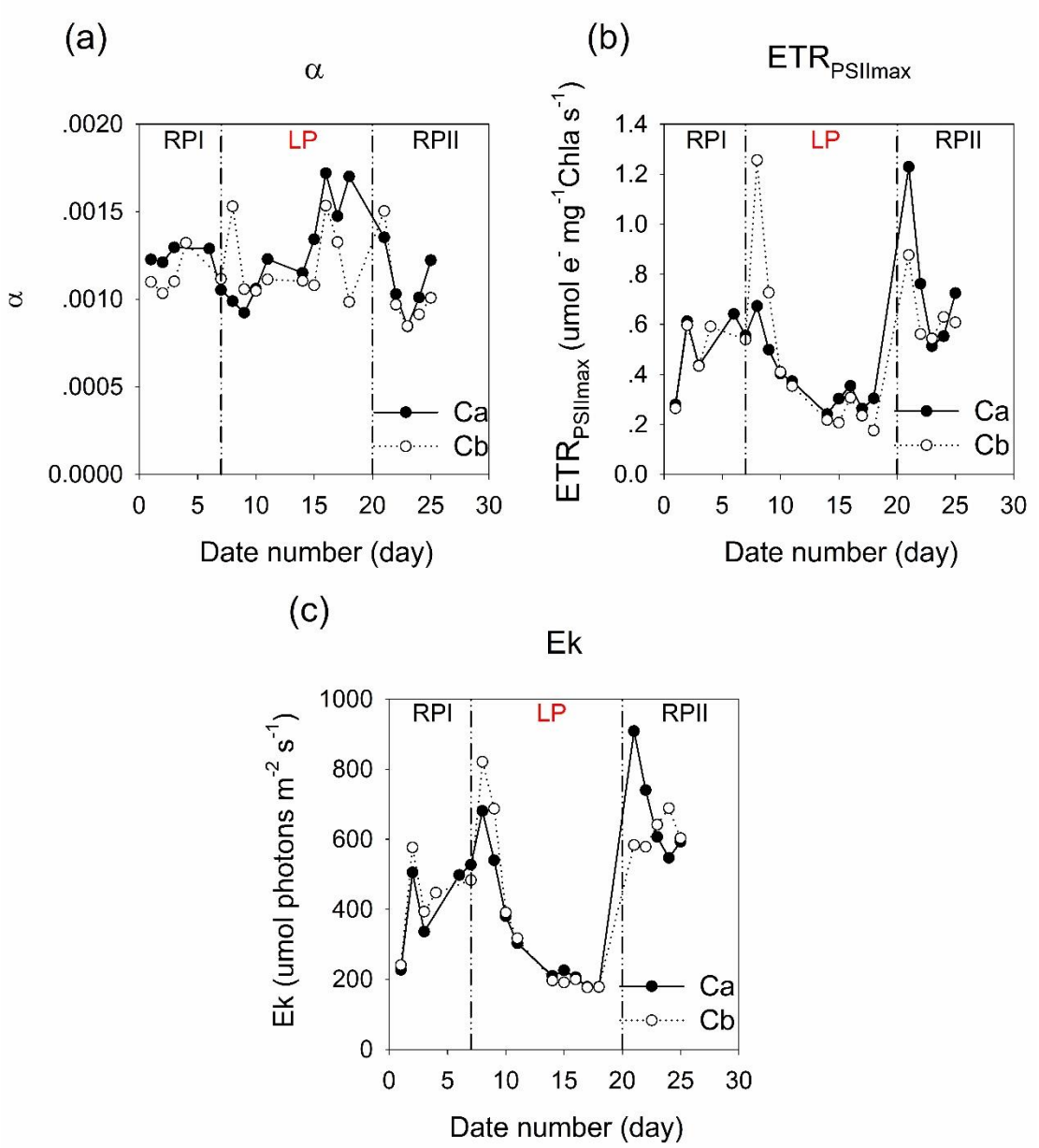

Figure 21 Fitted parameters α (a), $ETR_{PSIImax}$ (b) and Ek (c) of both Ca (solid line with black circle) and Cb (dotted line with white circle) throughout the experiment 2, with ETR_{PSII} data from FLCs. Day 1-7 is the P-replete phase-I (RPI), day 8-20 is the P-limited phase (LP), and day 21-26 is the P-replete phase-II (RPII) (see Table 8).

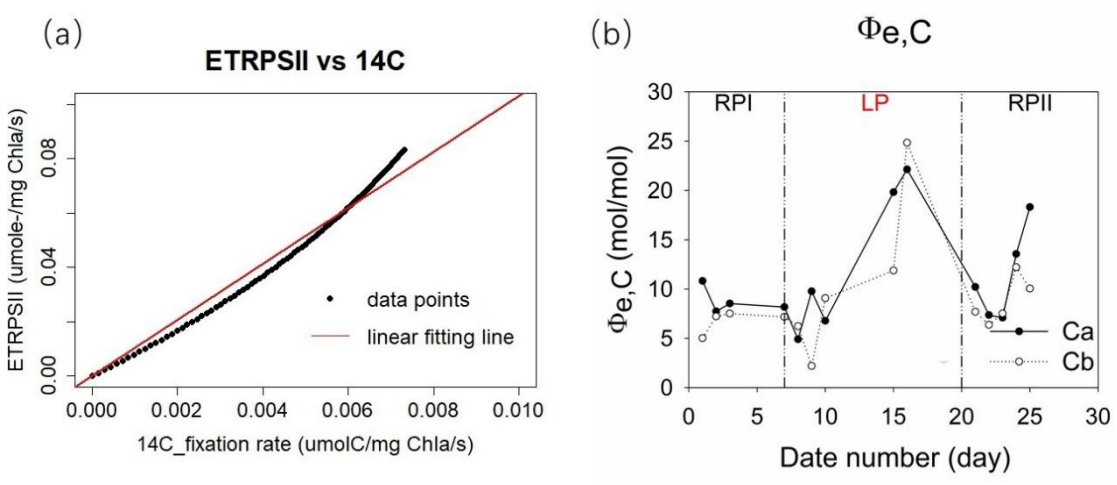

Figure 22 (a) An example of the derivation of electron requirement for carbon fixation ($\Phi_{e,C}$) from calculated photosynthetic rates within 80 µmol photons m^{-2} s^{-1} using the fitted parameters obtained from the FLCs and the 14C-based P-I curves. (b) Electron requirement for carbon fixation ($\Phi_{e,C}$) for both culture Ca (solid line with black circle) and Cb (dotted line with white circle) throughout the experiment 2. Day 1-7 is the P-replete phase-I (RPI), day 8-20 is the P-limited phase (LP), and day 21-26 is the P-replete phase-II (RPII) (see Table 8).

3.2.7 Diurnal change in light-dark cycle

As described above, we tracked ETR_{PSII} and C_fixation rates at four time points during the light period (09:30 am; 11:30 am; 13:30 pm; 15:30 pm) on day 4 during the first stage (P-replete) and day 18 during the second stage (P-limited). Changes in cell number, mean cell diameter and F_v/F_m are plotted in Figure 23. Both cell density and mean cell diameter (Figure 23(a)) slightly increased from 09:30 am to 15:30 pm. Their values are lower during the P-limited cindition than those during P-replete date. For F_v/F_m, patterns on two dates are different (Figure 23(b)). F_v/F_m on the P-replete date increased a little from 0.52 to 0.53 at 11:30 am but followed by a drop to 0.51 at 13:30 pm, then rose again to 0.55 at 15:30 pm. But F_v/F_m on P-limited date marginally climbed from 0.53 to 0.55. Basically, the F_v/F_m values on two dates were similar. That's because Fv/Fm has already recovered from the initial decline (Figure 15). We fitted the FRRf light curve data with P&G model, and plotted $ETR_{PSIImax}$ and α (Figure 24). Due to uncleaned sampling bottle, we lost the point at 09:30 am on P-replete date. The $ETR_{PSIImax}$ on P-replete date showed a valley, while that on P-limited date showed a "sine" wave. As to α, it decreased from 0.0016 to 0.0014 on day 4 during the P-replete stage, but showed also a "sine" wave on day 18 during the P-limited stage. The general values of $ETR_{PSIImax}$ in P-replete date are higher than those in P-limited stage. But there is no obvious difference in the value of α between two dates. The C_fixation rates at the growth light intensity both showed an increase at 13:30 pm and then decreased back to morning level but the dynamics were larger in the P-replete culture (Figure 25(a)). The electron requirement for carbon fixation $\Phi_{e,C}$ on both dates showed similar pattern (Figure 25(b)): increased at 11:30 am, decreased at 13:30 pm and then increased again at 15:30 pm. But the values on day 4 during the P-replete stage were much higher than the values on day 18 during the P-limited stage dut to higher C_fixation rates on day 4, which is also opposite with our expectation.

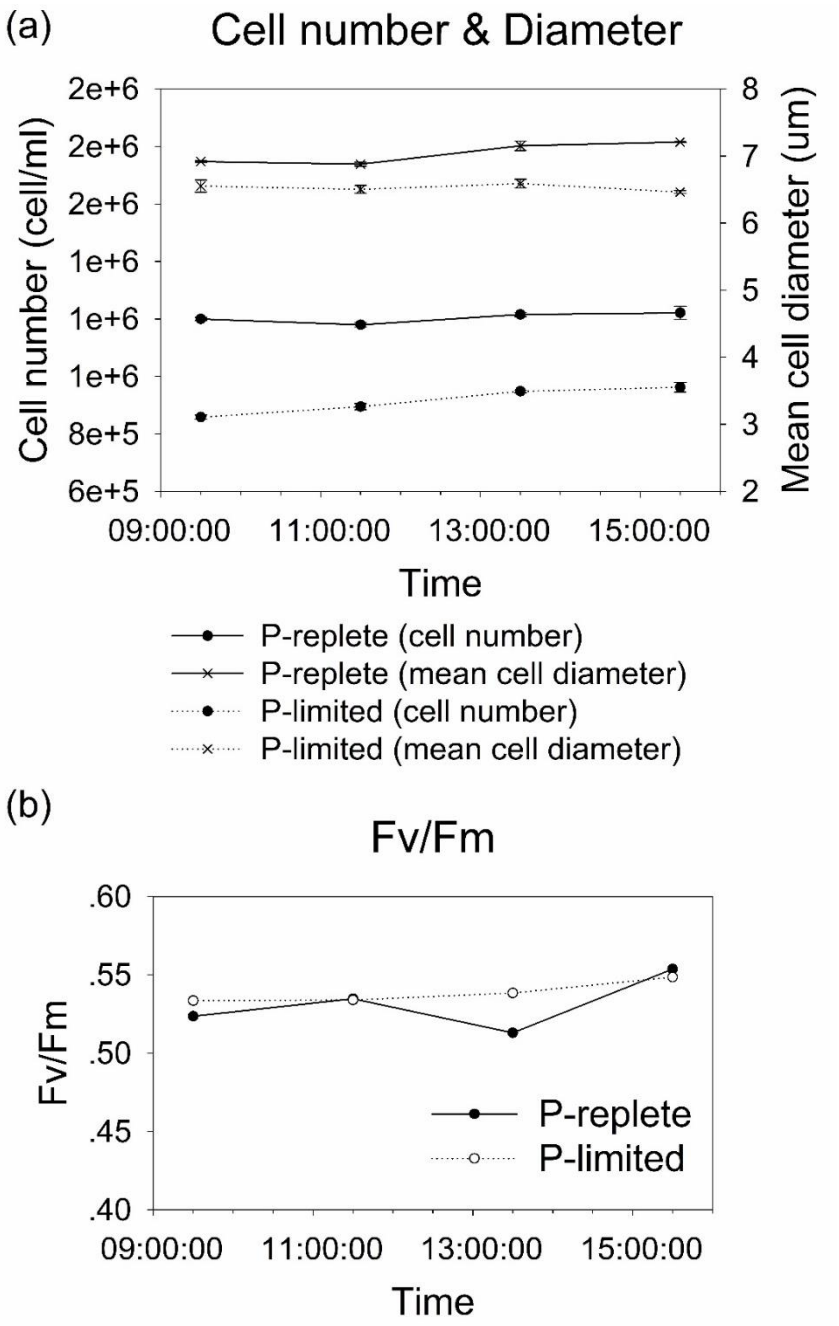

Figure 23 (a) The cell density (solid line) and mean cell diameter (dashed line) of Ca at different time o'clock during light period on day 4 in P-replete state (solid line) and day 18 in P-limited state (dotted line). (b) The F_v/F_m of Ca at different time o'clock during light period on day 4 in P-replete state (solid line) and day 18 in P-limited state (dotted line).

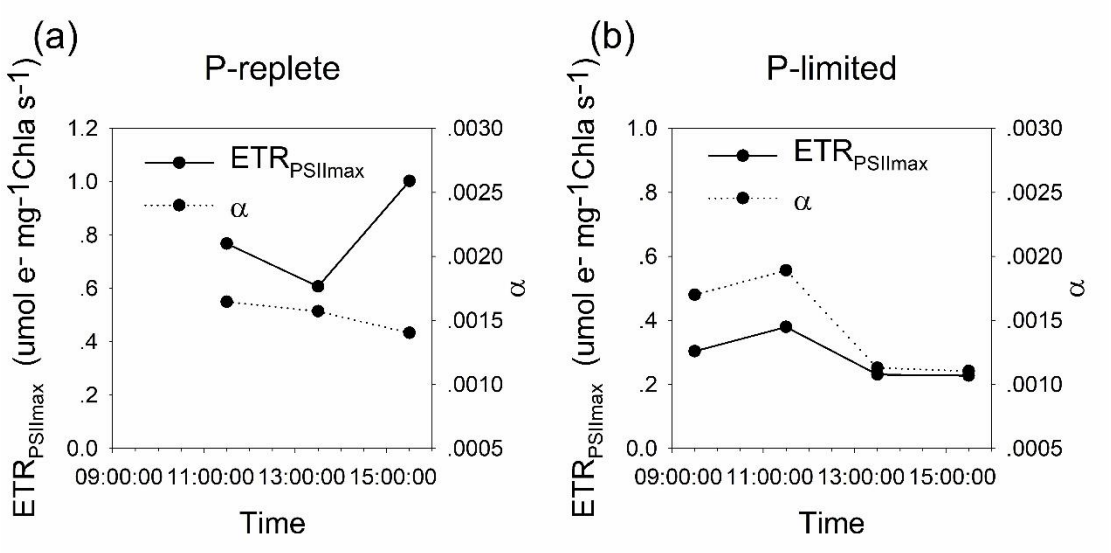

Figure 24 The $ETR_{PSIImax}$ (solid line) and α (dotted line) of Ca at different time during light period on day 4 in P-replete state (a) and day 18 in P-limited state (b). The data was obtained by fitting of FLCs data.

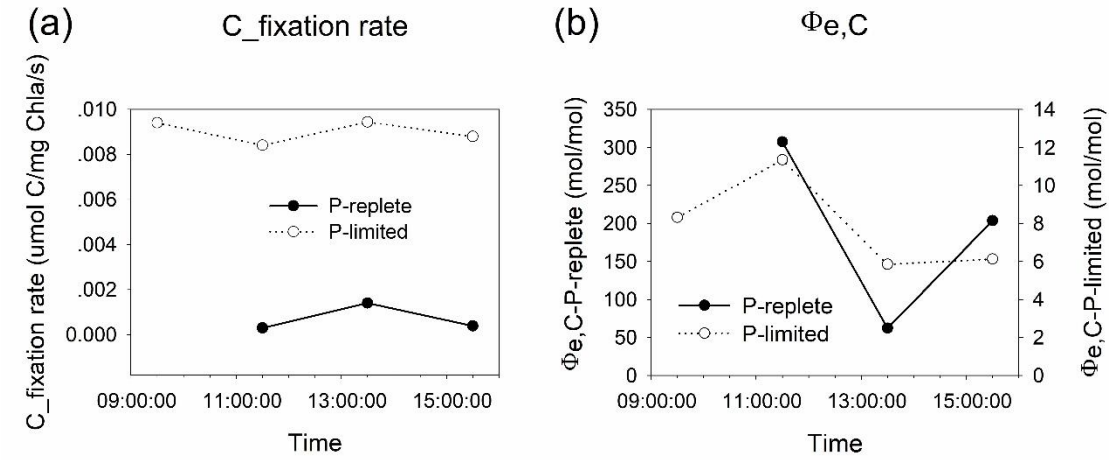

Figure 25 The C_fixation rate of culture Ca (a) and the electron requirement for carbon fixation $\Phi_{e,C}$ (b) under growth light intensity at different time o'clock during light period on day 4 in P-replete state (solid line with black circle) and day 18 in P-limited state (dotted line with white circle). Data were based on 2h incubations.

3.2.8 $^{13}C^{15}N$ incubation

Bulk analysis

C_fixation rates based on stable isotope analyses based on 2h (Fig. 26(a)) or 7h (Fig. 26(b)) incubations showed decreased rates during the P-limited phase, which recovered after the addition of DIP. This is contrary to the 24h incubations (Fig. 26(c)) which did not show a decrease in the C_fixation rate, which stayed more or less stable, apart from the first measurements on day 3, which showed lower rates. Contrary to the C_fixation rates, N_assimilation rates increased up to 5-fold

during the P-limited phase and went back to original level after the addition of extra P in 7h and 24h incubations (Figure 26(e)(f)). But this pattern is not observed in 2h incubations (Figure 26(d)). Therefore, because of these opposite patterns, the C/N_assimilation rate ratio decreased by about 3 times during the P-limited phase and went back to original level after the addition of extra P (Figure 26(g)(h)(i)). So, we conclude that the C-fixation rates were higher during the P-replete phase, but the N-assimilation rates were lower during the P-replete phase. Also, the C/N_ assimilation rate ratio, whatever in 2h, 7h or 24h incubations, decreased a lot when transferred into P-limited condition.

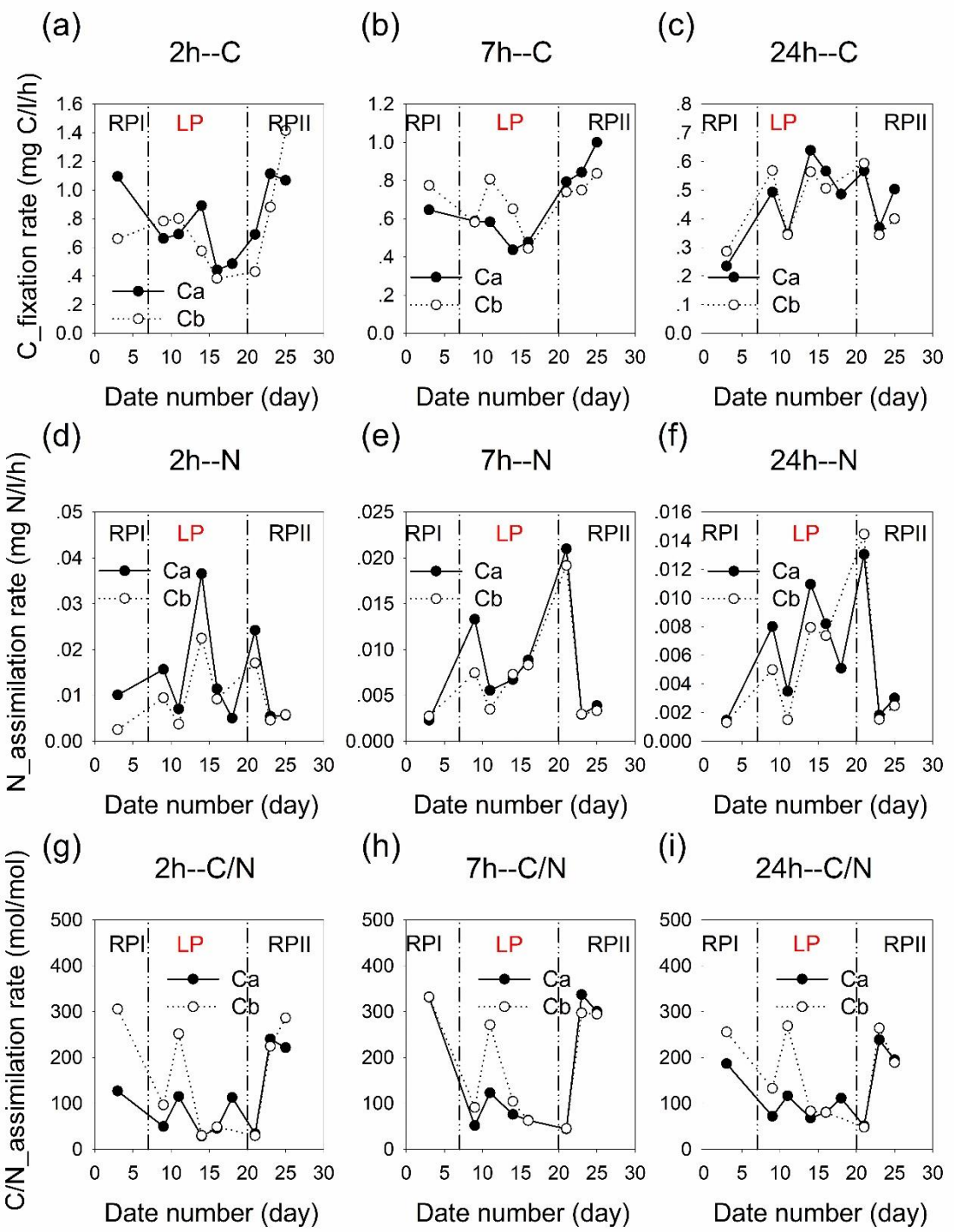

Figure 26 The change of C fixation rate, N_assimilation rate and C/N assimilation rate ratio for the 2h, 7h and 24h ^{13}C and ^{15}N enriched incubations of culture Ca (Ca) and Cb (Cb) with date. Day 1-7 is the P-replete phase-I (RPI), day 8-20 is the P-limited phase (LP), and day 21-26 is the P-replete phase-II (RPII) (see Table 8).

Single cell analysis

In order to know the C/N assimilation patterns in single cell level, we applied NanoSIMS measurements on the uptake of ^{13}C-DIC and ^{15}N-NO_3 patterns throughout the whole experiment. We represent the uptake of ^{13}C-DIC by ratio $^{13}C/(^{12}C+^{13}C)$, which was derived from NanoSIMS ^{12}C and ^{13}C ion counts. Similarly, the uptake of ^{15}N-NO_3 was represented as $^{12}C^{15}N/(^{12}C^{14}N+^{12}C^{15}N)$, which was derived from NanoSIMS $^{12}C^{14}N$ and $^{12}C^{15}N$ ion counts. We used CN ions here instead of N because N itself cannot be detected. Example of NanoSIMS secondary ion counting images are presented in Figure 27 (a)(b)(c) for one cell in the P-replete phase and in Figure 28 (a)(b)(c) for one cell in the P-limited phase. Using the ^{12}C, ^{13}C, $^{12}C^{14}N$ and $^{12}C^{15}N$ ion counts, we can derive the ratios of $^{13}C/(^{12}C+^{13}C)$ and $^{12}C^{15}N/(^{12}C^{14}N+^{12}C^{15}N)$. It seems that the enrichment of ^{13}C was scattered within cells. Although organelles with higher ^{13}C uptake within cells are clear, there is no certain patterns for its distribution in different cells, so the uptake of ^{13}C between cells were quite variable. However, for ^{15}N uptake, the enrichment of ^{15}N mainly converge on one area within cells. When cells were prolonged, those areas were more close to the end of cells. When cells were round or the shape of cells were not clear, that feature was less visible. This phenomenon occurred both in the P-replete phase (Figure 27 (d)(e)) and the P-limited phase (Figure 28 (d)(e)). Besides, although there is more N in the cell, we can also see a strong N signal outside the cell. That might be because excretion from cells or some leakage during sample preparation occured. As the cells of *Dunaliella tertiolecta* have no cell walls (Oukarroum et al., 2012), we think that cell leakage caused by rupture of the cell membrane during the filtering procedure is the more likely cause for the enriched 15N-signal outside cells. That phenomenon also exist in images of C but less visiable. That is because the signal of the ^{13}C is much stronger (compare values on x-axis in Figure 27 (d)(e)) and the scales are relative larger, so the leakage is suppressed by the scaling, but a halo caused by an enriched $^{13}C/(^{12}C+^{13}C)$ signal is still visible around the cells.

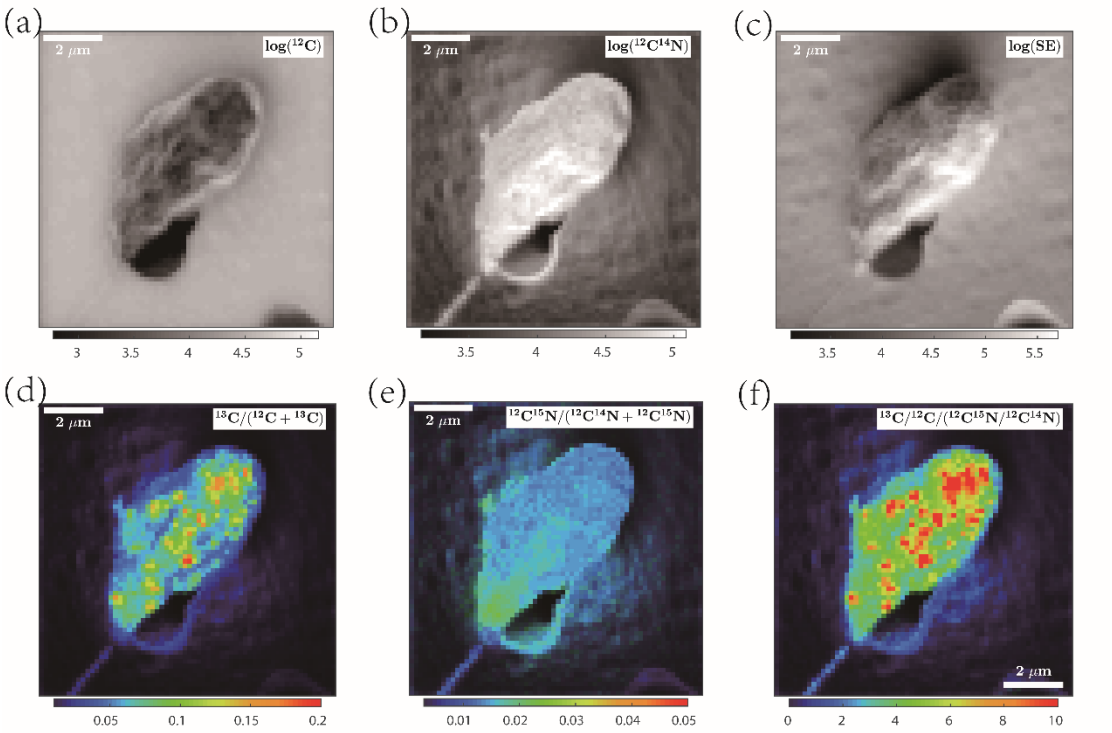

Figure 27 Example of NanoSIMS secondary ion counting images for log(^{13}C) (a), log(^{12}C^{14}N) (b), log(Secondary Electrons) (c), and derived ^{13}C/(^{12}C+^{13}C) (d), ^{12}C^{15}N /(^{12}C^{15}N +^{12}C^{15}N) (e) and ^{13}C/^{12}C /(^{12}C^{15}N /^{12}C^{14}N) (f) of one cell in the P-replete stage.

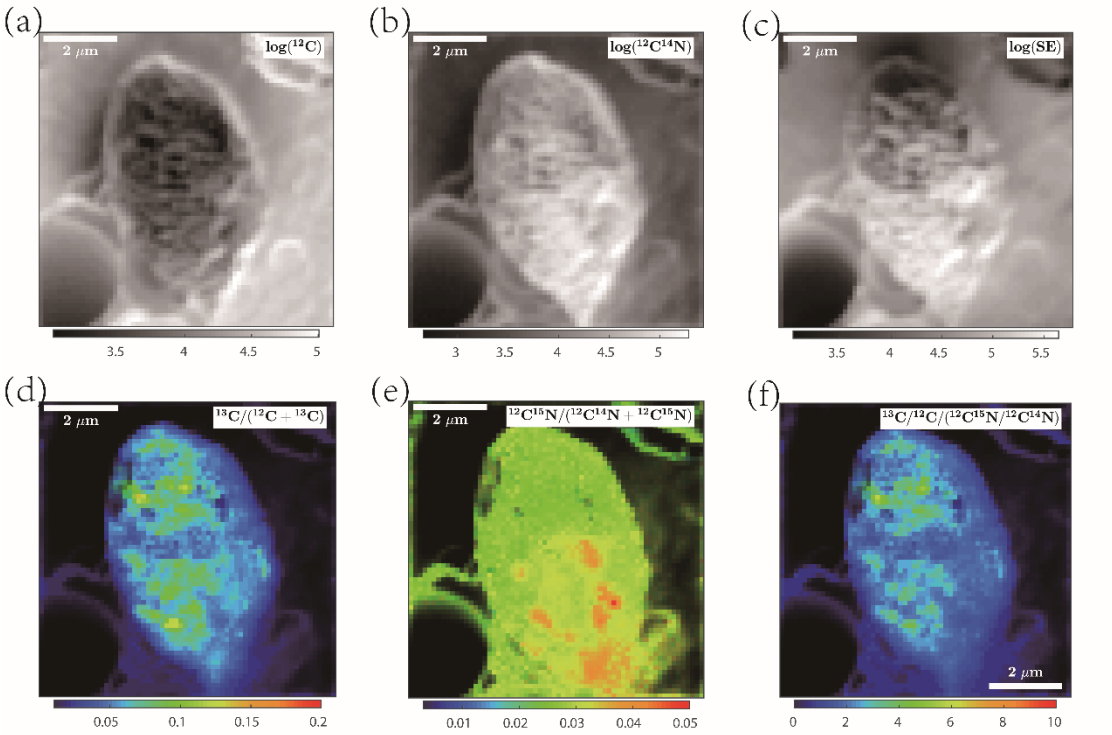

Figure 28 Example of NanoSIMS secondary ion counting images for log(^{13}C) (a), log(^{12}C^{14}N) (b), log(Secondary Electrons) (c), and derived ^{13}C/(^{12}C+^{13}C) (d), ^{12}C^{15}N /(^{12}C^{15}N +^{12}C^{15}N) (e) and ^{13}C/^{12}C /(^{12}C^{15}N /^{12}C^{14}N) (f) of one cell in the P-limited stage.

Restricted by the limited time and low cell density, we only measured cells from 7 h incubations from the following days since the start of the experiment: 3, 9, 11, 16, 25. Among those dates, day 3 was during the first P-replete stage; day 9, 11 and 16 were during the P-limited stage; day 25 was in the second P-replete stage. We plotted ^{13}C/(^{12}C+^{13}C) and ^{12}C^{15}N /(^{12}C^{15}N +^{12}C^{15}N) against each other for all the data from all dates (Figure 28 (a)). The result shows that there is no specific patterns for C/N uptake between the P-replete and P-limited phases. Even within the same phase, the variability is quite large. Then we plotted box plots for ^{13}C/(^{12}C+^{13}C) (Figure 28 (b)) and ^{12}C^{15}N /(^{12}C^{15}N +^{12}C^{15}N) (Figure 28 (c)) in different dates. The data number, mean value, standard deviation and standard error of mean information of data points in each date was summarized in Table 9. The mean value of ^{13}C/(^{12}C+^{13}C) on day 3 during the first P-replete phase was 0.0859± 0.00755, which is much higher than mean values of ^{13}C/(^{12}C+^{13}C) on day 9 (0.0398±0.00733), 11 (0.0415±0.00581) and 16 (0.0369±0.00175), which has less variability, during the P-limited phase. After the addition of P to normal level, the mean value showed an increase trend to 0.0510±0.00874. However, the N uptake showed opposite trend. The mean value of ^{12}C^{15}N /(^{12}C^{15}N +^{12}C^{15}N) in the P-replete phases (day 3 and day 25) are lower than that in the P-limited phase (day 9, 11 and 16). Within the P-limited phase, the N uptake was higher in the initial stage (day 9) and decreased gradually with time (day 11 and day 16). That is inconsistent with bulk analysis result in Figure 26 (e) where the N assimilation rate decreased from day 9 to day 11 but increased from day 11 to day

16. Statistic pairwise comparison results by one way ANOVA analysis (Table 10) also showed significant difference of $^{13}C/(^{12}C+^{13}C)$ between the first P-replete phase (day 3) and the P-limited phase (day 9, 11, and 16), but only significant difference of $^{12}C^{15}N/(^{12}C^{15}N+^{12}C^{15}N)$ between day 3 and day 9. The reason why there is no significant difference between the P-limited phase and the second P-replete phase might be that the cells in the second P-replete stage haven't reached steady state yet. Generally, the nitrogen/carbon uptake ratio by cells is lower in P-limited environment, compared with that in P-replete condition. This finding corroborates bulk analysis result above.

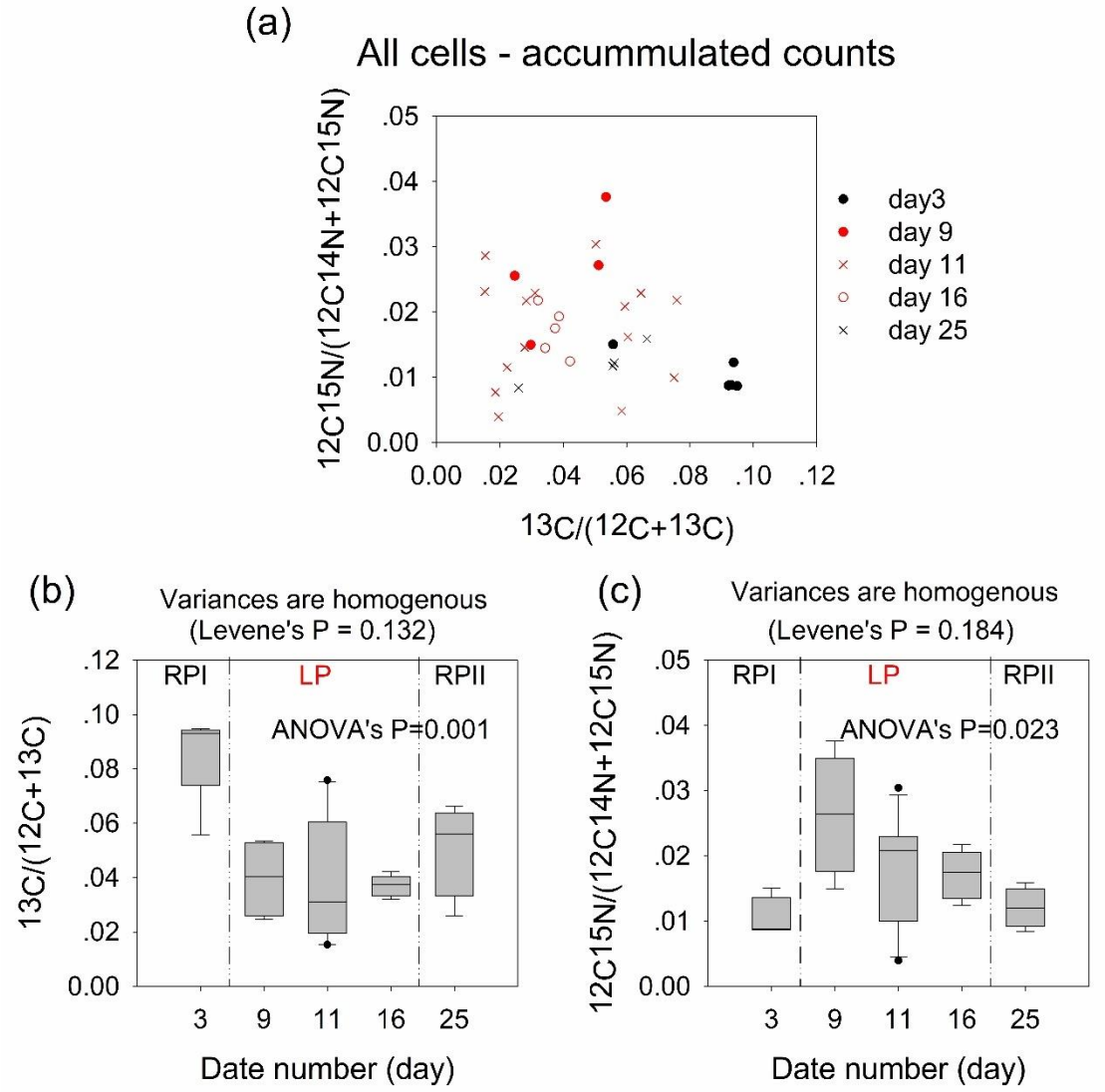

Figure 29 NanoSIMS counting results of $^{13}C/(^{12}C+^{13}C)$ and $^{12}C^{15}N/(^{12}C^{14}N+^{12}C^{15}N)$ for all cells counted from 7 h ^{13}C and ^{15}N enrichment incubations (a). And box plots of $^{13}C/(^{12}C+^{13}C)$ (b) and $^{12}C^{15}N/(^{12}C^{14}N+^{12}C^{15}N)$ (c) from different dates in 7 h ^{13}C and ^{15}N enrichment incubations. Day 3 was in the first P-replete phase (RPI), day 9, 11 and 16 were in the P-limited phase (LP), and day 25 was in the second P-replete phase (RPII).

Table 9 Data number (N), mean value (Mean), standard deviation (Std.Dev) and standard error of mean (SEM) of data points in every group (day 3, 9, 11, 16 and 25) in Figure 29 (b)(c).

	$^{13}C/(^{12}C+^{13}C)$				$^{12}C^{15}N/(^{12}C^{14}N+^{12}C^{15}N)$			
Date number	N	Mean	Std.Dev	SEM	N	Mean	Std.Dev	SEM
3	5	0.0859	0.0169	0.00755	5	0.0107	0.00286	0.00128
9	4	0.0398	0.0147	0.00733	4	0.0263	0.00927	0.00463
11	15	0.0415	0.0225	0.00581	15	0.0174	0.00833	0.00215
16	5	0.0369	0.00391	0.00175	5	0.0171	0.00373	0.00167
25	4	0.0510	0.0175	0.00874	4	0.0121	0.00308	0.00154

Table 10 Pairwise comparison results by one way ANOVA analysis for $^{13}C/(^{12}C+^{13}C)$ and $^{12}C^{15}N/(^{12}C^{14}N+^{12}C^{15}N)$ from NanoSIMS counts for 7 h ^{13}C and ^{15}N enrichment incubations in different dates (day 3, 9, 11, 16 and 25).

Pairwise comparison (day vs day)	$^{13}C/(^{12}C+^{13}C)$		$^{12}C^{15}N/(^{12}C^{14}N+^{12}C^{15}N)$	
	P value	P < 0.05	P value	P < 0.05
3 vs 9	<0.001	Yes	0.022	Yes
3 vs 11	0.003	Yes	0.358	No
3 vs 16	0.008	Yes	0.570	No
3 vs 25	0.066	No	0.948	No
9 vs 11	0.852	No	0.216	No
9 vs 16	0.905	No	0.337	No
9 vs 25	0.875	No	0.061	No
11 vs 16	0.953	No	0.931	No
11 vs 25	0.968	No	0.551	No
16 vs 25	0.874	No	0.639	No

4 Discussion

In this study, we conducted a lab-culture experiment of model photosynthetic eukaryotic micro-organism *Dunaliella tertiolecta* by manipulating the phosphorus content in medium. Specifically, we studied: 1) whether instrumental factor K_R, which is needed to quantify [RCII] in the sigma algorithm and a_{LHII} in the absorption algorithm in Oxborough et al., 2012, keeps constant in unbalanced growth from P-replete condition to P-limited condition; 2) whether the electron requirement for C-fixation ($\Phi_{e,C}$) remains stable during such transient phases. Paremeters of cell concentration, cell size, pH, pigments concentration, [RCII], DIP, POC/PON, FLC and P-I curve were monitored throughout the whole experiment to give a sense of cell conditions during such transient phases and also for parameter calculations. Besides, the roles of alternative sinks of electron during such transient phases were investigated from FLC responses of treatments with inhibitors dithiothreitol (DTT) and propyl gallate (PGal). Whether there is large diurnal variability in C-fixation rate was studied by stable isotope ^{13}C-DIC incubations at different timepoints in a light-dark cycle. Carbon and nitrogen assimilation patterns in such transient phases were investigated both in bulk level through ^{13}C-DIC and ^{15}N-NH_4 double stable isotope enrichment incubations and single cell level through NanoSIMS measurements.

4.1 General growth characteristics

Generally, the changes of most growth parameters in experiment 2 match our expectation: cell growth rates, cell concentrations and *Chla*/cell all decreased, as did the photosynthetic activity. Although the F/2 medium is frequently used for culture studies, a calculation based on the used cell concentration and assuming Redfield stoichiometry indicated that even during the P-replete phase the cells might actually have a (mild) P-shortage. As our cell concentrations did not differ from other studies (Ihnken et al., 2011; Ihnken et al., 2014), this might suggest that the nutrient replete conditions cited in these papers might not be true. Nevertheless, the transfer of the cells to the low-P-phase ensured strongly different P-availability during our experiment, so the prerequisite for our experiment (a strong decrease in the P-availability to induce unbalanced growth conditions) was met. The effect of cells handling during the transfer operation to low P-conditions was limited (Figure 6), so we don't take that into account. Some parameters still kept steady for several days after the transfer to low P-condition, or changed quite gentle, like the cell concentration, Chla concentration, POC and PON concentration, and F_v/F_m. That can be ascribed to the P stored in cells which could still support their growth for a few days. In most cases, Ca and Cb behaved in very similar, making the cultures good duplicates. Although sometimes the data were a bit noisy, but both cultures showed similar variation, that means such variation was not caused by measurement error but might induced by other factors.

Due to P shortage in the second period, there was not enough P to continue to grow and reproduce at the same rate. Therefore, the growth rate of cells decreased from 0.6 day^{-1} at the initial stage of the P-limited phase to about 0.4 day^{-1} at the end of that phase (figure8 (d)), and cell density decreased by about 40% until we added extra P into cultures (Figure 8 (a)). Some studies found an inverse

relationship between cells size and their growth rate (Kagami & Urabe 2001; Morin et al. 2008), but it is not the case in this study. The cell size decrease in the P-limited phase in this study might be a result of self-regulation with environment change (Figure 8 (b)). The change in P-availability further led to a decrease of average absorption (Figure 9 (a)), *Chla* content (Figure 9 (b)), POC and PON concentration (Figure 10 (b)(c)) but only a small change in the C:N-ratio (Figure 10 (d)). Because of that undesirable abrupt environmental change, the photosynthetic activity of cells, F_v/F_m, also decreased, although this only happened after a few days after the transfer to low P-medium, suggesting that the change in F_v/F_m was induced by depletion of the internal P-store. (Figure 15). Interestingly, the decrease in F_v/F_m was only temporary because after approximately 10 days after the onset of the decrease F_v/F_m had recovered (Figure 15). Young and Beardall (2003) also reported a great decrease in F_v/F_m in *Dunaliella tertiolecta* in response to nutrient starvation and a rapid recovery after nutrient resupply, but it was N in their case. The recovery of F_v/F_m before the supplement of P in our results is in accordance with the find of Kruskopf and Flynn 2006, where they suggested that F_v/F_m can recover as cells adapting to that nutrient lack. So, using F_v/F_m as an indicator of nutrient deficiency is difficult parameter to use as cells acclimated to low P may have high F_v/F_m values. Owing to that impairment of photosynthetic capacity, cells received much more light than they could use. They thus adopted two kinds of strategies to adapt to the new condition. The short term one is to increase NPQ to get rid of the extra light energy as heat, as we noticed in the behavior of control samples in Figure 16. The long term one is to reduce light-harvesting pigment concentration to diminish the light they capture. As a result, both Cha/cell (Figure 9(d)) and *Chla*/(*Zea*+*Viol*) (Figure 14(b)) showed a downward trend. As n_{PSII} did not change and the structure of a PSII unit did not change, thus, as *Chla*/cell decreased, the cells mainly reduced the number of PSII units per cell whilst keeping the structure intact. So, we can conclude that cells reduced their intracellular RCII numbers by the reduction of intracellular *Chla* concentration to weaken their light energy absorption ability but kept the size of the PSU constant. This would make the cells less sensitive to photodamage than increasing the PSU size, as this would have increased the ratio of pigment to RCII. This conclusion agrees with the result of a fundamental research on light-shade adaptation by Falkowski, P. G. and Owens, T. G. in 1980. They found that main chlorophyll content changes are linked with changes in the number of RCII but not the PSU size for chlorophyte *Dunaliella tertiolecta*. Suggett, D. J. et al (2007) also observed similar outcome in one calcifying strain of coccolithophorid *Emiliania huxleyi*. But one noncalcifying strain of *Emiliania huxleyi* and diatom *Skeletonema costatum* showed preference in adjusting PSU size instead of intracellular RCII number (Falkowski, P. G. and Owens, T. G., 1980; Suggett, D. J. et al, 2007), although Kromkamp and Limbeek (1993) for *Skeletonema costatum* showed that the structure of the PSII unit size depended on the light regime: cells exposed to fluctuations in the light climate decreased the PSU size and adjusted the number of PSII according the average irradiance experienced.

According to the package effect theory from previous studies (Latimer, 1983; Falkowski et al. 1985; Dubinsky, Z. et al. 1986; Finkel, Z. V., 2001), during the first transient phase, the drop of intracellular *Chla* concentration (*Chla*/cell) would cause a decrease in the self-shading by thylakoids within the chloroplasts or between chloroplasts. Furthermore, the self-shading effect should have been further relieved as the cell density was less. Thus, according to their theory, the chance for each pigment molecules to absorb light (a*) should have increased during P-limited stage despite

the fact that the incident irradiance did not change. An example is the study of Geider, R. J. et al in 1993. They demonstrated that a* of diatom *Phaeodactylum tricornutum* went up in P-starved condition compared with nutrient-saturated treatment. What's more, the change in a* could lead to a change in the scaling in PSU size and n_{PSII}. With the probability for each *Chla* molecule to absorb a photon increasing, the requirement of *Chla* to evolve one O_2 molecule decreases, hence PSU size could decline without affecting the rate of O_2-evolution and n_{PSII} is boosted (Finkel, Z. V., 2001). The finding of Sukenik et al. in 1990 that PSU size increased when D. tertiolecta was transferred from a high to low light environment is exactly an example of such theory. However, we didn't observe such changes -- there was no evident variation pattern of a*, PSU size or n_{PSII} with the concentration of P in medium (Figure 9 (c); Figure 11(a)(b)). So the cells preferred to keep their PSII units of constant size. Why we did not observe a change in the package effect is not clear yet.

For light absorption regulation, we found similar results of *Chla*/*Chlb* (Figure 14(a)), *Chla*/(*Zea*+*Viol*) (Figure 14(b)), *Chla*/POC and *Chlb*/POC (Figure 14(d)(e)) with previous studies (Falkowski, P. G. and Owens, T. G., 1980; Geider, R. J., and Osborne, B. A., 1986; Geider, R. J. et al. 1993; Esteban et al. 2015). Falkowski, P. G. and Owens, T. G. in 1980 observed an increase of *Chla*/*Chlb* in *Dunaliella tertiolecta* under high light intensity. The nutrients starvation experiment on diatom *Phaeodactylum tricornutum* by Geider, R. J. et al in 1993 revealed a rise in xanthophyll cycle pigments to *Chla* ratio in P-starved treatment. Recently, in the review paper of Esteban et al (2015), a positive relationship of *Chla*/*Chlb* and a negative relationship of VAZ/Chl (VAZ here contains xanthophyll cycle pigments: violaxanthin, antheraxanthin and zeaxanthin; Chl contains *Chla* and *Chlb*) with light intensity was also found. That is in accordance with our observation because our cells went from light limitation to P limitation, which at some point is the same thing with going from low light to high light. The *Chla*/*Chlb* here could be an indicator of sun/shade acclimation level and the structure of the photosynthetic apparatus (stoichiometry of PSII to PSI) (Anderson et al. 2008; Ballottari et al. 2014; Esteban et al. 2015). Because of its small variation, it could also be a reporter of traditional pigment measurements accuracy. The ratio *Chla*/(*Zea*+*Viol*) here reflects the relative proportion of photosynthetic pigments to the photoprotective xanthophyll cycle pigments. We showed that the proportion of accessory photosynthetic pigments decreased and after the transition from P-replete to P-limited condition. Because of the decrease in photosynthetic capacity, the light the cells absorbed was much more than they needed. For the sake of self-protection from photodamage, the cells up-regulated the ratio of photoprotective pigments as demonstrated by an decrease in the *Chla*/(*Zea* +*Viol*) ratio (Figure 14 (b)). However, contrary to our expectation, the de-epoxidation state (*Zea* (*Zea*+*Viol*) (Filella et al., 2009) also decreased. This indicates that regulation of light harvesting by NPQ driven by the xanthophyll cycle was not the main driver of photoprotection. This was corroborated by our DDT experiments which showed small role of the xanthophylls cycle in q_E of *Dunaliella tertiolecta*. The ratio of *Chla*/POC and *Chlb*/POC showed a valley in the second period (Figure 14 (d)(e)). This corresponds to the result of Geider, R. J., and Osborne, B. A. (1986) that POC/*Chla* greatly increased with light level.

F_{II} factor was almost doubled during the second period (Figure 9(e)). The reason for that doubling might be that the PSII is more capable in dissipating extra energy from light, compared with photosynthesis system I. As we already known, there are several choices for PSII to get rid of high light energy: NPQ, heading of electrons to other biochemical compounds apart from

carbohydrates… In order to effectively remove extra energy, a higher proportion of absorbed light is allocated to PSII during the P-limited stage. But this is only a hypothesis which need further test.

4.2 The robustness of K_R

The K_R values we calculated based on measured [RCII] values and the equation proposed by Oxborough et al. 2012 are generally 10 times higher than the value given by the manual of FRRf (Figure 12). That mismatch might arise from the different light unit we used. The light unit used to derive K_R value of 11800 photons m^{-3} s^{-1} generated blue light, while the light unit we used in this experiment generated white light with a higher light intensity. In addition, we cannot rule out that the output was truly saturating. So, light color and light intensity might be two factors that can alter K_R value. Further study is required for this aspect. Apart from that aspect, there was a near 30-40% decrease of K_R value from the P-replete period to the P-limited period (Figure 12). That means the assumption that the ratio of fluorescence (k_f) and photochemistry (k_p) rate constants in dark acclimated samples is constant (i.e. K_R is constant), based on which a easier method to calculate [RCII] based on the sigma algorithm was proposed by Oxborough et al. 2012, doesn't hold during transient between balanced growth and P-limited unbalanced growth. That also means the new absorption algorithm using calculated a_{LHII} to derive PSII electron transport rate per unit volume (JV_{PSII}) is not usable in such unbalanced condition. Further studies on K_R value of other species in transient phases between different availability of other nutrients are needed. If there exists any pattern, then we could build a specific model to derive K_R based on different nutrients with different concentrations, or even in different species.

4.3 The robustness of $\Phi_{e,C}$

We found that the electron requirement for carbon fixation $\Phi_{e,C}$ almost tripled after the transfer from balanced growth during the P-replete stage to unbalanced growth conditions in the P-limited stage (Figure 22 (b)). At the first P-replete stage, $\Phi_{e,C}$ was ~ 8 mol e^-/mol C, while it rose to ~ 25 mol e^-/mol C during the second period. That means $\Phi_{e,C}$ didn't remain stable in fluctuating natural environments with respect to P availability. The reason for that variation is related to below analysis on roles of alternative sinks of absorbed light energy which were activated activated during the P-transient. Cyclic electron flow around PSII (or PSI) by PTOX (plastid terminal oxidase) played important roles in this divergence. But the role of the xanthophyll cycle in thermal dissipation was limited. The role of PTOX and the xanthophyll cycle in thermal quenching didn't change much from balanced growth in P-replete medium to unbalanced growth in P-limited environment (see Section 4.4).

As summarized by Lawrenz, E. et al (2013), a mean value of 10.9±6.91 mol e^-/mol C was estimated on a global level. But abiotic factors like nutrient availability, temperature, salinity and light availability etc. were observed to affect the value of $\Phi_{e,C}$. These authors tried to summarize their characteristics and proposed specific algorithms for different regions based on several environmental variables. That gives us a clue that we could further test whether there is any variation of $\Phi_{e,C}$ for other species in the case of transient phase from nutrient replete growth to other nutrients

deficiency. Then a database could be builded and maybe a specific algorithm could be builded for this kind of fluctuating conditions.

4.4 Role of alternative sinks of absorbed light energy

There are generally three pathways of absorbed light energy: photochemical quenching, NPQ and fluorescence. NPQ includes mainly three components: q_E, q_T, q_I. For photochemical quenching, not all electrons produced from water-splitting are utilized in fixing carbon. Some electrons go into alternative electron cycling, which includes Water Water Cycle (WWC), cyclic electron flow around PSII (or PSI). Some electrons are headed to the synthesis of other biochemical compounds apart from carbohydrates. We conducted FLCs with DTT and PGal treatments to reveal the role of xanthophyll cycle in q_E, and the role of cyclic electron flow around PSII (or PSI) by PTOX in alternative electron cycling. NPQ did show a rise after cells went into P-limited stole of DTT treatment was limited, no matter in P-replete stages or P-lacking stage (Figure 16). That is to say, the xanthophylls cycle played a small role in NPQ mechanism of *Dunaliella tertiolecta*. The age. But the rrole of the xanthophyll cycle can be deducted from changes in ratio of *Zea*/(*Zea*+*Viol*) (the de-epoxiation state). But, although the contribution of the xanthophyll cycle pigments *Zea* and *Viol* increased relative to *Chla*, the de-epoxiation state actually decreased during the P-limited phase (Figure 14 (c)). This thus indicates that the xantophyll cycle plays a minor role in NPQ *in Dunaliella tertiolecta*. That means other components rather than the xanthophylls cycle play a more pronounced role in q_E of *Dunaliella tertiolecta*. According to Ihnken et al (2014), the fast component of q_E -- ΔpH gradient dependent thermal quenching -- seems more effective than the slower xanthophyll cycle component in *Dunaliella tertiolecta*.

Fq'/Fm' was largely reduced at the presence of PGal (Figure 17). In the quantification of $rETR_{PSII}$ change ratio at 276 μmol photons m^{-2} s^{-1} (Figure 18), we found that around 50% electrons were used by PTOX to reduce oxygen, and it decreased a lot when transformed into P-limited environment. Similarly, in the research of Mackey, K. R. et al (2008), they also found similar function of PTOX, but the percentage of photochemical electron flow blocked by PGal remains below 15% for phytoplankton at Pacific coastal sites. Moreover, that percentage was significantly higher in high-light, low-nutrient waters. This difference with our results might arise from different composition of phytoplankton community.

4.5 Allocation pattern of assimilated C and N

In bulk analysis of ^{13}C and ^{15}N enriched incubations, we found that during the P-limited phase the C_fixation rate decreased in 2h and 7h incubations, but increased over a 24h period, whilst the N_assimilation rate increased in 7h and 24h incubations. Therefore, the C/N assimilation rate ratio largely decreased in P-limited stage in all 2h, 7h and 24h incubations (Figure 26). Those results were confirmed by single cell level analysis by NanoSIMS where we found carbon uptake decreased but nitrogen uptake increased during the P-limited phase (Figure 29). It is noticeable that the C/N uptake rate ratio in bulk analysis were larger than 50, but the ratio of POC/PON were around 8, that disagreement might due to preferential excretion or leakage of carbon compared with nitrogen. In

the single cell level, allocation of carbon uptaken was scattered within cells and the variability was large. But nitrogen was more concentrated in one area inside cells, especially in the end part of prolonged cells. Maybe it is related to abundant enzyme protein near nucleus especially during cell division. This hypothesis needs further study.

4.6 Diurnal variability in C fixation and ETR_{PSII}

Basically, ETR_{PSII} changed a lot during light-dark cycle, but it is hard to say any specific pattern of its change, and it seems that the variation is larger in the P-replete phase than the P-limited phase (Figure 24). The pattern of C_fixation rate diurnal change seems opposite with ETR_{PSII} (Figure 25). But the significance of its change was also smaller in the P-limited phase. $\Phi_{e,C}$ also fluctuated a lot during light-dark cycle, and the change significance in the P-replete phase was much higher than tht in the P-limited phase. And it is strange that $\Phi_{e,C}$ in the P-replete phase were much larger than those in the P-limited phase, which is contrary to our results in Figure 22. The reason for that haven't been figured out yet.

Limited by experimental conditions and labor shortage, the timepoints we chose during light-dark cycle were not enough to figure out any obvious change pattern. Future studies on this aspect should take this into consideration and plan higher frequence measurements.

4.7 Limitations in this study

Firstly, the theoretical N:P ratio of the f/2 medium used in this study is 26.7:1, which is a bit higher than the Redfield ratio (C:N:P=106:16:1). That could cause P-limitation to algae. Although our algae did response to P concentration manipulation, future studies should pay attention to this aspect. Secondly, there is a problem in our experiment design that we didn't set control cultures with sufficient P from the start to the end. That makes it difficult to interpretate our results because we don't know to what extent the change was caused by different P concentration treatments or just occurred with time. Thirdly, the timepoints we set in monitoring diurnal variability of C fixation and ETR_{PSII} are too few that we cannot explicitly recognize any patterns in our results. Also, we only conducted this diurnal change experiment on one culture, it is hard to say whether the variability was random. More frequent measurements and more replicates for future studies on this aspect are required. Fourthly, we only studied the stability of $\Phi_{e,C}$ and K_R on one algae species and in the lacking of one nutrient element. Corresponding mechanisms in other species and other nutrients are still unknown. More studies of other common phytoplankton species and other frequent limiting nutrient elements are required to fully understand the conversion of fluorescence signal to carbon based primary production. Fifthly, our study is only based on laboratory experiments. But most primary production investigations are based on field work. Since the ecosystem community in real oceans and seas is much more diverse and complicated, field work needs to be combined with laboratory work.

5 Conclusion and outlook

$\Phi_{e,C}$ for *Dunaliella tertiolecta* is about 8 at nutrient sufficient environment. The reason why it is bigger than theoretical minimum value — 4 — arises from the contribution of cyclic electron flow around PSII (or PSI) by PTOX and heading of electrons to the synthesis of other biochemical compounds apart from carbohydrates. The role of the xanthophyll cycle in NPQ here is not large and the NPQ might be caused by state transitions. During transient phases in fluctuating environments with respect to P availability, $\Phi_{e,C}$ didn't remain stable and increased 3-fold from P-replete conditions to P-limited conditions. Further study on other species and other nutrient would be helpful in summarizing that variation, thus specific algorithms could be builded up in order to convert ETR_{PSII} measurements to C-based primary production.

The sigma algorithm-based method to calculate [RCII] and the absorption algorithm-based method to calculate a_{LHII} proposed by Oxborough et al. 2012 doesn't hold during fluctuating environment with different P concentrations. That is because of K_R's variation in P-replete condition and P-limited condition, with about 30-40% decrease in the P-limited condition. Besides, light color and light intensity might also alter K_R value. More studies on K_R value of other species in transient phases between different availability of other nutrients are needed for the testing of Oxborough et al.'s algorithm. Besides, studies about the effect of light color and light intensity on K_R value are also essential in improving Oxborough et al.'s algorithm.

The biggest obstacles in the application of variable fluorescence based method to measure PP in phytoplankton were: 1) how to measure absolute rates of photosynthetic electron transport and 2) the conversion of ETR_{PSII} into C fixation rates. Obstacle one was solved with the developments described by Oxborough et al. 2012, which allowed one to derive [RCII] concentrations and the optical absorption coefficient of PSII (a_{LHII}), which are vital in the calculation of ETR_{PSII} in respectively the sigma and absorption algorithm. If the assumptions on which these methods are based hold under all kinds of environmental conditions and for all phytoplankton species, then the application of FRRf could be used to obtain absolute rates of photosynthetic electron transport easily. Our study tested the assumptions of these two algorithms. The result turns out to be that the basic assumption underlying the derivation of K_R doesn't hold during transient phase inducing unbalanced growth caused by a changing P-supply rate, and the K_R values we got were quite higher than the default value. And the conversion factor of ETR_{PSII} into C fixation rates increased a lot during such transient phase. Therefore, the popularization of Chla fluorescence in measuring primary production still needs further development in understanding and predicting the K_R variability and electron requirement for C-fixation.

6 Acknowledgements

This study is a fruit of many people and institutions. Most materials and instruments were offered by the EDS department in Royal Netherlands Institute for Sea Research (NIOZ-Yerseke). The NanoSIMS measurements were supported by the professor Olaf Schuiling fund. The NanoSIMS facility at the Utrecht University was supported through the NWO large infrastructure funding awarded to dr. Jack Middelburg. For the persons involved in this study, I would like to thank Dr. J. C. Kromkamp and Dr. L. Polerecky for providing patient guidance throughout this master thesis research. I would also like to thank Jetta Vlaming and Jan Peene for their kind help during the experiments. Besides, I would also like to thank all the people in NIOZ-Yerseke and guesthouse who created a nice environment to work and live in. I'm very grateful for all your help.

7 Reference

Adams, W. W., and B. Demmig-Adams. 1995. The xanthophyll cycle and sustained thermal energy dissipation activity in Vinca minor and Euonymus kiaufschovicus in winter. Plant, Cell and.Environment **18**:117-127.

Anderson JM, Chow WS, De las Rivas J. 2008. Dynamic flexibility in the structure and function of photosystem II in higher plant thylakoid membranes: the grana enigma. Photosynthesis Research 98: 575–587.

Aro, E. M., S. McCaffery, and J. M. Anderson. 1993. Photoinhibition and D1 protein degradation in peas acclimated to different growth irradiances. Plant Physiol. **103**:835.

Asada, A. 2000. The water-water cycle as alternative photon and electron sinks. Philosophical Transaction of the Royal Society London., series B. **355**:1419-1431.

Baker NR, Oxborough K (2004) Chlorophyll fluorescence as a probe of photosynthetic productivity. In: Papageorgiou GC and Govindjee (eds) Chlorophylla fluorescence: a signature of photosynthesis. Springer, Dordrecht, pp 65–82.

Ballottari M, Alcocerb MJP, D'Andreab C, Violac D, Ahn TK, Petrozzab A, Poll D, Fleming GR, Cerullo C, Bassi R. 2014. Regulation of photosystem I light harvesting by zeaxanthin. Proceedings of the National Academy of Sciences, USA 111: 2431–2438.

Berg, G. M., Shrager, J., van Dijken, G., Mills, M. M., Arrigo, K. R., & Grossman, A. R. (2011). Responses of psbA, hli and ptox genes to changes in irradiance in marine Synechococcus and Prochlorococcus. Aquatic Microbial Ecology, 65(1), 1-14.

Berges JA, Charlebois DA, Mauzerall DC, Falkowski PG (1996) Differential effects of nitrogen limitation on photosynthetic efficiency of Photosystem I and II in microalgae. Plant Physiol 110:689–696

Bolhàr-Nordenkampf HR, Öquist G (1993) Chlorophyll fluorescence as a tool in photosynthesis research. In: Hall DO, Scurlock JMO, Bolhàr-Nordenkampf HR, Leegood RC, Long SP (eds) Photosynthesis and production in a changing environment: a field and laboratory manual. Chapman & Hall, London, pp 193–206

Boyd PW, LaRoche J, Gall M, Frew R, McKay RM (1999) Role of iron, light, and silicate in controlling algal biomass in subantarctic waters SE of New Zealand. J Geophys Res 104:13391–13404

Bradbury M, Baker NR (1984) A quantitative determination of photochemical and non-photochemical quenching during the slow phase of the chlorophyll fluorescence induction curve of

bean leaves. Biochim Biophys Acta 765:275–281.

Bukhov N, Carpentier R (2004) Alternative photosystem I-driven electron transport routes: mechanisms and functions. Photosynth Res 82:17–33.

BUTCHER, R.W. 1959. An introductory account of the smaller algae of the British Coastal Waters. Part 1: Introduction and Chlorophyceae. Fishery investigations. Ministry of Agriculture, Fisheries and Food. Series IV. Her Majesty's Stationery Office, London.

BUTLER, W. L., AND M. KITAJIMA. 1975. Fluorescence quenching in photosystcm II of chloroplasts. Biochim. Biophys. Acta 376: 116-l 25.

Campbell DA, Hurry V, Clarke A, Gustafsson P, O¨ quist G (1998) Chlorophyll fluorescence analysis of cyanobacterial photosynthesis and acclimation. Microbiol Mol Biol Rev 62:667–683.

Campbell, D., A. K. Clarke, P. Gustafsson, and G. Oquist. 1996. D1 exchange and the Photosystem II repair cycle in the cyanobacterium Synechococcus. Plant Science **115**:183-190.

Carr, M.-E., Friedrichs, M. A. M., Schmeltz, M., Aita, M. N., Antoine, D., Arrigo, K. R., Asanuma, I., Aumont, O., Barber, R., Behrenfeld, M., Bidigare, R., Buitenhuis, E. T., Campbell, J., Ciotti, A., Dierssen, H., Dowell, M., Dunne, J., Esaias, W., Gentili, B., Gregg, W., Groom, S., Hoepffner, N., Ishizaka, J., Kameda, T., Le Quere, C., Lohrenz, S., Marra, J., Melin, F., Moore, K., Morel, A., Reddy, T. E., Ryan, J., Scardi, M., Smyth, T., Turpie, K., Tilstone, G., Waters, K., and Yamanaka, Y.: A comparison of global estimates of marine primary production from ocean color, Deep-Sea Res. Part II-Top. Stud. Oceanogr., 53, 741-770, 2006.

Claquin, P., Kromkamp, J. C., and Martin-Jezequel, V.: Relationship between photosynthetic metabolism and cell cycle in a synchronized culture of the marine alga Cylindrotheca fusiformis (Bacillariophyceae), Eur J Phycol, 39, 33-41, 2004.

Cox, T. J., Maris, T., Soetaert, K., Kromkamp, J. C., Meire, P., & Meysman, F. (2015). Estimating primary production from oxygen time series: A novel approach in the frequency domain. Limnology and Oceanography: Methods, 13(10), 529-552.

Crow, J. F., & Kimura, M. (1970). An introduction to population genetics theory. An introduction to population genetics theory.

Dau, H. 1994. Short-term adaptation of plants to changing light intensities and its relation to Photosystem II photochemistry and fluorescence. Journal.of.Photochemistry.and.Photobiology.B.: Biology **26**:3-27.

Dubinsky, Z., Falkowski, P. G., & Wyman, K. (1986). Light harvesting and utilization by phytoplankton. Plant and Cell Physiology, 27(7), 1335-1349.

Elser, J. J., Acharya, K., Kyle, M., Cotner, J., Makino, W., Markow, T., ... & Hood, J. A. (2003). Growth rate–stoichiometry couplings in diverse biota. Ecology Letters, 6(10), 936-943.

Elser, J. J., Bracken, M. E., Cleland, E. E., Gruner, D. S., Harpole, W. S., Hillebrand, H., ... & Smith, J. E. (2007). Global analysis of nitrogen and phosphorus limitation of primary producers in freshwater, marine and terrestrial ecosystems. Ecology letters, 10(12), 1135-1142.

Esteban, R., Barrutia, O., Artetxe, U., Fernández-Marín, B., Hernández, A., & García-Plazaola, J. I. (2015). Internal and external factors affecting photosynthetic pigment composition in plants: a meta-analytical approach. New Phytologist, 206(1), 268-280.

Falkowski PG, Fujita Y, Ley A, Mauzerall D (1986) Evidence for cyclic electron flow around photosystem-II in Chlorella pyrenoidosa. Plant Physiol 81:310–312.

Falkowski, P. G., & Owens, T. G. (1980). Light—shade adaptation: two strategies in marine phytoplankton. Plant physiology, 66(4), 592-595.

Falkowski, P. G., & Raven, J. A. (2013). Aquatic photosynthesis. Princeton University Press.

Falkowski, P. G., Dubinsky, Z., & Wyman, K. (1985). Growth-irradiance relationships in phytoplankton. Limnology and Oceanography, 30(2), 311-321.

Filella, I., Porcar-Castell, A., Munné-Bosch, S., Bäck, J., Garbulsky, M. F., & Peñuelas, J. (2009). PRI assessment of long-term changes in carotenoids/chlorophyll ratio and short-term changes in de-epoxidation state of the xanthophyll cycle. International Journal of Remote Sensing, 30(17), 4443-4455.

Finazzi G, Forti G (2004) Metabolic flexibility of the green alga Chlamydomonas reinhardtii as revealed by the link between state transitions and cyclic electron flow. Photosynth Res 82:327–338.

Finkel, Z. V. (2001). Light absorption and size scaling of light-limited metabolism in marine diatoms. Limnology and Oceanography, 46(1), 86-94.

Flameling, I. A. and Kromkamp, J.: Light dependence of quantum yields for PSII charge separation and oxygen evolution in eucaryotic algae, Limnology and Oceanography, 43, 284-297, 1998.

Flood, S., Burkholder, J., & Cope, G. (2018). Assessment of atrazine toxicity to the estuarine phytoplankter, Dunaliella tertiolecta (Chlorophyta), under varying nutrient conditions. Environmental Science and Pollution Research, 1-15.

García-Mendoza, E., & Colombo-Pallotta, M. F. (2007). The giant kelp Macrocystis pyrifera presents a different nonphotochemical quenching control than higher plants. New Phytologist, 173(3), 526-536.

Geider, R. J., & Osborne, B. A. (1986). Light absorption, photosynthesis and growth of Nannochloris atomus in nutrient-saturated cultures. Marine Biology, 93(3), 351-360.

Geider, R. J., La Roche, J., Greene, R. M., & Olaizola, M. (1993). RESPONSE OF THE PHOTOSYNTHETIC APPARATUS OF PHAEODACTYLUM TRICORNUTUM (BACILLARIOPHYCEAE) TO NITRATE, PHOSPHATE, OR IRON STARVATION 1. Journal of phycology, 29(6), 755-766.

Genty B, Briantais J-M, Baker NR (1989) The relationship between the quantum yield of photosynthetic electron transport and quenching of chlorophyll fluorescence. Biochim Biophys Acta 990:87–92.

Goltsev, V. N., Kalaji, H. M., Paunov, M., Bąba, W., Horaczek, T., Mojski, J., ... & Allakhverdiev, S. I. (2016). Variable chlorophyll fluorescence and its use for assessing physiological condition of plant photosynthetic apparatus. Russian journal of plant physiology, 63(6), 869-893.

Goss, R., Pinto, E. A., Wilhelm, C., & Richter, M. (2006). The importance of a highly active and ΔpH-regulated diatoxanthin epoxidase for the regulation of the PS II antenna function in diadinoxanthin cycle containing algae. Journal of plant physiology, 163(10), 1008-1021.

Govindjee, Sixty-three years since Kautsky: chlorophyll a fluorescence, Aust. J. Plant Physiol. 22 (1995) 131^160.

Guillard R. R. and Ryther J. H., 1962. Studies of marine planktonic diatoms. I. *Cyclotella nana* Hustedt and *Detonula confervacea* Cleve. *Can J Microbiol*. 8: 229-239.

Hennige SJ, Smith DJ, Perkins R, Consalvey M, Paterson DM, Suggett DJ (2008) Photoacclimation, growth and distribution of massive coral species in clear and turbid waters. Mar Ecol Prog Ser 369:77–88.

Holt N, Fleming G, Niyogi KK (2004) Toward an understanding of the mechanism of nonphotochemical quenching in green plants. Biochemistry 43(26):8281–8289.

Horton, P., and A. Ruban. 1994. The role of light-harvesting complex II in energy quenching. Pages 111-128 *in* N. R. Baker, editor. Photoinhibition of photosynthesis: from molecular meachnisms to the field. Bios Scientific Publishers, Oxford.

Horton, P., and A. Ruban. 2005. Molecular design of the photosystem II light-harvesting antenna: photosynthesis and photoprotection. Journal of Experimental Botany **56**:365-373.

Ihnken, S., Kromkamp, J. C., & Beardall, J. (2011). Photoacclimation in Dunaliella tertiolecta reveals a unique NPQ pattern upon exposure to irradiance. *Photosynthesis research*, *110*(2), 123-137.

Ihnken, S., Kromkamp, J. C., Beardall, J., & Silsbe, G. M. (2014). State-transitions facilitate robust quantum yields and cause an over-estimation of electron transport in Dunaliella tertiolecta cells held at the CO2 compensation point and re-supplied with DIC. Photosynthesis research, 119(3), 257-272.

Ivanov AG, Hurry V, Prafullanchandra VS, Öquist G, Huner NPA (2008a) Reaction centre quenching of excess light energy and photoprotection of photosystem II. J Plant Biol 51:85–96.

Ivanov AG, Prafullanchandra VS, Hurry V, Öquist G, Huner NPA (2008b) Photosystem II reaction centre quenching: mechanisms and physiological role. Photosynth Res 98:565–574.

Johnsen, G., and E. Sakshaug. 2007. Biooptical characteristics of PSII and PSI in 33 species (13 pigment groups) of marine phytoplankton, and the relevance for pulse-amplitued-modulated and fast-repetition-rate fluorometry. Journal of Phycology **43**:1236-1251.

K Soetaert, Kromkamp, J. C., GM Silsbe (2014). FRRF: Phytoplankton Photosynthesis Irradiance Curve Fitting with R. R package.

Kagami, M., & Urabe, J. (2001). Phytoplankton growth rate as a function of cell size: an experimental test in Lake Biwa. Limnology, 2(2), 111-117.

Kalaji, H. M., Jajoo, A., Oukarroum, A., Brestic, M., Zivcak, M., Samborska, I. A., ... & Ladle, R. J. (2016). Chlorophyll a fluorescence as a tool to monitor physiological status of plants under abiotic stress conditions. Acta Physiologiae Plantarum, 38(4), 102.

Kautsky H, Hirsch A (1931) Neue Versuche zur Kohlensãureassimilation. Naturwissenschaften 19:964

Kirilovsky, D. 2007. Photoprotection in cyanobacteria: the orange carotenoid protein (OCP)-related non-photochemical-quenching mechanism. Photosynthesis Research **93**:7-16.

Kolber Z, Wyman KD, Falkowski PG (1990) Natural variability in photosynthetic energy-conversion efficiency – A field study in the Gulf of Maine. Limnol Oceanogr 35:72–79.

Kolber, Z. S., Prášil, O., & Falkowski, P. G. (1998). Measurements of variable chlorophyll fluorescence using fast repetition rate techniques: defining methodology and experimental protocols. Biochimica et Biophysica Acta (BBA)-Bioenergetics, 1367(1), 88-106.

Kolber, Z., & Falkowski, P. G. (1993). Use of active fluorescence to estimate phytoplankton photosynthesis in situ. Limnology and Oceanography, 38(8), 1646-1665.

Krause G, Weis E (1991) Chlorophyll fluorescence and photosynthesis: the basics. Annu Rev Plant Physiol Plant Molec Biol 42:313–349

Krause GH, Jahns P (2004). Non-photochemical energy dissipation determined by chlorophyll

fluorescence quenching: characterization and function. In: Papageorgiou G, Govindjee (eds) Chlorophyll a fluorescence: a signature of photosynthesis. Springer, Dordrecht, pp 463–495.

Krause GH, Weis E (1988) The photosynthetic apparatus and chlorophyll fluorescence: an introduction. In: Lichtenthaler HK (ed) Applications of chlorophyll fluorescence. Kluwer, Dordrecht, pp 3–12

Kromkamp, J. C., and R. M. Forster. 2003. The use of variable fluorescence measurements in aquatic ecosystems: differences between multiple and single turnover measuring protocols and suggested terminology. European Journal of Phycology **38**:103-112.

Kromkamp, J. C., Dijkman, N. A., Peene, J., Simis, S. G. H., and Gons, H. J.: Estimating phytoplankton primary production in Lake IJsselmeer (The Netherlands) using variable fluorescence (PAM-FRRF) and C-uptake techniques, Eur J Phycol, 43, 327 - 344, 2008.

Kromkamp, J., & Limbeek, M. (1993). Effect of short-term variation in irradiance on light harvesting and photosynthesis of the marine diatom Skeletonema costatum: a laboratory study simulating vertical mixing. Microbiology, 139(9), 2277-2284.

Kromkamp, J., Capuzzo, E., & Philippart, C. J. M. (2017). Measuring phytoplankton primary production: review of existing methodologies and suggestions for a common approach. EcApRHA Deliverable WP 3.2.

Kruskopf, M., & Flynn, K. J. (2006). Chlorophyll content and fluorescence responses cannot be used to gauge reliably phytoplankton biomass, nutrient status or growth rate. New Phytologist, 169(3), 525-536.

Latimer, P. (1983). THE DECONVULATION OF ABSORPTION SPECTRA OF GREEN PLANT MATERIALS—IMPROVED CORRECTIONS FOR THE SIEVE EFFECT. Photochemistry and photobiology, 38(6), 731-734.

Lavaud J (2007) Fast regulation of photosynthesis in diatoms: mechanisms, evolution and ecophysiology. In: Global Science Books—Functional plant science and biotechnology, pp 267–287.

Lavaud J, Rousseau B, van Gorkom HJ, Etienne A-L (2002) Influence of the diadinoxanthin pool size on photoprotection in a marine planktonic diatom Phaeodactylum tricornutum. Plant Physiol 129:1398–1406

Lawrenz, E., Silsbe, G., Capuzzo, E., Ylöstalo, P., Forster, R. M., Simis, S. G., ... & Forget, M. H. (2013). Predicting the electron requirement for carbon fixation in seas and oceans. PLoS One, 8(3), e58137.

Lemeille S, Rochaix J-D (2010) State transitions at the crossroad of thylakoid signaling pathways.

Photosynth Res 106:33–46. doi:10.1007/s11120-010-9538-8.

Lin, S., Litaker, R. W., & Sunda, W. G. (2016). Phosphorus physiological ecology and molecular mechanisms in marine phytoplankton. Journal of phycology, 52(1), 10-36.

Longhurst, A., Sathyendranath, S., Platt, T. and Caverhill, C. (1995). An estimate of global primary production in the ocean from satellite radiometer data. Journal of Plankton Research 17, 1245-1271.

Ly, J., Philippart, C. J., & Kromkamp, J. C. (2014). Phosphorus limitation during a phytoplankton spring bloom in the western Dutch Wadden Sea. Journal of Sea Research, 88, 109-120.

Mackey, K. R., Paytan, A., Grossman, A. R., & Bailey, S. (2008). A photosynthetic strategy for coping in a high-light, low-nutrient environment. Limnology and Oceanography, 53(3), 900-913.

Marra, J. (2002). Approaches to the measurement of plankton production. Phytoplankton productivity: Carbon assimilation in marine and freshwater ecosystems, 78-108.

Mauzerall DC (1972) Light-induced changes in Chlorella, and the primary photoreaction for the production of oxygen. Proc Nat Acad Sci USA 69:1358–1362

Maxwell K, Johnson GN (2000) Chlorophyll fluorescence – a practical guide. J Exp Bot 51:659–668

Milligan, A. J., Halsey, K. H., & Behrenfeld, M. J. (2015). Advancing interpretations of 14C-uptake measurements in the context of phytoplankton physiology and ecology. Journal of Plankton Research, 37(4), 692-698.

Moore, C. M., Mills, M. M., Arrigo, K. R., Berman-Frank, I., Bopp, L., Boyd, P. W., Galbraith, E. D. et al. 2013. Processes and patterns of oceanic nutrient limitation. Nature Geosci. 6:701–10.

Morin, S., Coste, M., & Delmas, F. (2008). A comparison of specific growth rates of periphytic diatoms of varying cell size under laboratory and field conditions. Hydrobiologia, 614(1), 285-297.

Myers, J., & Graham, J. R. (1971). The photosynthetic unit in Chlorella measured by repetitive short flashes. Plant physiology, 48(3), 282-286.

Nielsen, E. S. (1952). The use of radio-active carbon (C^) for measuring organic production in the sea. Journal de Conseil, 18, 117-140.

Nielsen, G. Æ., & Bresta, A. M. (Eds.). (1984). Guidelines for the measurement of phytoplankton primary production. Baltic Marine Biologists.

Nieuwenhuize, J., Y. E. M. Maas, and J. J. Middelburg. 1994. Rapid analyses of organic carbon and nitrogen in particulate materials. Marine Chemistry **44**:217-224.

Nilkens M, Kress E, Lambrev P, Miloslavina Y, Mu¨ller M, Holzwarth AR, Jahns P (2010) Identification of a slowly inducible zeaxanthin-dependent component of non-photochemical quenching of chlorophyll fluorescence generated under steady-state conditions in Arabidopsis. Biochim Biophys Acta 1797:466–475. doi:10.1016/j.bbabio.2010.01.001.

Oukarroum, A., Bras, S., Perreault, F., & Popovic, R. (2012). Inhibitory effects of silver nanoparticles in two green algae, Chlorella vulgaris and Dunaliella tertiolecta. Ecotoxicology and Environmental Safety, 78, 80-85.

Oxborough K, Baker NR (1997) Resolving chlorophyll a fluorescence images of photosynthetic efficiency into photochemical and non-photochemical components – calculation of qP and Fv'/Fm' without measuring Fo'. Photosynth Res 54:135–142.

Oxborough, K., Moore, C. M., Suggett, D. J., Lawson, T., Chan, H. G., and Geider, R. J.: Direct estimation of functional PSII reaction centre concentration and PSII electron flux on a volume basis: a new approach to the analysis of Fast Repetition Rate fluorometry (FRRf) data, Limnology and Oceanography-Methods, 10, 142-154, 2012.

Papageorgiou G, Tsimilli-Michael M, Stamatakis K (2007) The fast and slow kinetics of chlorophyll a fluorescence induction in plants, algae and cyanobacteria: a viewpoint. Photosynth Res 94:275–290

Perkins, R. G., Kromkamp, J. C., Serôdio, J., Lavaud, J., Jesus, B., Mouget, J. L., ... & Forster, R. M. (2010). The application of variable chlorophyll fluorescence to microphytobenthic biofilms. In Chlorophyll a fluorescence in aquatic sciences: methods and applications (pp. 237-275). Springer, Dordrecht.

Platt T., Gallegos C.L. and W.G. Harrison, 1980. Photoinhibition of photosynthesis in natural assemblages of marine phytoplankton. J. Mar. Res., 38, 687–701

Pocock, T. H., A. Koziak, D. Rosso, S. Falk, and N. P. A. Huner. 2007. Chlamydomonas raudensis (UWO 241), Chlorophyceae, exhibits the capacity for rapid D1 repair in response to chronic photoinhibition at low temperature. Journal of Phycology **43**:924-936.

Porcar-Castell, A., Tyystjärvi, E., Atherton, J., van der Tol, C., Flexas, J., Pfündel, E. E., ... & Berry, J. A. (2014). Linking chlorophyll a fluorescence to photosynthesis for remote sensing applications: mechanisms and challenges. Journal of experimental botany, 65(15), 4065-4095.

Prasil, O., Kolber, Z., Berry, J., and Falkowski, P. G.: Cyclic electron flow around photosystem II in vivo, Photosynthesis.Research., 48, 395-410, 1996.

Ralph, P. J., & Gademann, R. (2005). Rapid light curves: a powerful tool to assess photosynthetic activity. Aquatic botany, 82(3), 222-237.

REDFIELD, A. C. 1958. The biological control of the chemical fac-tors in the environment. Am. Sci. 46: 205–221.

Reed, M. L., Pinckney, J. L., Keppler, C. J., Brock, L. M., Hogan, S. B., & Greenfield, D. I. (2016). The influence of nitrogen and phosphorus on phytoplankton growth and assemblage composition in four coastal, southeastern USA systems. Estuarine, Coastal and Shelf Science, 177, 71-82.

Riley, G. A. (1939). Plankton studies. II. The western North Atlantic, May-June, 1939. J. mar. Res, 2(2), 145-162.

Ritchie, R. J. (2006). Consistent sets of spectrophotometric chlorophyll equations for acetone, methanol and ethanol solvents. Photosynthesis research, 89(1), 27-41.

Schreiber U (2004). Pulse-Amplitude-Modulation (PAM) fluorometry and saturation pulse method: an overview. In: Papageorgiou G, Govindjee (eds) Chorophyll a fluorescence: a signature of photosynthesis. Springer, Dordrecht, pp 279–319.

Schreiber, U., Schliwa, U., & Bilger, W. (1986). Continuous recording of photochemical and non-photochemical chlorophyll fluorescence quenching with a new type of modulation fluorometer.Photosynthesis research, 10(1-2), 51-62.

Serôdio J, Vieira S, Cruz S, Coelho H (2006) Microphytobenthos vertical migratory photoresponse as characterized by light response curves. Photosynth Res 90:29–43.

Silsbe, G. M., and J. C. Kromkamp. 2012. Modeling the irradiance dependency of the quantum efficiency of photosynthesis. Limnology and Oceanography-Methods **10**:645-652.

Silsbe, G. M., Oxborough, K., Suggett, D. J., Forster, R. M., Ihnken, S., Komárek, O., Lawrenz, E., Prášil, O., Röttgers, R., Šicner, M., Simis, S. G. H., Van Dijk, M. A., and Kromkamp, J. C.: Toward autonomous measurements of photosynthetic electron transport rates: An evaluation of active fluorescence-based measurements of photochemistry, Limnology and Oceanography: Methods, 13, 138-155, 2015.

Steemann Nielsen, E. 1952. The use of radio-active carbon 14C for measuring organic production in the sea. J. Con. Perm. int. Explor. Mer 18(2), 117-140 **18**:117-140.

Suggett DJ, Oxborough K, Baker NR, MacIntyre HL, Kana TM, Geider RJ (2003) Fast Repetition Rate and Pulse Amplitude Modulation chlorophyll a fluorescence measurements for assessment of photosynthetic electron transport in marine phytoplankton. Eur J Phycol 38:371–384.

Suggett, D. J., Le Floc'H, E., Harris, G. N., Leonardos, N., & Geider, R. J. (2007). Different strategies of photoacclimation by two strains of Emiliania huxleyi (Haptophyta) 1. Journal of Phycology, 43(6), 1209-1222.

Suggett, D. J., Prášil, O., & Borowitzka, M. A. (2010). Chlorophyll a fluorescence in aquatic sciences: methods and applications (pp. 427-433). Dordrecht, The Netherlands: Springer.

Sukenik, A., Bennett, J., Mortain-Bertrand, A., & Falkowski, P. G. (1990). Adaptation of the photosynthetic apparatus to irradiance in Dunaliella tertiolecta: a kinetic study. Plant physiology, 92(4), 891-898.

Taiz, L., & Zeiger, E. (2006). Plant physiology. 4th. Sinauer Associate, Sunderland, Mass., EUA. 764 pp.

Van Kooten, O., & Snel, J. F. (1990). The use of chlorophyll fluorescence nomenclature in plant stress physiology. Photosynthesis research, 25(3), 147-150.

White AJ, Critchley C (1999) Rapid light curves: a new fluorescence method to assess the state of the photosynthetic apparatus. Photosynth Res 53:63–72.

Young EB, Beardall J. 2003. Rapid ammonium- and nitrate-induced perturbations to chl a fluorescence in nitrogen-stressed Dunaliella tertiolecta (Chlorophyta). Journal of Phycology 39: 332–342.

8 Appendices

Appendix I. Recipe of f/2 medium used in this study.

Table i. Recipe of f/2 medium used in this study.

	Stock (g/L)	Final (g/L)
Artificial seawater		
NaCl	241	24.1
Na_2SO_4	32.9	3.2
$MgCl_2 \cdot 6H_2O$	435	8.7
KCl	54	0.54
$CaCl_2 \cdot 2H_2O$	160	1.6
Minerals		
$NaNO_3$	150	0.075
$NaH_2PO_4 \cdot 2H_2O$	6.9	5.00×10^{-3}
$Na_2SiO_3 \cdot 9H_2O$	21.3	0.03
$NaHCO_3$	18	0.18
H_3BO_3	11	0.011
KBr	39	0.039
$SrCl_2 \cdot 6H_2O$	10	0.01
Trace metals		
Na_2-EDTA$\cdot 2H_2O$	4.16	4.16×10^{-3}
$FeCl_3 \cdot 6H_2O$	3.15	3.15×10^{-3}
$MnCl_2 \cdot 4H_2O$	0.18	1.8×10^{-4}
$ZnSO_4 \cdot 7H_2O$	0.022	2.2×10^{-5}
$CoCl_2 \cdot 6H_2O$	0.01	1×10^{-5}
$CuSO_4 \cdot 5H_2O$	0.01	1×10^{-5}
$Na_2MoO_4 \cdot 2H_2O$	0.006	6×10^{-6}
Vitamins		
Thiamine-HCl	0.1	1×10^{-4}
d-biotin*	0.0005	5×10^{-7}
Vitamin B12**	0.0005	5×10^{-7}

Appendix II. Abbreviations used in this report.

Table ii. Abbreviations used in this report.

	Full expression
PP	Primary production
LHC	Light harvesting complex
RCII	Reaction center II
PSI	Photosystem I
PSII	Photosystem II
DIC	Dissolved inorganic carbon
POC	Particulate organic carbon
PON	Particulate organic nitrogen
WWC	Water water cycle
PTOX	Plastid terminal oxidase
DCMU	3-(3,4-dichlorophenyl)-1,1-dimethylurea
DTT	Dithiothreitol
PGal	Propyl gallate
PQ	Plastoquinone pool
ST	Single-turnover
MT	Multiple-turnover
FLCs	Fluorescence-light response curves
PAM	Pulse amplitude modulated
FRRf	Fast repetition rate fluorescence
P&P	Pump and probe
Chla	Chlorophyll a
Chlb	Chlorophyll b
Zea	Zeaxanthin
Viol	Violaxanthin

Appendix III. Culture settings.

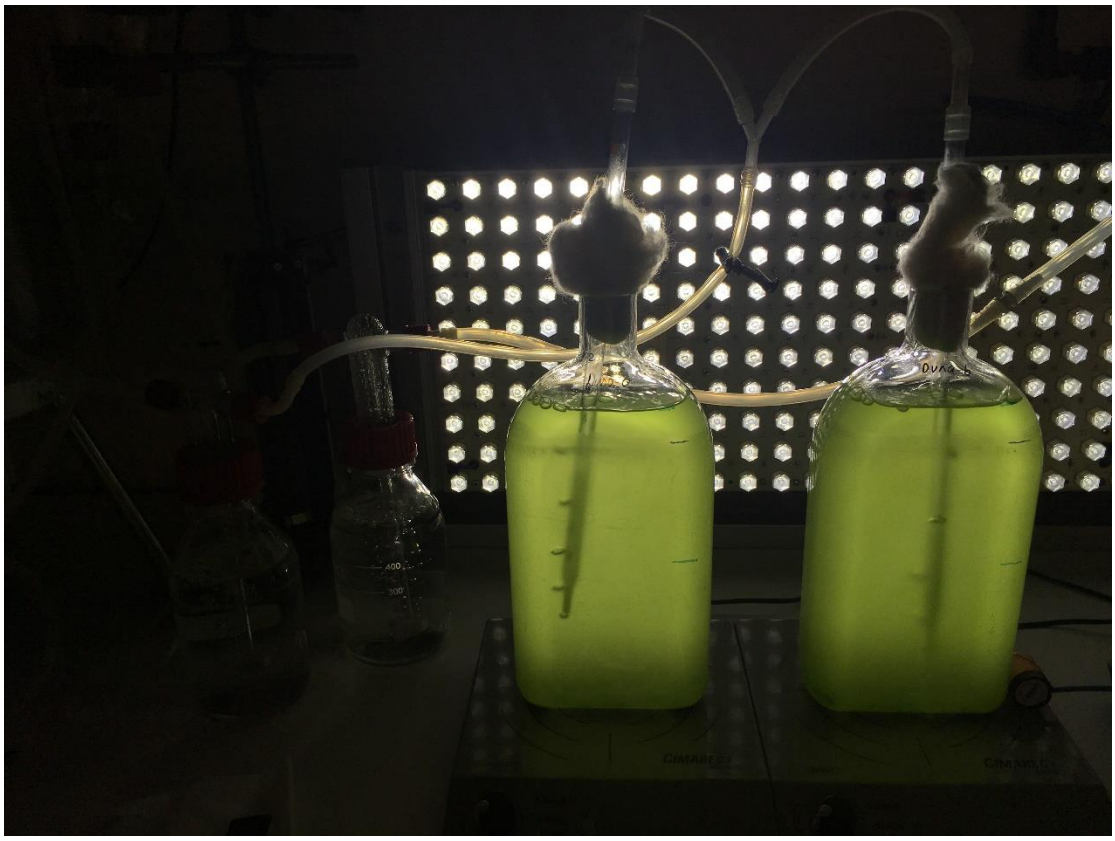

Figure i. One photo of the cultures.